NACA

RESEARCH MEMORANDUM

for the

Bureau of Aeronautics, Navy Department

WIND-TUNNEL INVESTIGATION OF A 1/5-SCALE MODEL OF THE RYAN XF2R AIRPLANE

By Park Y. Wong

Ames Aeronautical Laboratory
Moffett Field, Calif.

NATIONAL ADVISORY COMMITTEE
FOR AERONAUTICS

WASHINGTON

June 27, 1947

NATIONAL ADVISORY COMMITTEE FOR AERONAUTICS

RESEARCH MEMORANDUM

for the

Bureau of Aeronautics, Navy Department

WIND-TUNNEL INVESTIGATION OF A 1/5-SCALE MODEL OF THE RYAN XF2R AIRPLANE

By Park Y. Wong

SUMMARY

Wind-tunnel tests on a 1/5-scale model of the Ryan XF2R airplane were conducted to determine the aerodynamic characteristics of the air intake for the front power plant, a General Electric TG-100 gas turbine, and to determine the stability and control characteristics of the airplane. The results indicated low-dynamic-pressure recovery for the air intake to the TG-100 gas turbine with the standard propeller in operation. Propeller cuffs were designed and tested for the purpose of improving the dynamic-pressure recovery. Data obtained with the cuffs installed and the gap between the spinner and the cuff sealed indicated a substantial gain in dynamic pressure recovery over that obtained with the standard propeller and with the cuffed propeller unsealed.

Stability and control tests were conducted with the sealed cuffs installed on the propeller. The data from these tests indicated the following unsatisfactory characteristics for the airplane:

1. Marginal static longitudinal stability
2. Inadequate directional stability and control
3. Rudder-pedal-force reversal in the climb condition
4. Negative dihedral effect in the power-on approach and wave-off conditions

INTRODUCTION

At the request of the Bureau of Aeronautics, Navy Department, tests were conducted on a 1/5-scale model of the Ryan XF2R airplane in the Ames Aeronautical Laboratory 7- by 10-foot wind tunnel No. 2. The XF2R airplane was designed primarily for the development of the cowl for the front power-plant installation, a General Electric TG-100 gas turbine. The turbine and the resultant cowl design were intended for incorporation in a later airplane. Therefore, the primary purpose of these tests was to determine the aerodynamic characteristics of the air-intake system for the TG-100 gas turbine. These tests included measurements of the dynamic pressure recovery in the ducting system, the cowl pressure distribution, and the velocity distribution at the simulated entrance to the TG-100 turbine.

Since relatively few XF2R airplanes were to be constructed, stability and control tests were considered to be of secondary importance. Only a limited investigation was made of the longitudinal-, directional-, and lateral-stability and -control characteristics of the model to reveal any unsafe or undesirable handling characteristics that might be present in the airplane. Some comparisons were made of the predicted characteristics of the XF2R and the FR-1 to facilitate a comparative analysis based on the known handling qualities of the FR-1 airplane.

DESCRIPTION OF MODEL AND APPARATUS

The RYAN XF2R airplane, a single-place, low-wing, carrier-based, fighter-type aircraft with a fully retractable tricycle landing gear, differs from the FR-1 airplane only in the front power plant. The Wright R-1820 reciprocating engine of the FR-1 is replaced by a General Electric TG-100 gas turbine accompanied by a resultant modification in cowl and propeller design. The rear power plant, however, remains a General Electric I-16 jet motor located aft of the cockpit, supplied by air from leading-edge wing ducts and exhausting out the rear of the fuselage. A three-view drawing of the airplane is presented in figure 1. The basic physical characteristics of the airplane and the configuration notation used in these tests may be found in appendixes A and B. Photographs of the model mounted in the tunnel in various configurations are presented in figures 2 to 4, inclusive.

A 110-horsepower electric motor was utilized to drive the four-blade model propeller (Aeroproducts H20-156-28) used in these tests. Photographs of the model propeller with and without the cuffs installed are presented in figures 5 to 7. Presented in figure 8 are the geometric characteristics of the propeller and of the propeller cuffs developed. Ordinates for the blade cuffs are presented in table I. The aerodynamic characteristics of the propeller with and without cuffs, as determined on the 1/5-scale model, are presented in figure 9 for maximum power output (1800 bhp) of the TG-100 unit.

The quantity of air flow through the cowl entrance was controlled by an air pump located outside the test chamber and was determined by means of an ASME standard 5-inch-diameter orifice-meter located in the air pipe. A pressure rake containing 44 total pressure tubes and 4 static pressure tubes was located in the model at the position corresponding to the entrance to the TG-100 gas turbine. The pressures were measured by an averaging manometer from which the average pressure loss in the cowl ducting was determined. Similarly, air flow through the oil-cooler duct on the underside of the cowl was measured with a pressure rake consisting of nine total pressure and three static pressure tubes. The rate of air flow through the oil-cooler duct, however, was adjusted by varying the exit area at the rear of the fuselage. The relative location of the rakes may be seen on figure 10, which is a sketch of the model showing the various pressure-tube locations and the numbering system employed in identifying these tubes. A detail drawing of the tube locations in the cowl rake is given in figure 11. Photographs of the model showing the pressure orifice locations are presented in figures 12, 13, and 14.

TESTS AND TEST METHODS

The air-flow tests, which included measurements of dynamic-pressure recovery, pressure distribution, and velocity distribution, were conducted with the model having the flaps and gear retracted, tail off, and with the exit pipe for the cowl air installed on the under side of the fuselage. (See fig. 2 for a photograph of the model in this configuration.) To simulate flight conditions, various inlet-velocity ratios at the cowl entrance were obtained by the adjustment of the air-pump output and the tunnel airspeed. Presented in figure 15 is the predicted variation of cowl inlet-velocity ratio with free-stream velocity as furnished by the Ryan Aeronautical Company for the XF2R airplane. The variation of lift coefficient

with geometric angle of attack[1] as measured for the model in this series of tests is presented in figure 16.

For all stability and control tests, the TG-100 gas turbine jet-exhaust outlets on both sides of the fuselage were plugged and faired. Tuft studies indicated this advisable, since air bleeding through the cowl and out the side exhaust channels had an adverse effect on the air flow over the wing. Accordingly, to provide air flow through the cowl, the cowl air was allowed to discharge from a 3-inch-diameter hole on the underside of the fuselage. (See fig. 17.) This did not produce an appreciable flow disturbance. The air from the oil cooler and wing ducts was exhausted out the rear of the fuselage. For the stability and control tests, the oil-cooler inlet-velocity ratio was about 0.9 and the cowl inlet-velocity ratio was about 0.7.

Propeller calibrations were made at 0° angle of attack, and no corrections were applied to the thrust coefficients for differences in model attitude or configuration. Presented in figures 18 and 19 are the variations of thrust coefficient with lift coefficient and airplane velocity for various power conditions as furnished by the Ryan Aeronautical Company.

Constant power polars were obtained by testing the model throughout the angle-of-attack range at various values of T_c and cross-plotting the results for the power condition desired. Full-scale flight conditions matched in directional-stability and-control tests are listed in table II.

SYMBOLS, COEFFICIENTS, AND CORRECTIONS

All results are presented as standard NACA coefficients and are corrected for tares, tunnel-wall interference (reference 1) and stream inclination. All coefficients are referred to the wind axis with the exception of the rolling and pitching-moment coefficients C_l' and C_m', which are given about the stability axis. The coefficients used are defined as follows:

C_L lift coefficient $\left(\frac{\text{lift}}{qS}\right)$

C_D drag coefficient $\left(\frac{\text{drag}}{qS}\right)$

[1]Uncorrected for tunnel-wall effects and stream inclination.

C_Y lateral force coefficient $\left(\frac{\text{lateral force}}{qS}\right)$

C_m pitching-moment coefficient $\left(\frac{\text{pitching moment}}{qS\bar{c}}\right)$

$C_{m'}$ pitching-moment coefficient about the stability axis $\left(\frac{\text{pitching moment}}{qS\bar{c}}\right)$

C_n yawing-moment coefficient $\left(\frac{\text{yawing moment}}{qSb}\right)$

$C_{l'}$ rolling-moment coefficient about the stability axis $\left(\frac{\text{rolling moment}}{qSb}\right)$

C_{h_e} elevator hinge-moment coefficient $\left(\frac{\text{elevator hinge moment}}{qb_e\bar{c}_e^2}\right)$

C_{h_r} rudder hinge-moment coefficient $\left(\frac{\text{rudder hinge moment}}{qb_r\bar{c}_r^2}\right)$

J propeller advance ratio $\left(\frac{V}{nD}\right)$

T_c thrust coefficient $\left(\frac{\text{thrust}}{\rho V^2 D^2}\right)$

C_T thrust coefficient $\left(\frac{\text{thrust}}{\rho n^2 D^4}\right)$

C_p power coefficient $\left(\frac{\text{power}}{\rho n^3 D^5}\right)$

$1-\frac{\Delta H}{q_o}$ dynamic-pressure-recovery coefficient

P pressure coefficient $\left(\frac{\Delta p}{q_o}\right)$

where

q_o free-stream dynamic pressure ($\frac{1}{2}\rho V^2$), pounds per square foot

S wing area, square feet

$\bar{c}$ wing mean aerodynamic chord, feet

b wing span, feet

b_e elevator span, feet

$\bar{c}_e$ elevator root-mean-square chord aft of hinge line, feet

b_r rudder span, feet

$\bar{c}_r$ rudder root-mean-square chord aft of hinge line, feet

ρ mass density of air, slugs per cubic foot

V airspeed, feet per second

D propeller diameter, feet

b' propeller-blade width, feet

h propeller-blade thickness, feet

n propeller speed, revolutions per second

Δp pressure differential between the free-stream static and the local static pressures, pounds per square foot

q_L local dynamic pressure as determined by the individual rake tube readings, pounds per square foot

ΔH total head loss, pounds per square foot

In addition to the coefficients defined, the following symbols are utilized in the presentation of results:

α angle of attack of the fuselage reference line corrected for stream inclination and tunnel-wall effects, degrees

α_u uncorrected angle of attack of the fuselage reference line, degrees

ψ angle of yaw measured from the plane of symmetry, degrees

β propeller-blade angle, degrees

δ_e elevator deflection, degrees

δ_r rudder deflection, degrees

i_t tail incidence, degrees

Moment coefficients are presented about a center of gravity located at 18.3 percent of the mean aerodynamic chord aft of the wing leading edge and 2.06 percent of the mean aerodynamic chord above the fuselage reference line. This is the predicted center-of-gravity location for the airplane with wheels up and a normal gross weight of 10,450 pounds. Various center-of-gravity locations with corresponding weights of the airplane are listed in table III.

RESULTS AND DISCUSSION

Air-Flow Tests

Dynamic-pressure recovery.- The results of the dynamic-pressure-recovery tests are presented in figures 20 to 29, inclusive. Figure 20 presents data obtained with the propeller removed at several values of cowl inlet-velocity ratio with varying angle of attack. The oil-cooler inlet-velocity ratio for these tests was approximately 0.9. Variation of oil-cooler inlet-velocity ratio on the pressure recovery at the entrance to the TG-100 unit was found to be negligible. These data indicate that for the airplane at speeds above 150 miles per hour (α_u less than 4°) the effect of angle of attack on the dynamic pressure recovery will be small. For speeds below 150 miles per hour to the stall (α_u greater than 4°), the pressure recovery drops off 10 to 20 percent of the free-stream dynamic pressure. It is also noted from these data that the peak-pressure recovery of about 82 percent occurs at a cowl-inlet-velocity ratio between 0.7 and 0.8; whereas 74-percent recovery is obtained at 0.4, the inlet-velocity ratio for high-speed flight.

Presented in figure 21 is the variation of dynamic-pressure-recovery coefficient with cowl-inlet-velocity ratio for the propeller operating under conditions simulating high-speed flight. With the standard propeller, an additional 12- to 30-percent loss in dynamic pressure is obtained over that measured with the propeller removed. Since the dynamic-pressure recovery for high-speed flight ($V_i/V_o = 0.4$) with the standard propeller is only 58 percent of the free-stream dynamic pressure, the predicted high-speed performance of the airplane will be impaired considerably. Consequently blade cuffs were designed for the propeller to improve the dynamic-pressure-recovery characteristics in the cowl. Data for two

conditions of the cuffed blades are also presented in figure 21. With the cuffs installed, but with a small gap between the spinner and the base of the cuff to allow clearance for blade-angle changes, a considerable gain is experienced over results obtained with the standard propeller. Additional gain is obtained with the cuffs installed and the gap sealed making the dynamic-pressure recovery greater with the propeller on than with the propeller off. However, the peak-recovery-pressure coefficient of 0.82 occurs at an inlet-velocity ratio of 0.7, and at the high-speed inlet-velocity ratio (0.4) the dynamic-pressure-recovery coefficient is only 0.76.

To determine the effect of propeller parameters on the pressure recovery in the cowl in the high-speed flight range, measurements were taken for propeller-blade angles of 50°, 55°, and 60° at a constant thrust coefficient T_c and for various thrust coefficients at a constant blade angle. These results, summarized in figures 22 and 23, indicate that the effect of these parameters in the high-speed-flight range is minor.

Various flight conditions were investigated throughout the cowl inlet velocity and angle-of-attack range. Dynamic-pressure-recovery data for the following flight conditions are presented in the figures indicated.

Condition	Airplane velocity (mph)	Propeller blade angle (deg)	Thrust coefficient, T_c	Cowl-inlet-velocity ratio, V_i/V_o	Angle of attack (deg)	Figure number
High speed	445	55	0.01	0.4	- 1.5	21, 24
Climb	245	45	0.07	0.7	1.0	25, 26
Take-off	74	35	1.00	2.0	1.0 10.0	27, 28

For each condition investigated, a considerable gain in dynamic-pressure recovery is obtained with the propeller cuffs installed and sealed.

Figure 29 presents a summary of the dynamic-pressure-recovery data for maximum TG-100 power utilizing information presented in figures 9, 15, and 16. These data indicate that at 450 miles per hour

an additional 15-percent loss in dynamic-pressure recovery is incurred with the installation of the standard propeller over that obtained with propeller removed. The addition of the propeller cuffs with the gaps unsealed regains 11 percent of the dynamic-pressure recovery and sealing the gaps regains another 6 percent. This gives a dynamic-pressure recovery of 75 percent which is 2 percent better than that obtained with propeller removed.

It is doubtful that any further gain could be obtained utilizing the pumping action of the cuffs at the high-speed blade angles. However, the peak recovery pressure (as shown in fig. 22) occurs at an inlet-velocity ratio of approximately 0.7 and the high-speed inlet-velocity ratio for the existing cowl is 0.4. Since it is more important to have a high pressure recovery for high-speed flight, better pressure-recovery characteristics throughout the high-speed flight range may be obtained by increasing the cowl velocity ratio at a given airplane velocity. It is believed that by reducing the cowl-entrance area, thus increasing the inlet-velocity ratios, an increase in dynamic-pressure recovery may be obtained for the high-speed flight condition with the cuffed propeller sealed. Estimated values for a 40-percent reduction of entrance area, not considering any change in internal ducting efficiency, are shown in figure 29 for the propeller with sealed cuffs.

It should be pointed out that the cuff developed for these tests has a high thickness ratio at the spinner surface ($h/b' = 0.32$) which is the minimum possible because of the propeller-shank thickness. In high-speed flight, greater pressure losses than those indicated by the data are expected because the flow Mach number at the cuff will exceed the critical value for the cuff sections. Therefore, a propeller design with thinner root sections should be considered.

Cowl pressure distribution.- The pressure-distribution data are presented in the form of pressure coefficient versus distance[2] in inches from the cowl leading edge. The term "pressure coefficient" is defined as $\Delta p/q_o$ where Δp is the pressure differential between the free-stream static pressure and the local static pressure, and q_o is the free-stream dynamic pressure. The pressure coefficient

[2]This distance is measured normal to the plane of the cowl leading edge with distances toward the tail considered positive and those toward the nose considered negative.

is negative when the local static pressure is less than the free-stream static pressure.

In the presentation of the data, the cowl is divided into six sections as follows (fig. 10):

1. Upper center line, tubes 54 to 57 and 123 to 135.

2. Lower center line, tubes 86 to 101.

3. Spinner fairing, upper, tubes 65 to 74.

4. Spinner fairing, lower, tubes 58 to 64.

5. Oil-cooler fillet, tubes 102 to 122.

6. Oil cooler, upper center line, tubes 49 to 53 and 75 to 85.

The flagged symbols, as used in the presentation of results, indicate the pressure coefficients of the internal surfaces.

Pressure-distribution data for the model in various configurations and power conditions are presented in figures 30 to 35, inclusive. Figure 30 presents the effect of cowl inlet-velocity ratio on the pressure distribution over the various sections of the cowl with the propeller removed at -1.5° angle of attack. All external pressure distributions appear to be satisfactory with the exception of a pressure peak over the oil-cooler fillet leading edge. This is due to a flat spot (fig. 13) at the leading edge of the juncture of the oil-cooler duct and the cowl. No attempt was made to alleviate this pressure peak as the model is not an exact duplicate of the prototype airplane at this point. The high negative pressure coefficients occurring on the interior of the ducts at high inlet-velocity ratios are not detrimental to flow over the external surfaces. Figure 31 presents the effect of the variation of oil-cooler inlet-velocity ratio with propeller off, a cowl inlet velocity of 0.4, and -1.5° angle of attack.

The effect of various propeller modifications (figs. 5, 6, and 7) is presented in figure 32 for the model in the high-speed condition ($\beta = 55^\circ$, $T_c = 0.01$, $V_i/V_o = 0.4$, and $\alpha_u = -1.5^\circ$). These data indicate that the effect on the external surfaces is small, while, for the internal surfaces, the installation of the sealed cuffs increases the pressure coefficient positively, resulting in a favorable reduction in internal recovery losses.

The effects of angle of attack and cowl-inlet-velocity ratio on pressure distribution are presented in figures 33 and 34, respectively, for the model in the high-speed condition with sealed, cuffed propeller. These data show no undesirably high pressure peaks. The effect of small variations of cowl inlet velocity on external pressure distribution is negligibly small, while, internally, the pressure coefficient decreases with increase in inlet-velocity ratio.

Presented in figure 35 is a comparison of the pressure distributions for the model in the high-speed, climb, and take-off conditions. These data were obtained for the propeller with sealed cuffs.

Velocity distribution.- Velocity-distribution studies at the simulated entrance to the TG-100 gas turbine were made for various model configurations and flight conditions. The results for the high-speed, climb, and take-off conditions for various propeller configurations are presented in table IV in the form of local dynamic-pressure coefficients at the various tube locations of the pressure-measuring rake. The local dynamic-pressure coefficient q_L/q_o is defined as the ratio of the local dynamic pressure to the free-stream dynamic pressure. The local dynamic pressure was determined from the local total pressure indicated by the individual total-pressure tubes and the average static pressure in the duct as indicated by an average of the four static pressure tubes.

Aerodynamic characteristics in pitch.- The longitudinal aerodynamic characteristics of the Ryan XF2R model with various configurations are presented in figures 36 to 42, inclusive.

Figures 36 and 37 present the effect of power on the characteristics of the model with flaps deflected 40°, gear extended, and with flaps and gear retracted. Predicted variations of the stick-fixed neutral-point[3] location with lift coefficient (determined from figs. 36 and 37) are presented in figures 38 and 39 for various power conditions, flaps and gear deflected and retracted. Figure 38 indicates that the airplane with flaps deflected 40° and gear extended will be stable in the landing condition ($T_c = 0$) and in the approach condition with 40-percent maximum power but will only be marginally stable at lift coefficients above 1.0 with maximum power at the most aft center-of-gravity location. As indicated in figure 39, the

[3]Computed by method of reference 2.

airplane will be stable in the glide condition ($T_c = 0$) with flaps and gear retracted, but only marginally stable with maximum continuous power at the most aft center-of-gravity location for lift coefficients above 0.6. Above $C_L = 1.1$ (fig. 38) and $C_L = 0.6$ (fig. 39), an aft movement of the neutral point was noted for the respective conditions. This rearward shift in neutral point is probably due to the change in downwash associated with the slight reduction in the lift-curve slope for these conditions. It is possible that the reduction in lift-curve slope and hence the aft movement of the neutral point may not occur for the airplane at full-scale Reynolds number.

The effect of elevator deflection on the aerodynamic characteristics is presented in figures 40 and 41 for the model in the flaps 40°, gear-extended, and in the flaps- and gear-retracted conditions, respectively. These data were obtained with the normal horizontal tail incidence of 1.5° and at zero thrust coefficient. Also shown in figure 41 is the effect of the removal of the propeller cuffs. Presented in figure 42 is the effect of elevator deflection on the aerodynamic characteristics of the model with flaps deflected 40°, gear extended, horizontal-tail incidence at 6.4°, and at zero thrust coefficient. The increase in tail incidence approximates the change in angle of attack of the tail in the presence of the ground. These figures indicate that the airplane should possess adequate elevator control for the normal center-of-gravity location. It is estimated[4] that approximately 25° up-elevator deflection is required for landing with the center of gravity located at 18.3 percent M.A.C. The elevator hinge moments are not applicable in the computation of stick forces for the airplane as the elevator balance seal of the XF2R was not duplicated on the 1/5-scale model.

Aerodynamic characteristics in yaw.- The directional, lateral, and longitudinal characteristics of the model in yaw are presented in figures 43 to 48, inclusive. Data for the high-speed, climb, and glide conditions[5] were obtained with a propeller-blade angle of 45° and the model with flaps and gear retracted; whereas data for the power-off approach, the power-on approach, and the wave-off conditions were obtained with a propeller-blade angle of 35° and with flaps and gear extended. Two blade-angle settings were used to simplify testing, as exact simulation of the variable-pitch-propeller conditions

[4]By method of reference 3

[5]See table II for matched power conditions.

through the speed range would require a different blade-angle setting for each power condition.

The directional characteristics of the model in the high-speed condition are presented in figure 43(a). The data indicate a low value for the directional stability of the XF2R airplane. The static directional-stability parameter $dC_n/d\psi$ is -0.00065 as compared with -0.00165 for the FR-1 airplane. (See reference 4.) Also shown is the effect of propeller cuff removal, which increased $dC_n/d\psi$ to -0.00085, yielding a net gain of -0.0002. Figure 44(a) presents the directional characteristics of the model in a simulated maximum power climb. The occurrence of a rudder-pedal-force reversal[6] is evident for the airplane at positive angles of yaw. The data also indicate that the airplane does not balance with more than 18° left rudder and 22° right rudder for the yaw range investigated. Presented in figure 45(a) are the directional characteristics of the model in the simulated glide condition which appears marginally satisfactory.

The directional characteristics of the model for the power-off approach, the power-on approach, and the wave-off conditions are presented in figures 46(a), 47(a), and 48(a), respectively. A lightening of the pedal force beyond 30° right rudder is noticed for the power-off approach condition. For the power-on approach, the data indicate that the airplane will not balance with more than 17° left rudder and 33° right rudder. Figure 48(a) shows that the airplane will not balance beyond 8° left rudder in the wave-off condition.

The angle of left sideslip available $\Delta\beta_L$ beyond the angle of sideslip for wings level $C_Y = 0 = C_n$ and the incremental yawing-moment coefficient available ΔC_n at the angle of sideslip for wings level can be used as an indication of the rudder control existing for the critical power-on approach and wave-off conditions of figures 47 and 48. Marginal, if not inadequate, rudder control is available for the airplane in both these flight conditions. A comparison of the rudder control available for the XF2R airplane and the FR-1 airplane (obtained from reference 4) under similar

---

[6]Indicated by the variation of C_{h_r} with ψ at $C_n = 0$.

---

flight conditions is given in the following table:

Airplane	Rudder deflection (deg)	Power-on approach condition		Wave-off condition	
		$\Delta\beta_L$ (deg)	ΔC_n	$\Delta\beta_L$ (deg)	ΔC_n
XF2R	-35	4.1	0.016	1.0	0.004
	-30	3.6	0.012	0.6	-0.003
FR-1	-30	6.5	0.017	2.6	0.010

As indicated by the preceding data, the airplane will possess unsatisfactory directional-stability and -control characteristics. It is believed that the installation of a considerably larger dorsal fin will improve the directional characteristics of the airplane in the various power conditions.

Lateral-stability characteristics of the model in the high-speed, climb, and glide conditions are presented in figures 43(b), 44(b), and 45(b). As indicated by these data, the airplane will possess positive lateral stability in these conditions. For the high-speed condition, the parameter $dC_l'/d\psi$ is 0.0012 as compared to 0.0014 for the FR-1 airplane. (See reference 4.) Presented in figures 46(b), 47(b), and 48(b) are the lateral-stability characteristics of the model in the power-off approach, the power-on approach, and the wave-off conditions. Lateral instability is revealed for the power-on-approach and wave-off conditions. The following table includes a tabulated comparison of $dC_l'/d\psi$ for the XF2R and FR-1 airplanes.

Flight condition	$\partial C_l'/\partial\psi$	
	XF2R	FR-1
Power-off approach	0.0013	0.0010
Power-on approach	-0.0001	-0.0001
Wave-off	-0.0012	-0.0011

CONCLUSIONS

The following aerodynamic characteristics are revealed by these tests on the 1/5-scale model of the Ryan XF2R airplane:

Air-Flow Tests

1. Poor dynamic pressure recovery (58 percent) for the cowl duct is indicated for the model in the high-speed condition with the standard propeller. A gain of 17 percent in pressure recovery is realized with the installation of the propeller with sealed cuffs.

2. The peak dynamic-pressure recovery (82 percent) occurs at an inlet-velocity ratio of approximately 0.7 for the propeller with sealed cuffs. Since the high-speed inlet-velocity ratio is about 0.4 for the existing cowl, it is believed that some increase in dynamic-pressure recovery may be obtained by increasing the inlet-velocity ratio at a given airplane velocity.

3. Pressure distribution over various parts of the cowl investigated appears to be satisfactory.

Stability and Control Tests

1. Marginal stick-fixed static longitudinal stability

2. Adequate elevator control

3. Low directional stability ($dC_n/d\psi$) is -0.00065 for high-speed condition.)

4. Rudder-pedal-force reversal in climb condition

5. Inadequate rudder control in the power-on approach and wave-off conditions

6. Negative dihedral effect in the power-on approach and wave-off conditions

Ames Aeronautical Laboratory,
National Advisory Committee for Aeronautics,
Moffett Field, Calif.

APPENDIX A

Physical Characteristics of the Ryan XF2R-1 Airplane
[All dimensions are full scale.]

General	
Design gross weight, lb	10,450
Overload gross weight, lb	12,563
Fuel	
Normal, gal	180
Maximum (including external tanks), gal	480
Wing Dimensions	
Airfoil section description	
Root	NACA 65,2-117, a = 1.0
Tip	NACA 65,2-115, a = 0.5
Total wing area, sq ft	275
Chord	
Root, in.	112
Tip, in.	56
Mean aerodynamic, in.	87.55
Span, ft	40
Incidence at root, deg	1
Twist, deg	0
Dihedral	
Center section, deg	0

Outer panel, deg	7½
Sweepback of leading edge, deg	0

Horizontal Tail

Airfoil section	NACA 65,2-015 (modified)
Span,	17 ft 6 in.
Aera, sq ft	68.85
Aspect ratio	4.45
Taper ratio	1.5:1
Elevators	
Span (each), ft	7.85
Chord	
Percent stabilizer chord,	35
Root-mean-square, ft	1.365
Area, sq ft	20.84
Balance	
Type	sealed internal
Chord (percent elevator chord)	45 (approx.)
Angular displacement	
Down, deg	12.5
Up, deg	27.5
Total, deg	40.0

Vertical Tail

Airfoil section	NACA 63,2-012 (modified)

Span, ft	6.792
Area, sq ft	31.85
Aspect ratio	1.45
Taper ratio	2.83:1
Rudder	
Span, ft	5.98
Chord	
Percent fin chord,	28 to 48.3
Root-mean-square, ft	1.490
Area, sq ft	8.69
Balance	
Type	Overhanging
Chord (percent rudder chord)	27.9
Angular displacement, deg	30
Aileron	
Type	Internal sealed balance
Span, ft	7.46
Chord (aft hinge line), percent wing chord	17
Area (aft of hinge line), sq ft	12.8
Flaps	
Type	NACA single-slotted flap
Chord	25-percent wing chord
Span of inner flap	4 ft $6\frac{1}{2}$ in.

Span of outer flap	4 ft 8½ in.
Total area, sq ft	30.25
Travel, deg	40

Landing gear

Type	Retractable tricycle
Ground angle of thrust line, deg	1

Power plant

Forward engine	General Electric TG-100 gas turbine
Gear ratio	0.0881
Rear engine	General Electric I-16 (centrifugal compressor type J.P.M.)

Propeller

Type	Aeroproducts
Hub	A542-X
Blade	H-20-156-28M
Number of blades	Four
Diameter	10 ft 8 in.
h/b at 0.75R	0.0712
Activity factor	137.4

APPENDIX B

CONFIGURATION KEY

1/5-SCALE MODEL OF THE RYAN XF2R AIRPLANE

W	Wing (with duct entrances)
B	Bare fuselage
K	Cockpit enclosure
X_w	Wing fillets
X_t	Tail fillets
H	Horizontal tail with internal-sealed-balance elevators
V	Vertical tail
f_D	Dorsal fin
F^o	0° flap deflection
F^{40}	40° flap deflection
S	Standard configuration = $WBKX_wHVX_tf_DF^o$
G	Tricycle landing gear down
E_X	Exit pipe(TG-100 unit)
P	Standard propeller
P^1	Propeller + cuffs (unsealed)
P^2	Propeller + cuffs (sealed)

REFERENCES

1. Swanson, Robert S., and Schuldenfrei, Marvin J.: Jet-Boundary Corrections to the Downwash Behind Powered Models in Rectangular Wind Tunnels with Numerical Values for 7- by 10-Foot Closed Wind Tunnels. NACA ARR, Aug. 1942.

2. Schuldenfrei, Marvin: Some Notes on the Determination of the Stick-Fixed Neutral Point From Wind-Tunnel Data. NACA RB No. 3I20, 1943.

3. Katzoff, S., and Sweberg, Harold H.: Ground Effect on Downwash Angles and Wake Location. NACA Rep. No. 738, 1943.

4. Sacks, Alvin H.: Wind-Tunnel Investigation of a 1/5-Scale Model of the Ryan XFR-1 Airplane with Various Modifications. (TED No. 2370) NACA CMR No. A6J18, 1946.

TABLE I.- PROPELLER-BLADE CUFF ORDINATES,
RYAN XF2R AIRPLANE
[Radius station (r/R) = 0.1875]

Station (Percent chord)	Station (Percent chord)
0	0
2.5	4.80
5.0	6.56
10.0	9.00
20.0	12.14
30.0	14.00
40.0	14.82
50.0	15.00
60.0	14.04
70.0	12.00
80.0	8.83
90.0	4.80
95.0	2.60
100.0	0
T.E. radius = 0.5.	

Cuff ordinates match blade ordinates at radius station (r/R) = 0.375.

Cuff contour formed of straight constant percent chord lines between radius stations 0.1875 and 0.375.

TABLE II.- TEST CONDITIONS FOR DIRECTIONAL CHARACTERISTICS OF THE 1/5-SCALE MODEL OF THE RYAN XF2R AIRPLANE

Full-Scale Airplane Conditions [1]						Model Conditions						
Attitude	Airspeed at S. L. (mph)	Power	Flaps and gear	C_L	T_c	α_u	C_L	T_c	β	Propeller speed (rpm)	q_o (lb/sq ft)	Fig. No.
High-speed	450	Military and J.P.M.[2]	Retracted	0.075	0.013	-1	0.09	0	45	2000	40.5	43
Climb	156	Military	Retracted	.61	.22	5	.73	.22	45	4000	33.0	44
Glide	116	Zero thrust	Retracted	1.11	0	10	1.11	0	45	2000	40.5	45
Approach	99.6	Zero thrust	Flaps 40° and gear extended	1.50	0	8	1.50	0	35	2400	28.7	46
	95.2	40% maximum	Flaps 40° and gear extended	1.64	.4	8	1.63	.4	35	5000	25.0	47
Wave-off	94.8	Take-off	Flaps 40° and gear extended	1.66	.69	8	1.72	.69	35	5000	16.0	48

[1]Based on design gross weight of 10,450 pounds.
[2]Jet-propulsion motor.

TABLE III.- WEIGHTS AND CORRESPONDING CENTER-OF-GRAVITY LOCATIONS FOR THE RYAN XF2R AIRPLANE

Condition	Weight (lb)	Wheels down			Wheels up		
		Horizontal c. g.		Vertical c.g.	Horizontal c.g.		Vertical c.g.
		[1] Aft of station 0 (in.)	Percent M.A.C.	From fuselage H.R.L.[2] (in.)	[1] Aft of station 0 (in.)	Percent M.A.C.	From fuselage H.R.L.[2] (in.)
Weight empty	8324	122.0	14.8	0	123.0	16.0	1.5
Light weight most forward center-of-gravity	9309	121.5	14.3	-.30	122.0	14.8	1.10
Light weight most aft center-of-gravity	10,150	126.0	19.4	1.0	126.5	20.0	2.3
Normal gross weight	10,450	124.70	17.94	.60	125.0	18.30	1.80
Overload gross weight 1-100 gallon auxiliary tank	11,151	- - -	- - -	- - -	126.0	19.4	-2.00

[1] Station 0 is 109 inches forward of the leading edge of the outer panel.

[2] Horizontal reference line is the same as the thrust line of model FR-1.

TABLE IV.- LOCAL DYNAMIC PRESSURE COEFFICIENTS AT THE SIMULATED ENTRANCE TO THE TG-100 GAS TURBINE. 1/5-SCALE MODEL OF THE RYAN XF2R AIRPLANE.

Flight condition	High speed			Climb			Take - off					
Propeller config.	Off	Standard	Cuffed, sealed	Off	Standard	Cuffed, sealed	Off	Standard	Cuffed, sealed	Off	Standard	Cuffed, sealed
β	---	55	55	---	45	45	---	35	35	---	35	35
T_c	---	0.01	0.01	---	0.07	0.07	---	1.0	1.0	---	1.0	1.0
q_o	40.5	42.3	35.5	40.5	41.7	42.9	10.4	10.0	4.2	10.4	10.2	4.0
V_i/V_o	0.40	0.39	0.40	0.71	0.69	0.69	1.96	2.00	1.95	1.94	1.98	1.99
α_u	-1	-1.5	-1.5	2	2	2	1	1	1	10	10	10
Tube no.	q_L/q_o	q_L/q_o	q_L/q_o	q_L/q_o	q_L/q_o	q_L/q_o	q_L/q_o	q_L/q_o	q_L/q_o	q_L/q_o	q_L/q_o	q_L/q_o
1	0.293	0.300	0.283	1.063	0.846	0.988	7.96	8.12	7.99	6.72	7.60	8.56
3	.238	.315	.306	.896	.900	.826	7.90	7.90	7.45	7.70	7.72	7.99
4	.202	.290	.254	.668	.841	.759	7.96	7.92	7.35	7.98	7.80	8.04
5	.314	.329	.363	.966	.866	.869	6.71	7.38	7.16	6.84	7.32	7.58
6	.218	.300	.283	.845	.826	.774	7.84	7.60	7.06	7.88	7.52	7.66
7	.319	.339	.387	.956	.846	.855	6.88	7.36	6.96	7.23	7.44	7.42
8	.238	.315	.300	.865	.816	.778	7.58	7.43	6.91	7.70	7.48	7.53
9	.319	.344	.387	.926	.841	.869	6.35	7.30	7.16	6.76	7.52	7.42
10	.228	.320	.300	.814	.792	.759	7.02	7.26	6.96	7.50	7.46	7.38
11	.349	.358	.415	.946	.836	.869	6.71	7.39	6.96	7.08	7.48	7.17
12	.243	.329	.306	.825	.786	.754	7.42	7.32	6.82	7.70	7.50	7.22
13	.354	.358	.410	.956	.806	.874	6.49	7.36	7.11	6.97	7.24	7.17
15	.369	.358	.410	.966	.826	.874	6.47	7.51	7.26	6.88	7.32	7.22
16	.233	.329	.294	.865	.742	.726	7.06	7.47	6.91	7.51	7.46	7.12
17	.374	.344	.410	1.027	.831	.907	7.20	7.76	7.30	7.34	7.44	7.27
18	.233	.320	.300	.830	.776	.730	7.88	7.72	6.96	7.86	7.66	7.17
19	.299	.329	.352	1.022	.826	.821	5.33	7.53	6.57	7.66	7.42	7.32
20	.192	.305	.288	.800	.767	.678	7.75	7.51	6.42	7.62	7.50	6.81
21	.218	.334	.311	.814	.846	.759	6.81	7.65	7.50	6.64	7.34	7.22
22	.187	.281	.254	.602	.742	.635	7.33	7.37	6.66	7.31	7.24	6.65
23	.283	.328	.329	1.017	.850	.836	7.98	7.84	5.10	7.50	6.92	4.43
24	.253	.295	.271	.890	.757	.654	7.36	7.02	4.90	7.00	6.20	4.43
25	.329	.290	.329	1.083	.944	.888	7.98	8.06	7.79	8.00	8.14	8.35
27	.354	.300	.306	1.047	.895	.883	6.61	7.47	7.06	7.74	7.76	7.68
28	.197	.266	.265	.774	.816	.754	7.94	7.72	7.06	7.90	7.60	7.53
29	.364	.281	.329	.794	.875	.888	6.06	7.30	7.11	5.68	7.52	7.84
30	.278	.257	.260	.936	.836	.778	7.57	7.47	6.96	6.52	7.56	7.58
31	.374	.281	.311	1.043	.914	.917	7.58	7.63	7.16	7.18	7.62	7.78
32	.248	.247	.265	.865	.816	.754	7.67	7.37	6.76	7.15	7.28	7.27
33	.293	.295	.277	.921	.885	.826	6.78	7.33	6.82	6.21	7.20	7.89
34	.263	.271	.260	.941	.866	.774	7.20	7.49	6.86	7.17	7.26	5.78
35	.304	.286	.283	.840	.856	.878	6.39	6.76	4.56	6.95	6.08	4.38
36	.319	.257	.300	1.012	.895	.682	7.94	6.41	3.97	7.93	4.78	2.78
37	.395	.257	.335	1.083	.924	1.026	7.94	8.08	8.04	7.80	8.16	9.13
39	.258	.290	.277	.774	.895	.916	6.81	7.36	7.26	6.15	7.32	8.20
40	.248	.242	.231	.966	.836	.798	7.26	7.10	6.82	6.50	6.82	7.58
41	.395	.271	.283	1.027	.900	.964	6.62	7.45	7.31	6.48	7.30	7.58
42	.258	.232	.225	.900	.846	.840	7.37	7.43	7.06	6.64	7.12	7.73
43	.369	.252	.260	1.083	.954	.978	7.14	7.67	7.45	6.64	7.66	7.84
44	.207	.213	.219	.779	.816	.788	7.64	7.36	6.76	7.38	7.30	7.42
45	.319	.261	.237	.976	.930	.874	7.04	7.51	6.86	7.42	7.64	7.94
46	.177	.223	.213	.845	.856	.783	7.92	7.71	7.31	8.00	7.70	8.40
47	.304	.242	.207	1.087	.964	.998	8.00	7.92	6.08	8.00	8.00	8.40
48	.253	.213	.167	1.022	.920	.893	7.76	7.38	5.98	7.97	7.70	7.32

NOTE: Tubes 2, 14, 26, and 38 are static tubes.

FIGURE LEGENDS

Figure 1.– Three-view drawing of the Ryan XF2R airplane. (Full-scale airplane dimensions.)

Figure 2.– Front view of 1/5-scale model of the Ryan XF2R airplane mounted in the Ames 7- by 10-foot wind tunnel for the cowl-duct investigation.

Figure 3.– Front view of the 1/5-scale model of the Ryan XF2R airplane with 40° flap deflection and landing gear extended.

Figure 4.– Rear view of the 1/5-scale model of the Ryan XF2R airplane with flaps and landing gear retracted.

Figure 5.– Standard propeller on the 1/5-scale model of the Ryan XF2R airplane.

Figure 6.– Propeller with cuffs unsealed on the 1/5-scale model of the Ryan XF2R airplane.

Figure 7.– Propeller with cuffs sealed on the 1/5-scale model of the Ryan XF2R airplane.

Figure 8.– Geometric characteristics of the aeroproducts H-20-156-28 propeller on the Ryan XF2R airplane.

Figure 9.– Aerodynamic characteristics of the aeroproducts H-20-156-28 propeller as determined on the 1/5-scale model of the Ryan XF2R airplane for maximum power output of the TG-100 unit.

Figure 10.– Pressure-tube locations. 1/5-scale model of the Ryan XF2R airplane.

Figure 11.– Tube locations of the pressure rake in the simulated entrance to the TG-100 gas turbine. 1/5-scale model of Ryan XF2R-airplane.

Figure 12.– Pressure orifices atop spinner fairing and cowl. 1/5-scale model of the Ryan XF2R airplane.

Figure 13.– Pressure orifices on lower side of spinner fairing and oil cooler on the 1/5-scale model of the Ryan XF2R airplane.

Figure 14.- Pressure orifices in the oil-cooler fillet. 1/5-scale model of Ryan XF2R airplane.

Figure 15.- Variation of cowl inlet-velocity ratio with free-stream velocity for the Ryan XF2R airplane. (Obtained from Ryan Aeronautical Company).

Figure 16.- Variation of lift coefficient with uncorrected angle of attack for the 1/5-scale model of the Ryan XF2R airplane.

Figure 17.- Detail view of the 1/5-scale model of the Ryan XF2R airplane showing the 3-inch-diameter hole used for discharging air from the cowl.

Figure 18.- Predicted variations of the lift coefficient with thrust coefficient of the Ryan XF2R airplane with various power conditions. (Normal gross weight = 10,450 lb).

Figure 19.- Predicted variations of the thrust coefficient with velocity of the Ryan XF2R airplane at various power conditions.

Figure 20.- Variation of the Dynamic-pressure-recovery coefficient, at the entrance to the TG-100 unit, with angle of attack for various cowl-inlet-velocity ratios with propeller off. 1/5-scale model of the Ryan XF2R airplane. (a) V_i/V_o = 0 to 0.8.

Figure 20.- Concluded. (b) V_i/V_o = 1.0 to 1.8.

Figure 21.- Variation of dynamic-pressure-recovery coefficient, at the entrance to the TG-100 unit, with cowl inlet-velocity ratio for the various propeller modifications. Simulated high-speed conditions.

Figure 22.- Effect of Propeller-blade angle on the variation of dynamic-pressure-recovery coefficient at the entrance to the TG-100 unit, with cowl-inlet-velocity ratio for various propeller modifications.

Figure 23.- Effect of propeller thrust coefficient on the variation of dynamic-pressure-recovery coefficient, at the entrance to the TG-100 unit, with cowl-inlet-velocity ratio for various propeller modifications.

Figure 24.- Variation of dynamic-pressure-recovery coefficient, at the entrance to the TG-100 unit, with angle of attack for various cowl-inlet-velocity ratios and propeller modifications. Simulated high-speed conditions.

Figure 25.– Variation of dynamic–pressure–recovery coefficient, at the entrance to the TG–100 unit, with cowl–inlet–velocity ratio for various propeller modifications. Simulated climb conditions.

Figure 26.– Variation of dynamic–pressure–recovery coefficient, at the entrance to the TG–100 unit, with angle of attack for various propeller modifications. Simulated climb conditions.

Figure 27.– Variation of dynamic–pressure–recovery coefficient, at the entrance to the TG–100 unit, with cowl–inlet–velocity ratio for various propeller modifications. Simulated take–off conditions.

Figure 28.– Variation of dynamic–pressure–recovery coefficient, at the entrance to the TG–100 unit, with angle of attack for various cowl–inlet–velocity ratios and propeller modifications. Simulated take–off conditions.

Figure 29.– Variation of dynamic–pressure–recovery coefficient, at the entrance to the TG–100 unit, with airplane velocity as determined on a 1/5–scale model of the XF2R airplane maximum TG–100 power.

Figure 30.– Effect of variation of cowl–inlet–velocity ratio, power–off, $\alpha_u = -1.5^\circ$, for the 1/5–scale model of the Ryan XF2R airplane. (a) Upper center line.

Figure 30.– Continued. (b) Lower center line.

Figure 30.– Continued. (c) Spinner fairing, upper. (d) Spinner fairing, lower.

Figure 30.– Concluded. (e) Oil–Cooler fillet. (f) Oil cooler, upper center line.

Figure 31.– Effect of variation of oil–cooler inlet–velocity ratio, propeller off, $V_i/V_o = 0.4$, $\alpha_u = -1.5^\circ$ for the 1/5–scale model of the Ryan XF2R airplane. (a) Lower center line. (b) Spinner fairing, lower.

Figure 31.– Concluded. (c) Oil–cooler fillet. (d) Oil cooler, upper center line.

Figure 32.– Effect of propeller modification with $\beta = 55^\circ$, $T_c = 0.01$, $V_i/V_o = 0.4$, $\alpha_u = -1.5^\circ$, for the 1/5–scale model of the Ryan XF2R airplane. (a) Upper center line. (b) Lower center line.

Figure 32.– Continued. (c) Spinner fairing, upper. (d) Spinner fairing, lower.

Figure 32.– Concluded. (e) Oil-cooler fillet. (f) Oil cooler, upper center line.

Figure 33.– Effect of variation of angle of attack, $V_j/V_o = 0.4$, $T_c = 0.01$, $\beta = 55^\circ$ cuffs sealed for the 1/5-scale model of the Ryan XF2R airplane. (a) Upper center line. (b) Lower center line.

Figure 33.– Continued. (c) Spinner fairing, upper. (d) Spinner fairing, lower.

Figure 33.– C oncluded. (e) Oil-cooler fillet. (f) Oil cooler, upper center line.

Figure 34.– Effect of the variation of cowl inlet-velocity ratio, $\beta = 55^\circ$ with cuffs sealed, $T_c = 0.01$, $\alpha_u = -1.5^\circ$, for the 1/5-scale model of the Ryan XF2R airplane. (a) Upper center line. (b) Lower center line.

Figure 34.– Continued. (c) Spinner fairing, upper. (d) Spinner fairing, lower.

Figure 34.– Concluded. (e) Oil-cooler fillet. (f) Oil cooler, upper center line.

Figure 35.– Pressure distribution for the high speed, climb, and take-off conditions with the propeller with sealed cuffs. 1/5-scale model of the Ryan XF2R airplane. (a) Upper center line. (b) Lower center line.

Figure 35.– Contined. (c) Spinner fairing, upper. (d) Spinner fairing, lower.

Figure 35.– Concluded. (e) Oil-cooler fillet. (f) Oil Cooler, upper center line.

Figure 36.– Effect of power on the aerodynamic characteristics of the 1/5-scale model of the Ryan XF2R airplane. Flaps 40° gear extended, elevator deflections 0° and -10°. (a) C_L vs α.

Figure 36.– Concluded. (b) C_L vs C_m, C_{h_e}.

Figure 37.– Effect of power on the aerodynamic characteristics of the 1/5-scale model of the Ryan XF2R airplane. Flaps and gear retracted. Elevator deflections 0° and -5°. (a) C_L vs α.

Figure 37.– Concluded. (b) C_L vs C_m, C_{h_e}.

Figure 38.– Predicted variation of stick-fixed neutral-point location with lift coefficient. Ryan XF2R airplane with flaps at 40° and gear extended.

Figure 39.– Predicted variation of stick-fixed neutral-point location with lift coefficient. Ryan XF2R airplane with flaps and gear retracted.

Figure 40.– Effect of elevator deflection on the aerodynamic characteristics of the 1/5-scale model of the Ryan XF2R airplane. Flaps deflected 40° and gear extended. Horizontal-tail incidence = 1.5°. $T_c = 0$.

Figure 41.– Effect of elevator deflection on the aerodynamic characteristics of the 1/5-scale model of the Ryan XF2R airplane. Flaps and gear retracted. Horizontal-tail incidence = 1.5°. $T_c = 0°$.

Figure 42.– Effect of elevator deflection on the aerodynamic characteristics of the 1/5-scale model of the Ryan XF2R airplane. Flaps deflected 40° and gear extended. Horizontal-tail incidence = 6.4°. $T_c = 0°$.

Figure 43.– Aerodynamic characteristics of the 1/5-scale model of the Ryan XF2R airplane in yaw. High-speed condition with flaps and gear retracted. (a) C_n, C_{h_r} vs ψ.

Figure 43.– Continued. (b) C_l', C_Y vs ψ.

Figure 43.– Concluded. (c) C_L, C_D, C_m' vs ψ.

Figure 44.– Aerodynamic characteristics of the 1/5-scale model of the Ryan XF2R airplane in yaw. Climb condition with flaps and gear retracted. (a) C_n, C_{h_r} vs ψ.

Figure 44.– Continued. (b) C_l', C_Y vs ψ.

Figure 44.– Concluded. (c) C_L, C_D, C_m' vs ψ.

Figure 45.- Aerodynamic characteristics of the 1/5-scale model of the Ryan XF2R airplane in yaw. Glide condition with flaps and gear retracted. (a) C_n, C_{h_r} vs ψ.

Figure 45.- Continued. (b) C_l', C_Y vs ψ.

Figure 45.- Concluded. (c) C_L, C_D, C_m' vs ψ.

Figure 46.- Aerodynamic characteristics of the 1/5-scale model of the Ryan XF2R airplane in yaw. Power-off approach condition with flaps deflected 40° and gear extended. (a) C_n, C_{h_r} vs ψ.

Figure 46.- Continued. (b) C_l', C_Y vs ψ.

Figure 46.- Concluded. (c) C_L, C_D, C_m' vs ψ.

Figure 47.- Aerodynamic characteristics of the 1/5-scale model of the Ryan XF2R airplane in yaw. Power-on approach condition with flaps deflected 40° and gear extended. (a) C_n, C_{h_r} vs ψ.

Figure 47.- Continued. (b) C_l', C_Y vs ψ.

Figure 47.- Concluded. (c) C_L, C_D, C_m' vs ψ.

Figure 48.- Aerodynamic characteristics of the 1/5-scale model of the Ryan XF2R airplane. Wave-off condition with flaps deflected 40° and gear extended. (a) C_n, C_{h_r} vs ψ.

Figure 48.- Continued. (b) C_l', C_Y vs ψ.

Figure 48.- Concluded. (c) C_L, C_D, C_m' vs ψ.

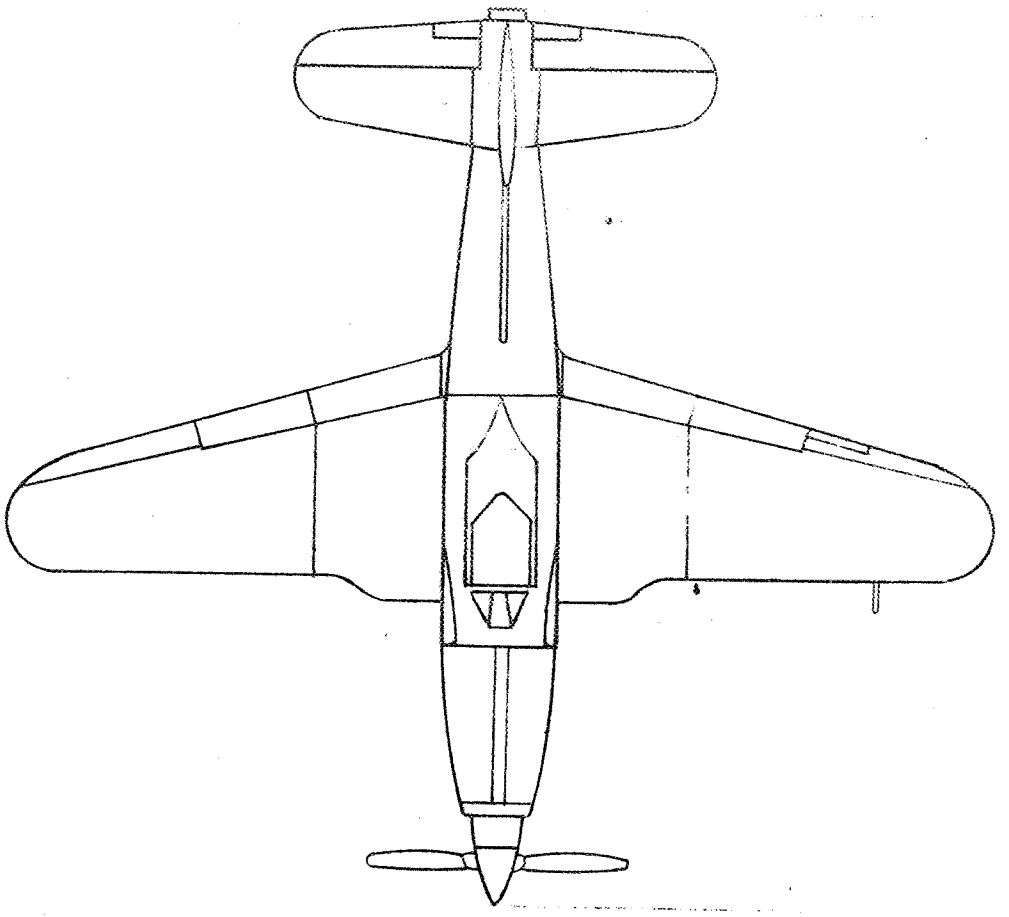

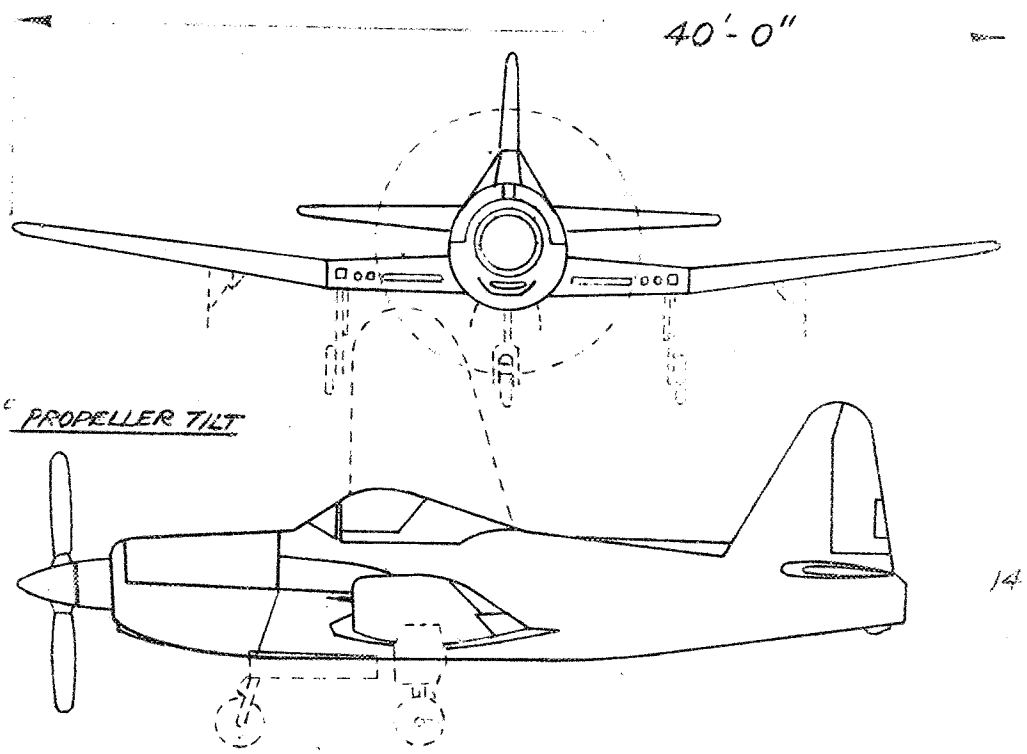

FIGURE 1.- THREE-VIEW DRAWING OF THE RYAN XFR-1 AIRPLANE. (FULL-SCALE AIRPLANE - U.S. Navy)

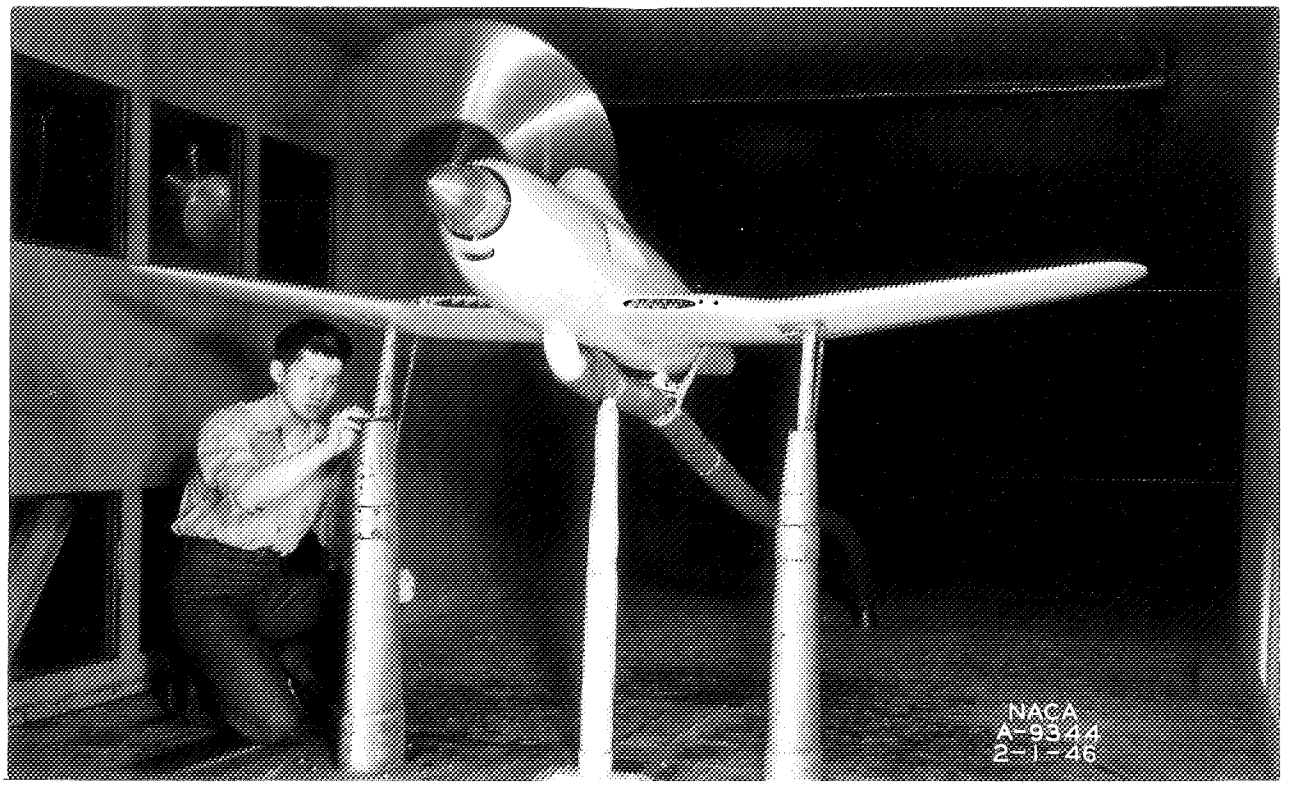

Figure 2.- Front view of 1/5-scale model of the Ryan XF2R airplane mounted in the Ames 7- by 10-foot wind tunnel for the cowl-duct investigation.

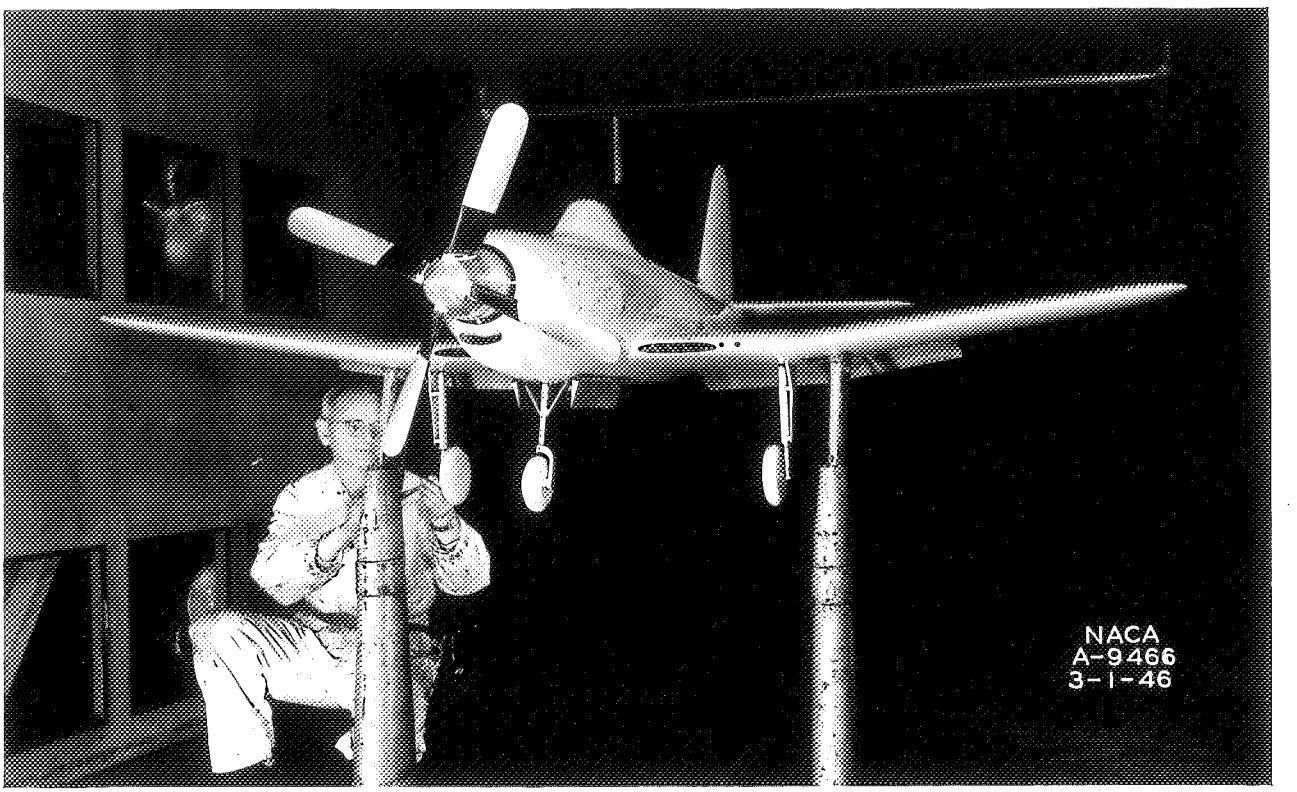

Figure 3.- Front view of the 1/5-scale model of the Ryan XF2R airplane with 40° flap deflection and landing gear extended.

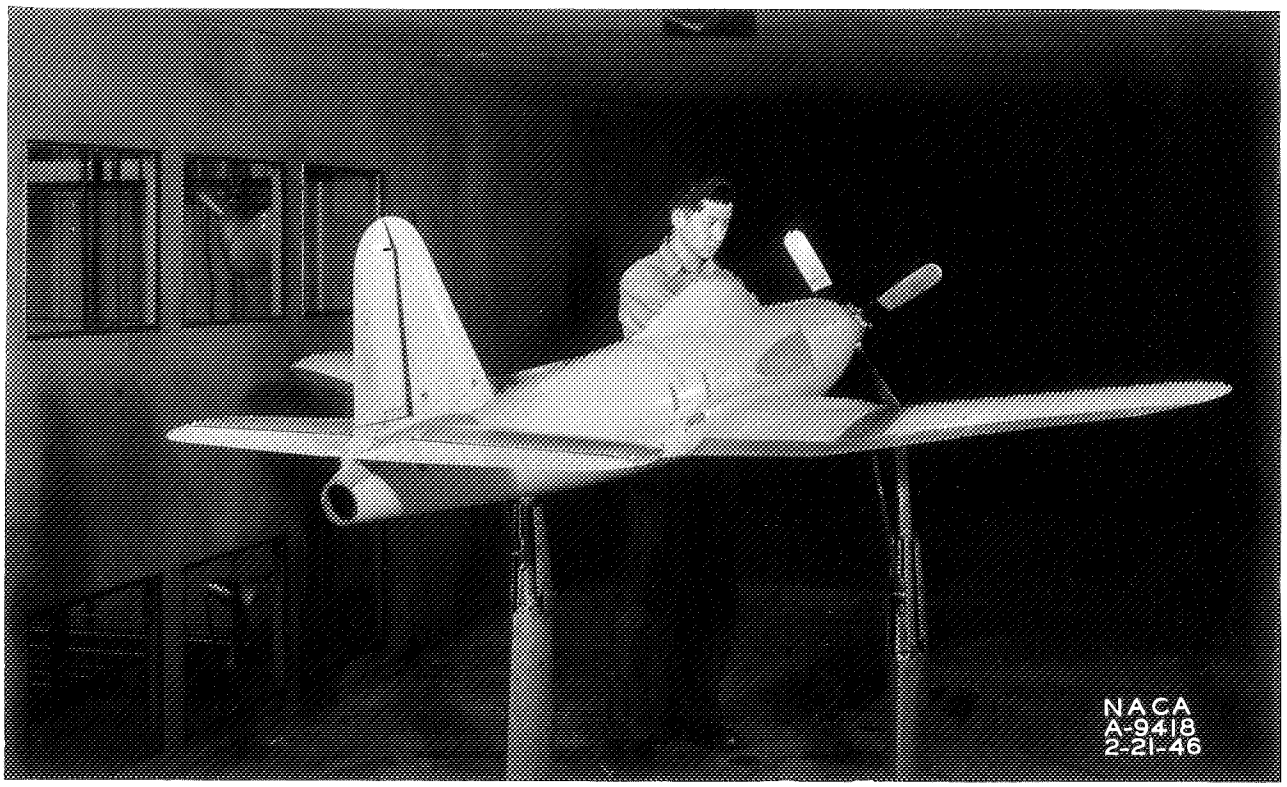

Figure 4.- Rear view of the 1/5-scale model of the Ryan XF2R airplane with flaps and landing gear retracted.

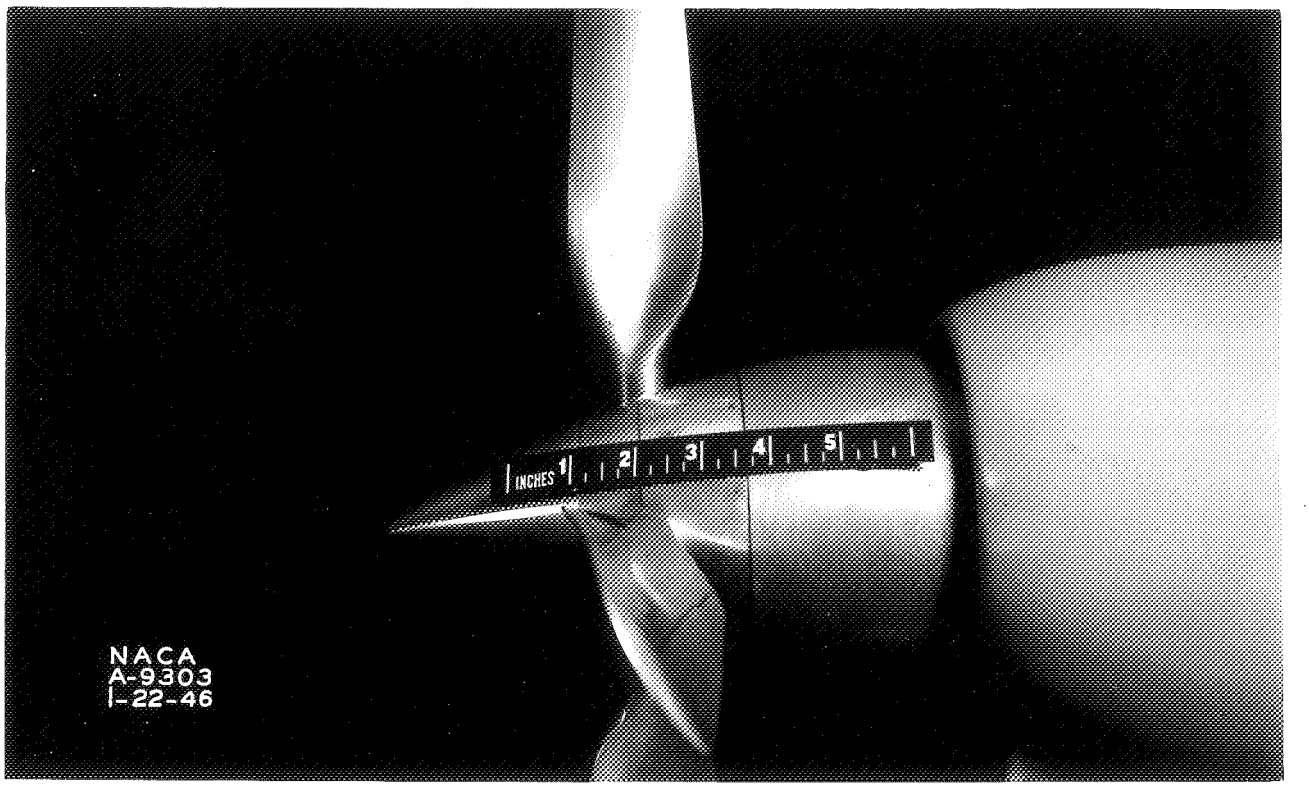

Figure 5.- Standard propeller on the 1/5-scale model of the Ryan XF2R airplane.

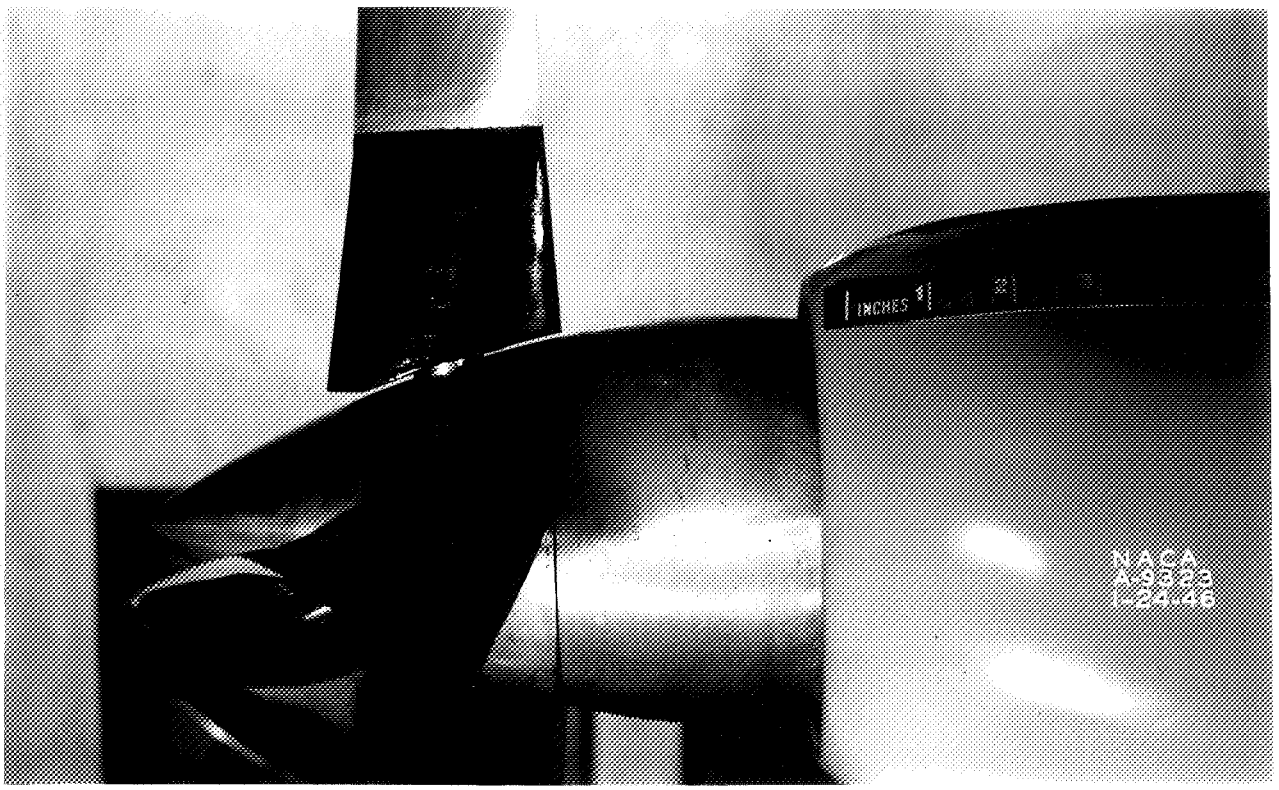

Figure 6.- Propeller with cuffs unsealed on the 1/5 scale model of the Ryan XF2R airplane.

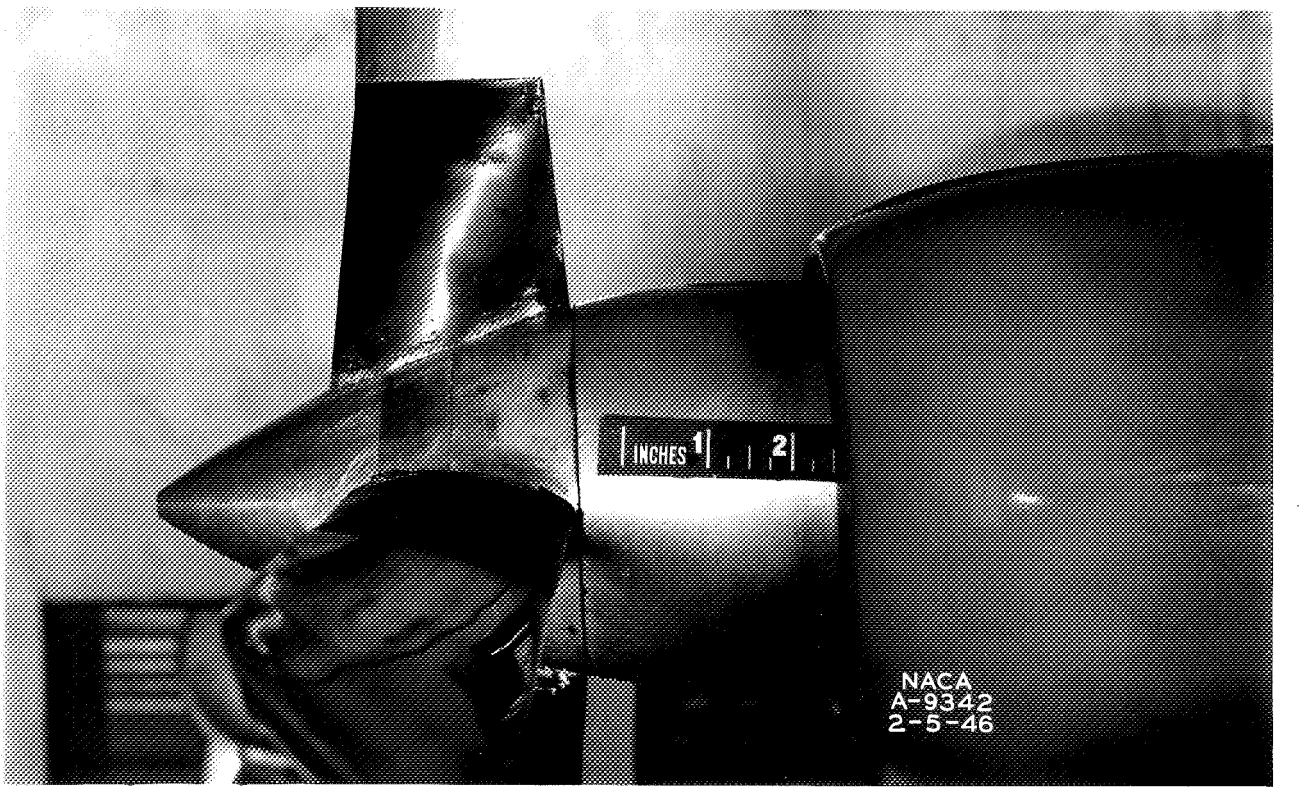

Figure 7.- Propeller with cuffs sealed on the 1/5-scale model of the Ryan XF2R airplane.

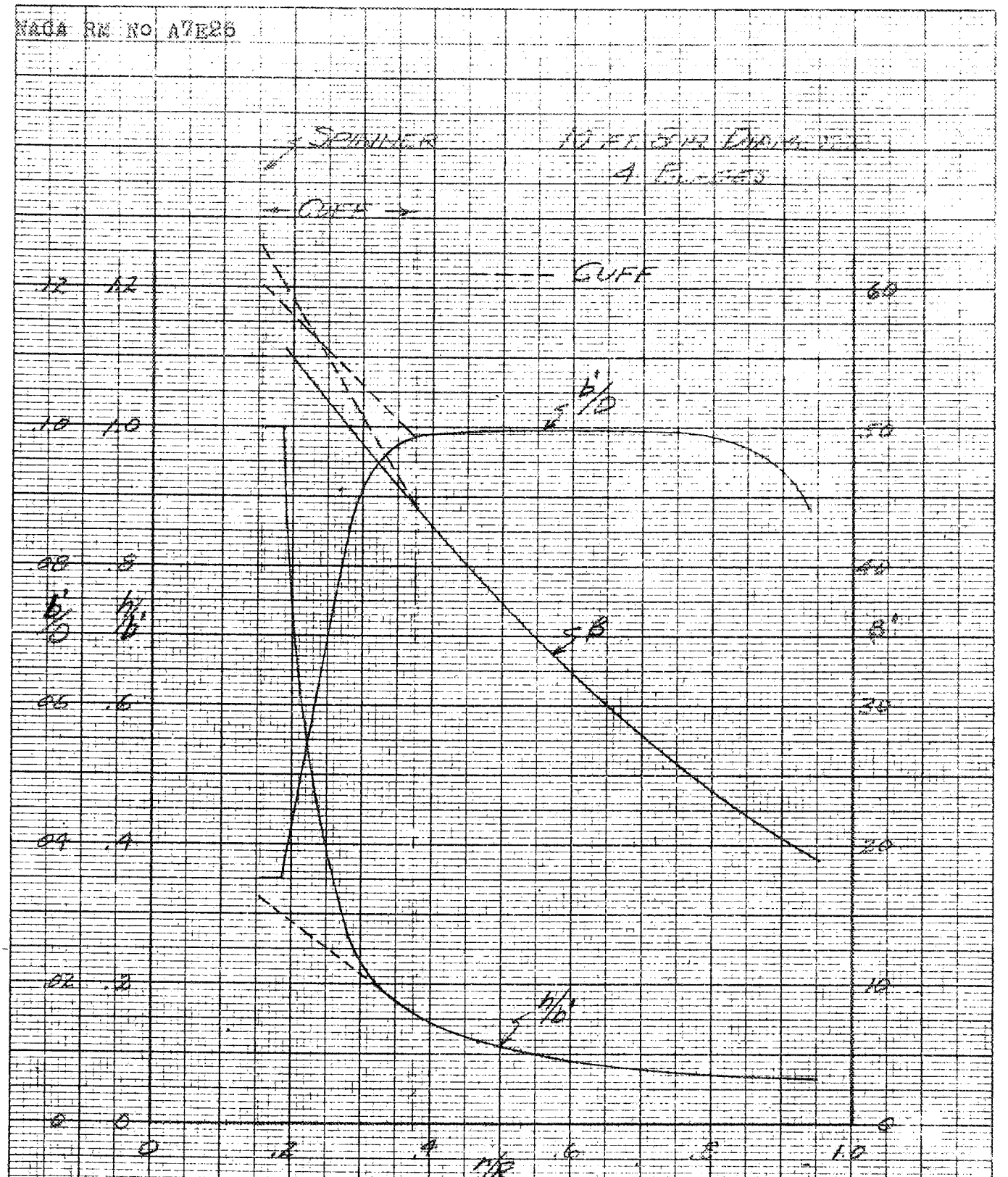

FIGURE 6. GEOMETRIC CHARACTERISTICS OF THE PROPELLERS 4-26-156-28 FROM THE NACA YF-80 AIRPLANE.

FIGURE 9 AERODYNAMIC CHARACTERISTICS OF THE AIRCRAFT
W-20-156-28 AS DETERMINED ON THE
OF THE

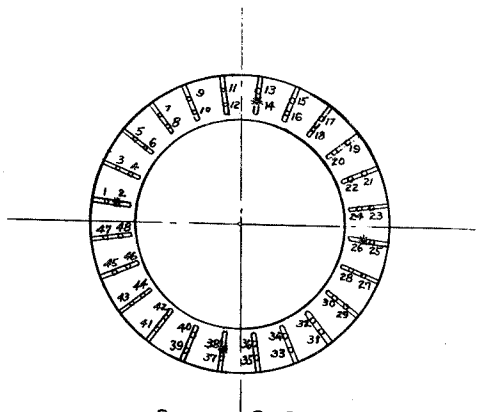

SECTION B-B

RAKE AT COMPRESSOR FACE

NOTE: TUBES 2, 14, 26, AND 38 MARKED THUS * ARE STATIC TUBES.

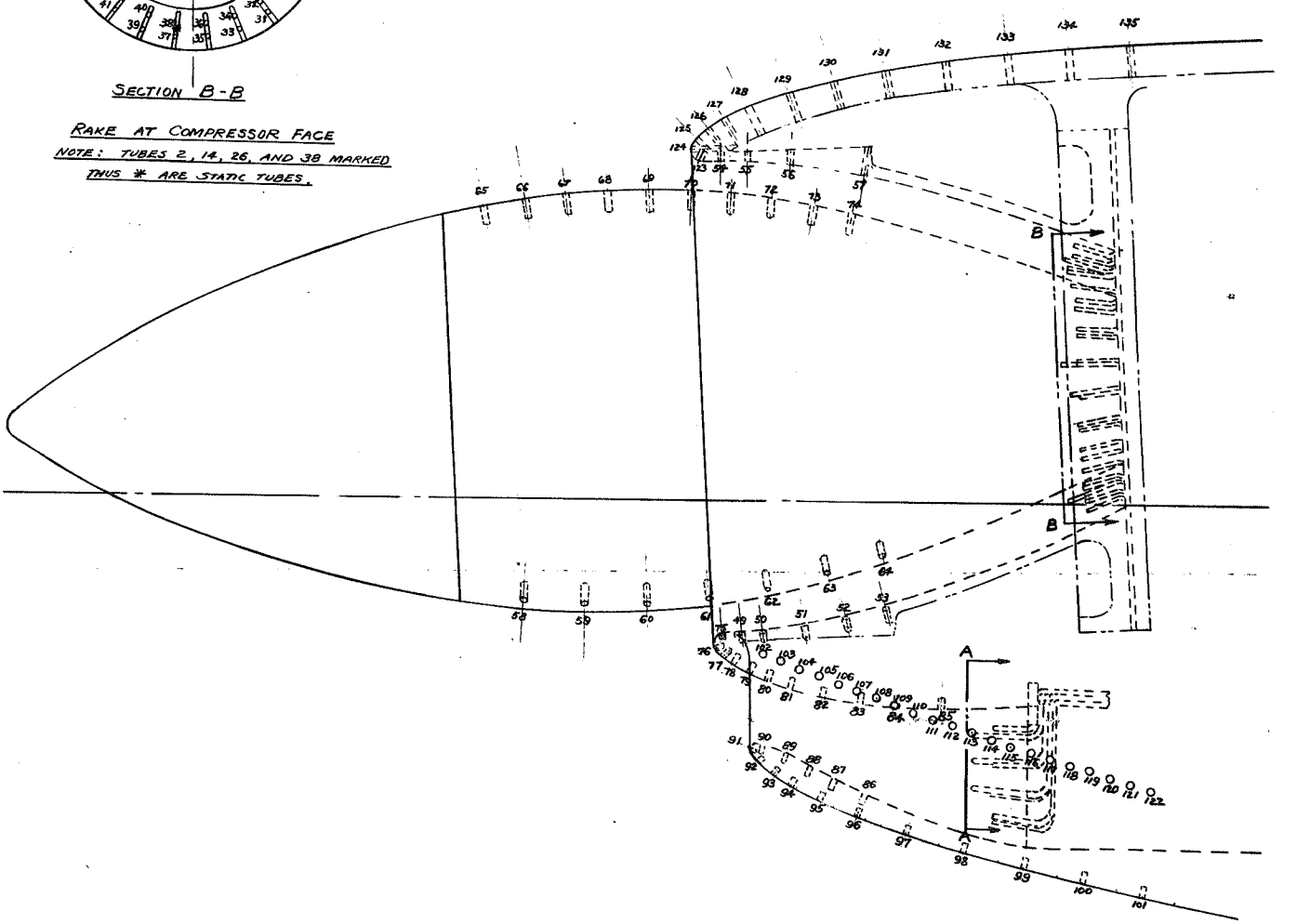

FIGURE 10.- PRESSURE-TUBE LOCATIONS. 1/5 SCALE MODEL OF THE RYAN XF2R AIRPLANE.

NOTE: TUBES 2, 14, 26, AND 38 ARE STATIC TUBES.

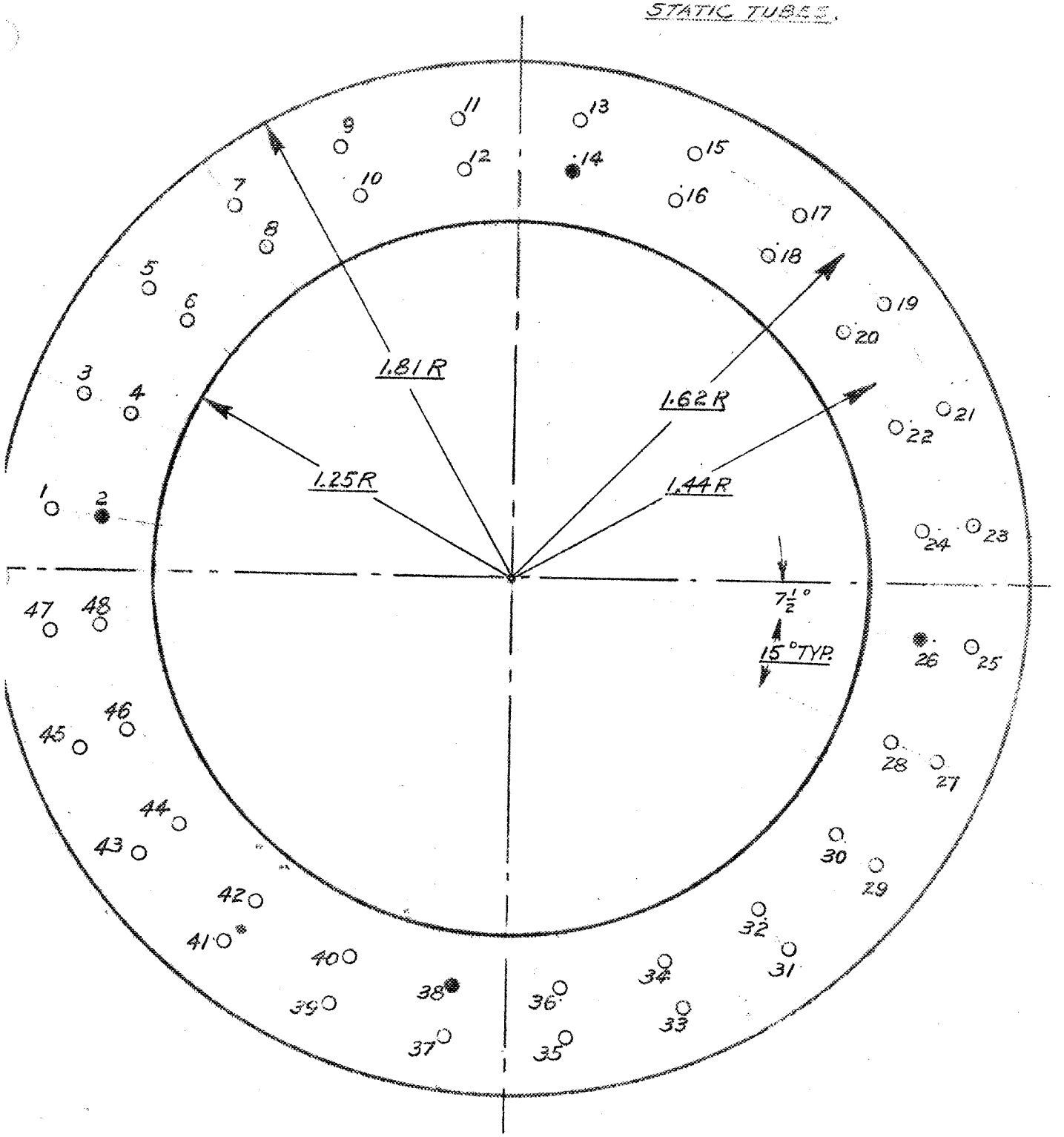

VIEW LOOKING AFT.

FIGURE 11. TUBE LOCATIONS OF THE PRESSURE RAKE IN THE SIMULATED ENTRANCE TO THE TG-100 GAS TURBINE. 1/5-SCALE MODEL OF RYAN XF2R AIRPLANE.

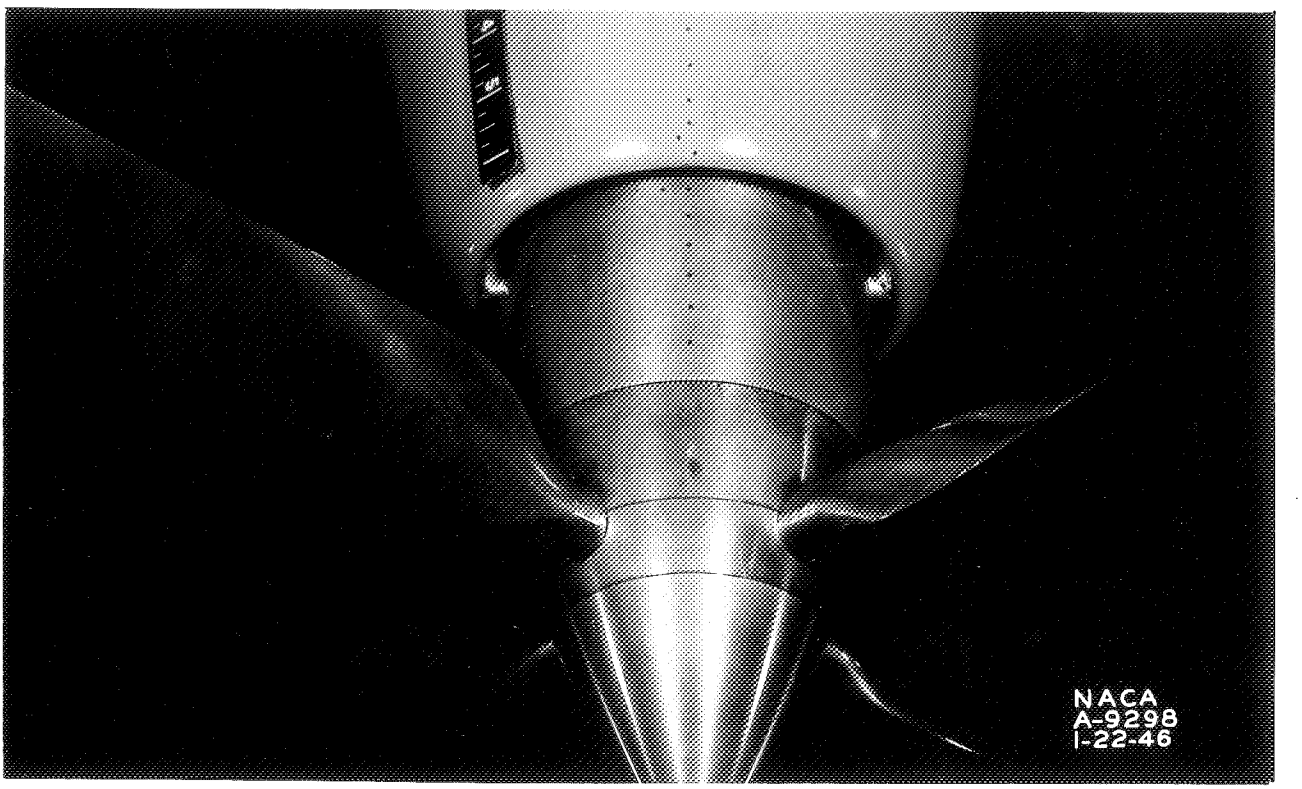

Figure 12.- Pressure orifices atop spinner fairing and cowl. 1/5-scale model of the Ryan XF2R airplane.

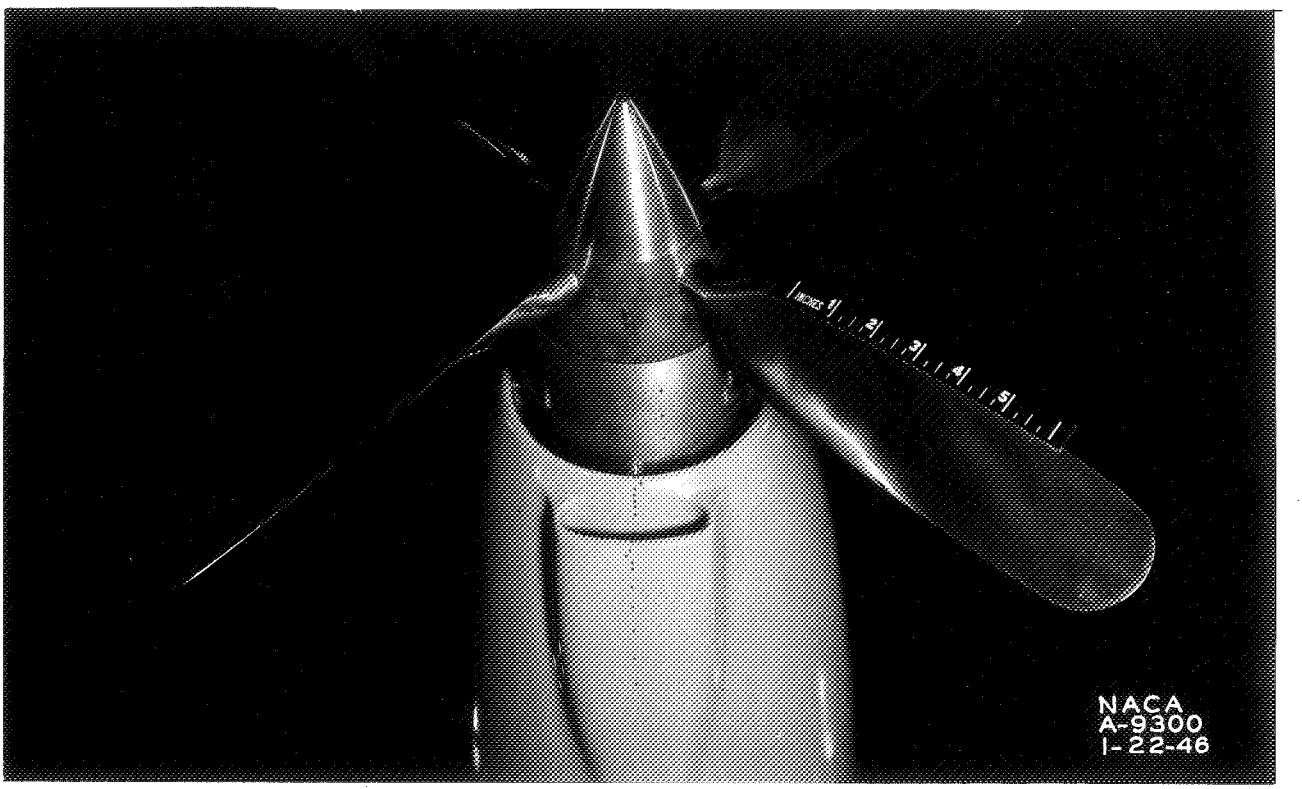

Figure 13.- Pressure orifices on lower side of spinner fairing and oil cooler on the 1/5-scale model of the Ryan XF2R airplane.

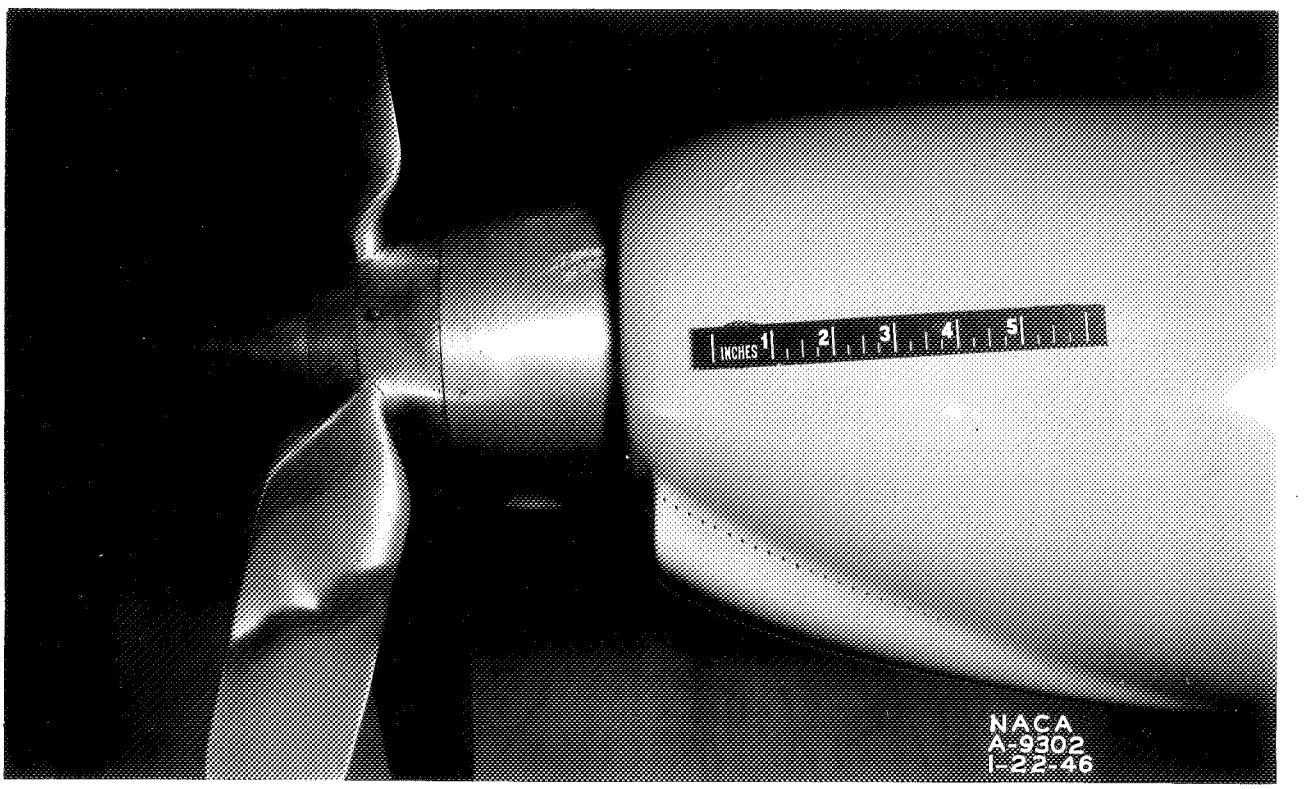

Figure 14.- Pressure orifices in the oil-cooler fillet.
1/5-scale model of Ryan XF2R airplane.

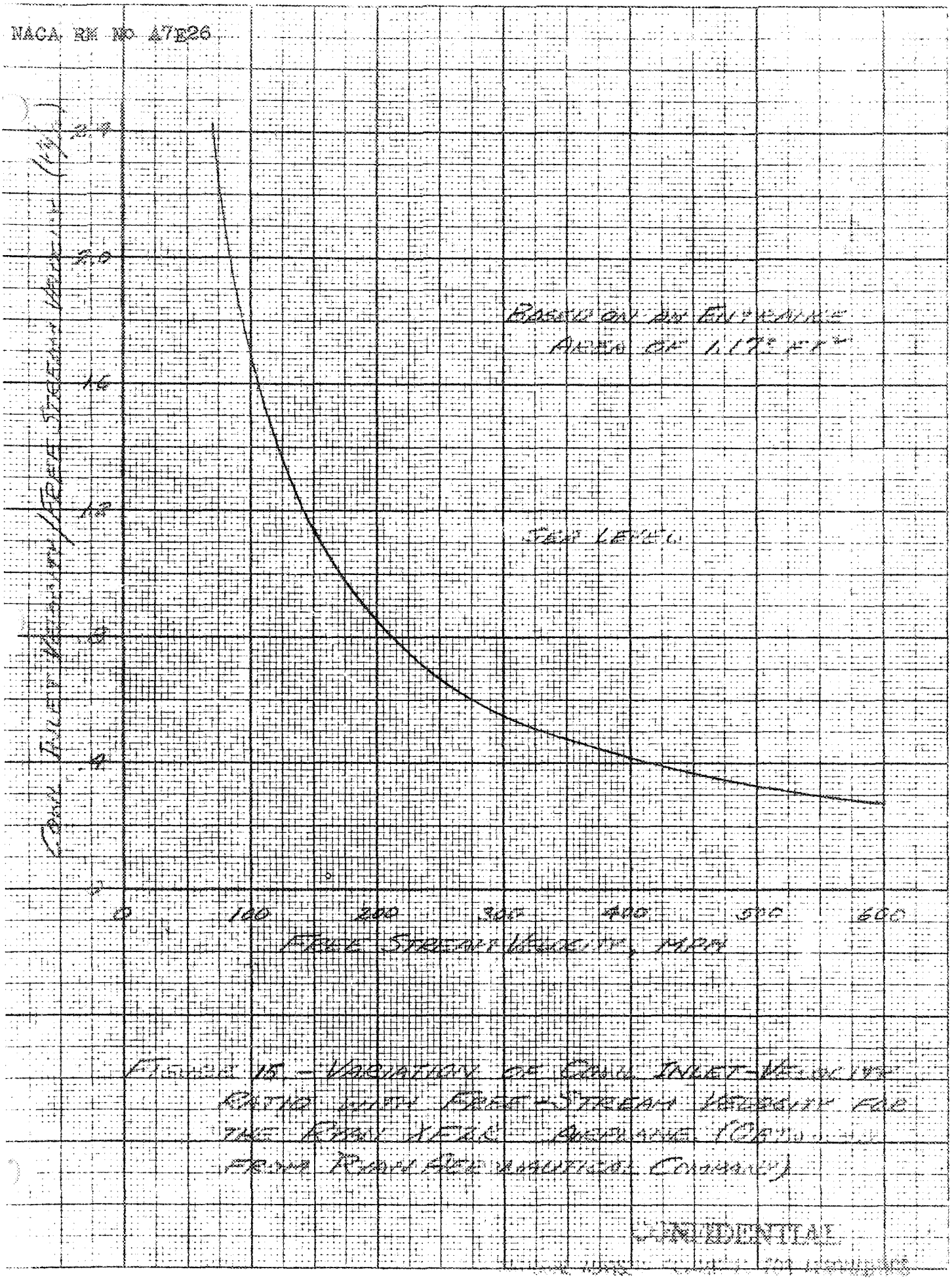

Figure 15. - Variation of fan inlet-duct total-pressure loss with free-stream velocity for fan inlet area and free-stream static pressure equal to sea-level standard conditions.

CONFIDENTIAL

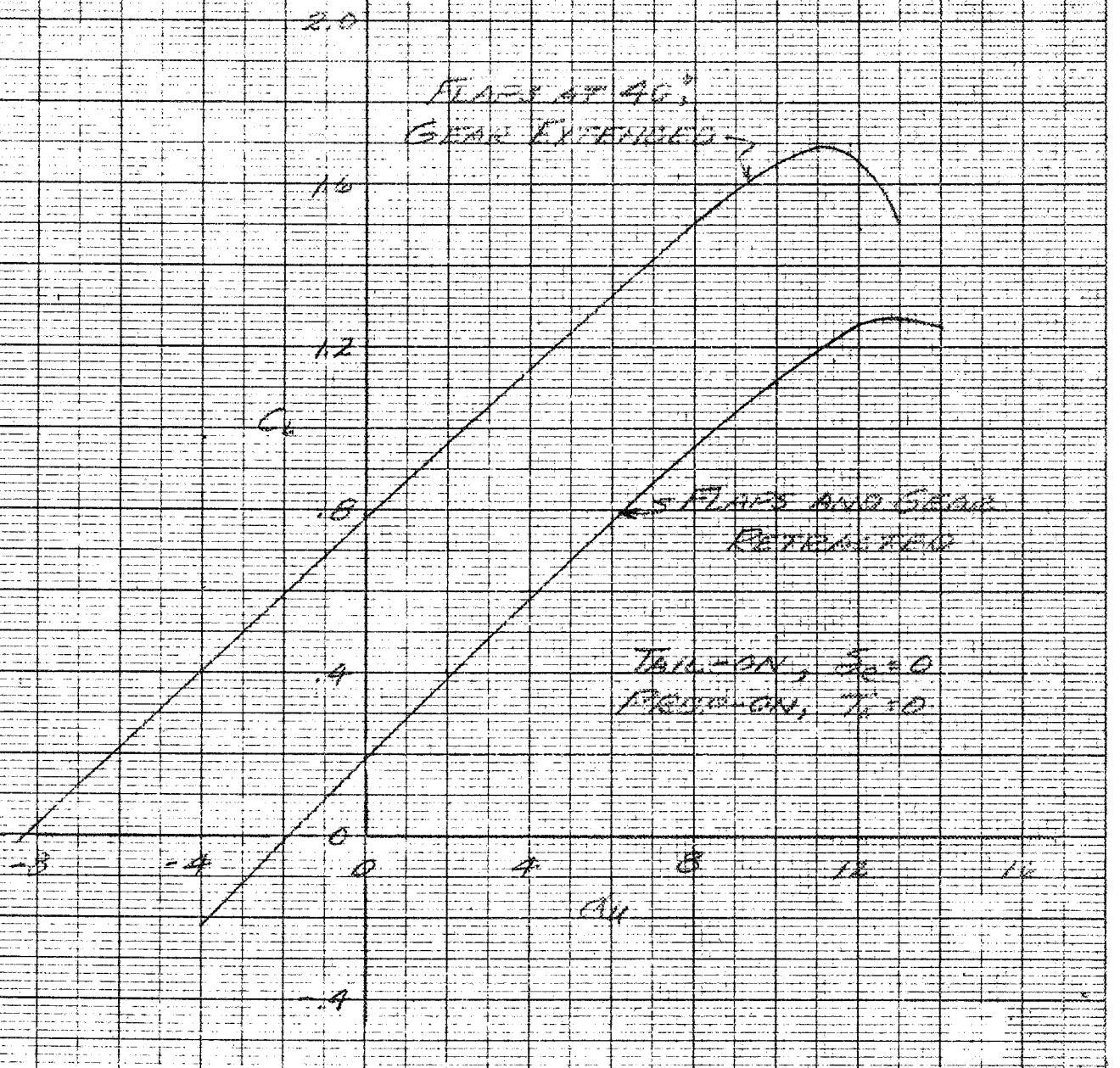

FIGURE 16.- VARIATION OF LIFT COEFFICIENT WITH UNCORRECTED ANGLE OF ATTACK FOR THE 1/4-SCALE MODEL OF THE KAISER XF7K-1

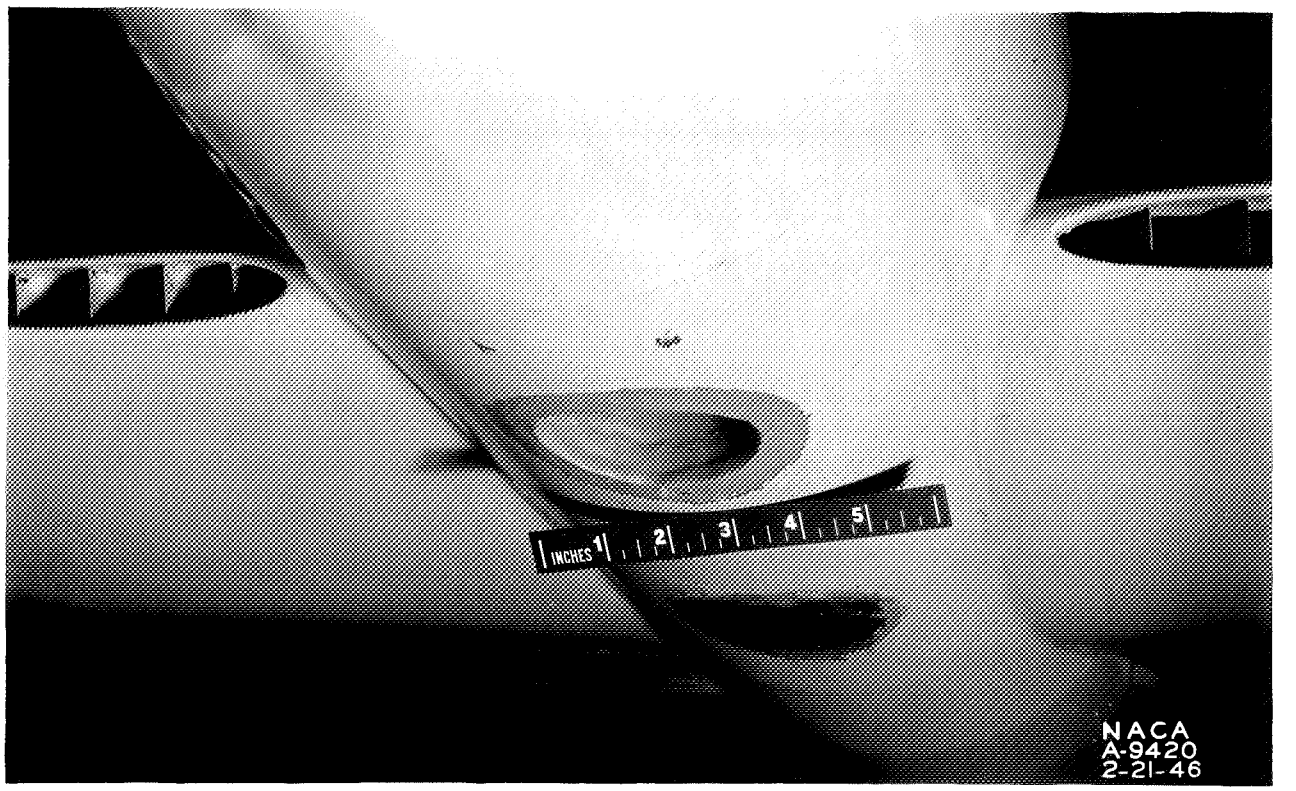

Figure 17.- Detail view of the 1/5-scale model of the Ryan XF2R airplane showing the 3-inch-diameter hole used for discharging air from the cowl.

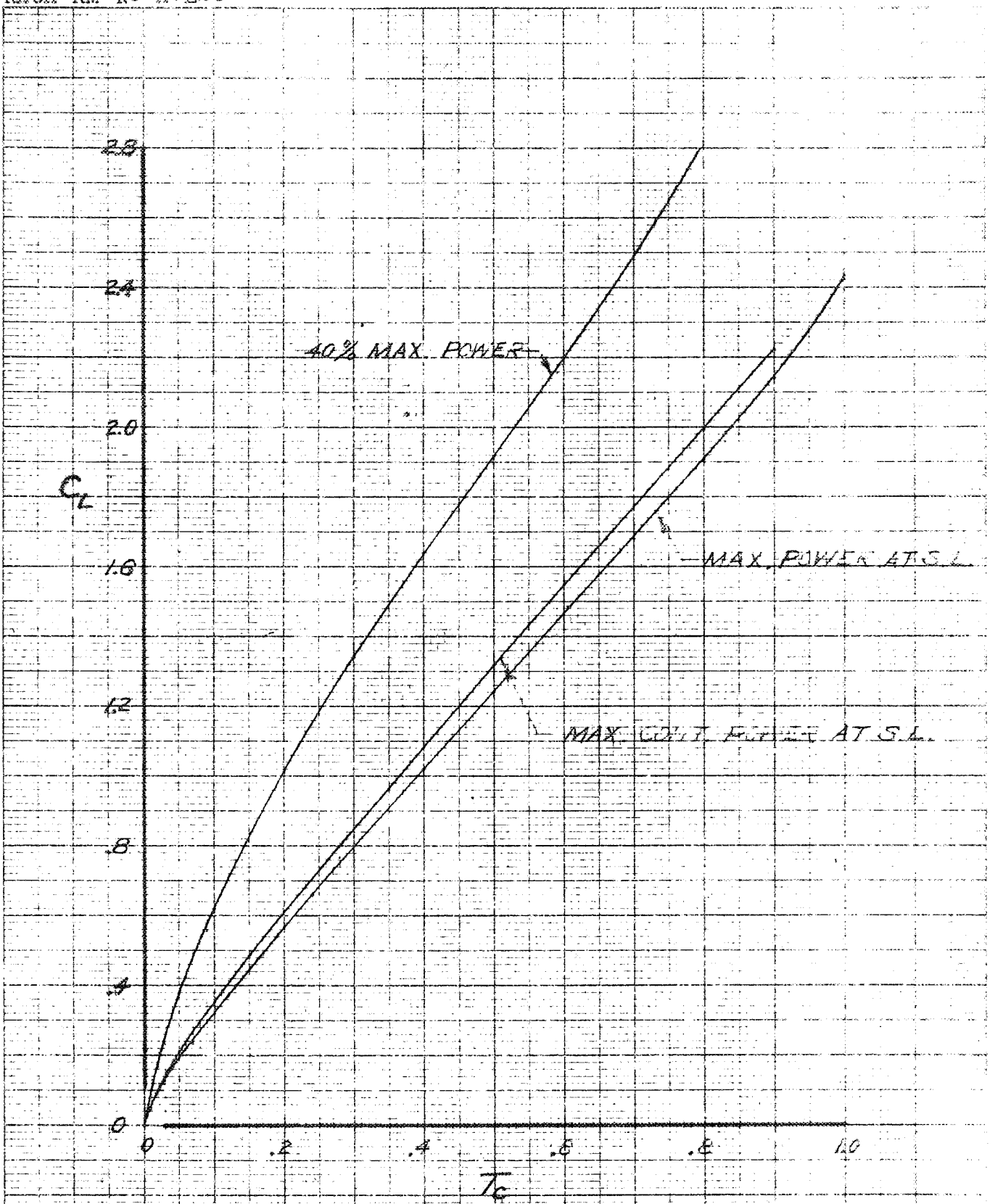

FIGURE 12 - PREDICTED VARIATIONS OF THE LIFT COEFFICIENT WITH THRUST COEFFICIENT OF THE F4H-1 AIRPLANE WITH VARIOUS POWER CONDITIONS. (NAVY FIGHTER WEIGHT = 16450 LB.)

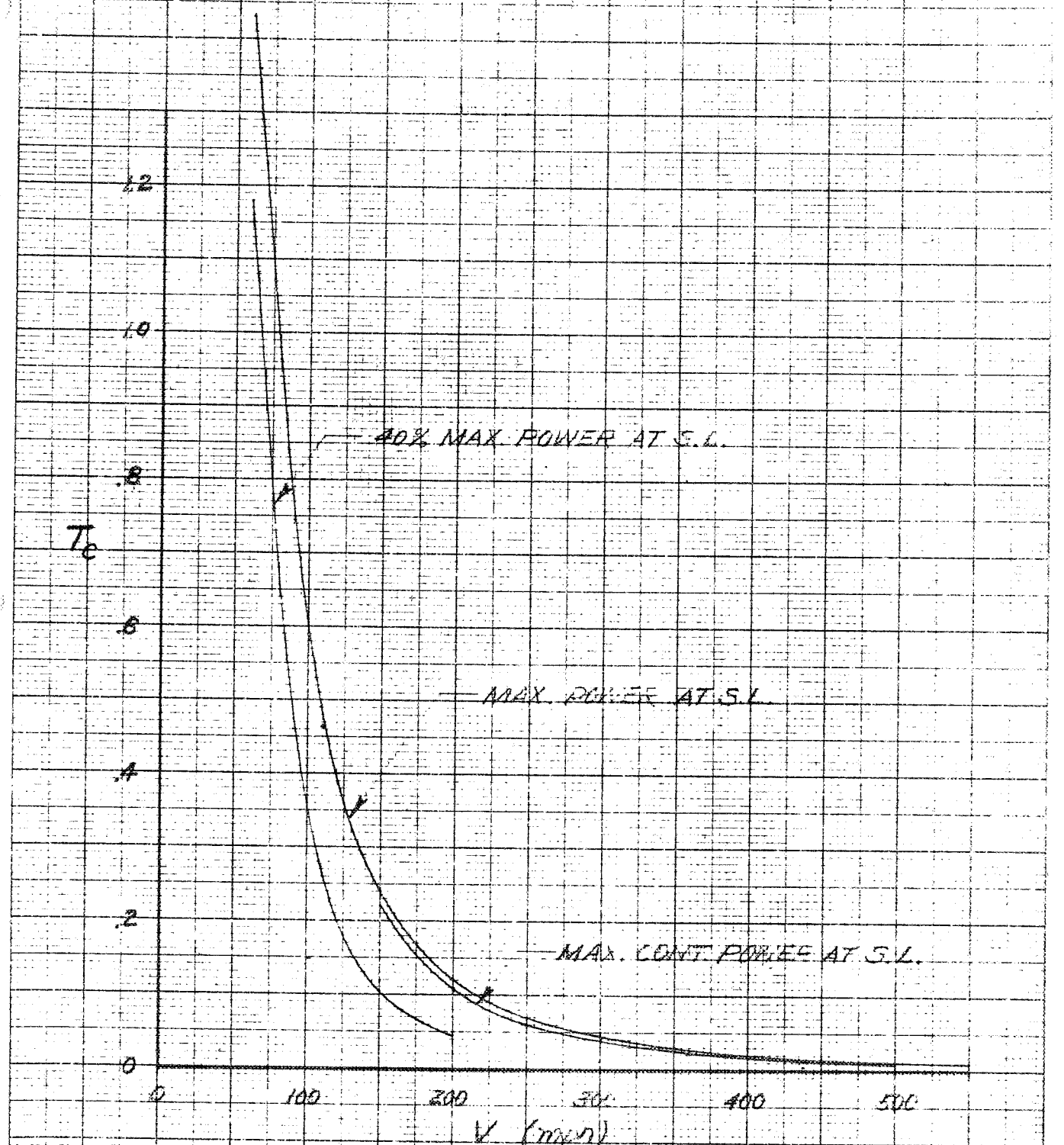

FIGURE 19.—PREDICTED VARIATIONS OF THE THRUST COEFFICIENT WITH VELOCITY OF THE RYAN XFER AIRPLANE AT VARIOUS POWER CONDITIONS.

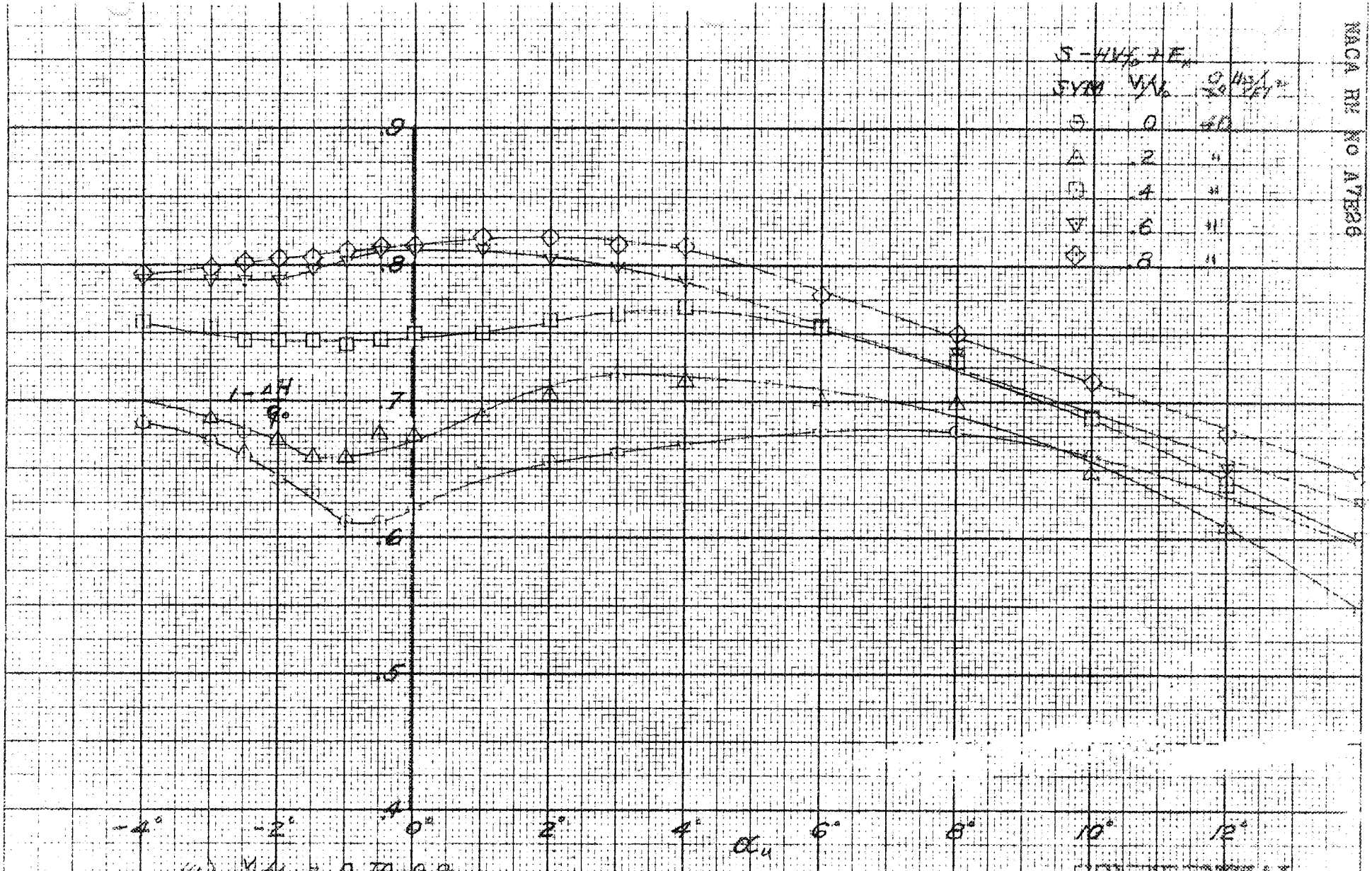

(a) $V_j/V_\infty = 0$ TO 0.8

CONFIDENTIAL

FIGURE 20 - VARIATION OF THE DYNAMIC-PRESSURE-RECOVERY COEFFICIENT AT THE ENTRANCE TO THE TG-100 UNIT, WITH ANGLE OF ATTACK FOR VARIOUS CONV-INLET-VELOCITY RATIOS WITH PROPELLER OFF. 1/5-SCALE MODEL OF THE RYAN XFR-1 AIRPLANE

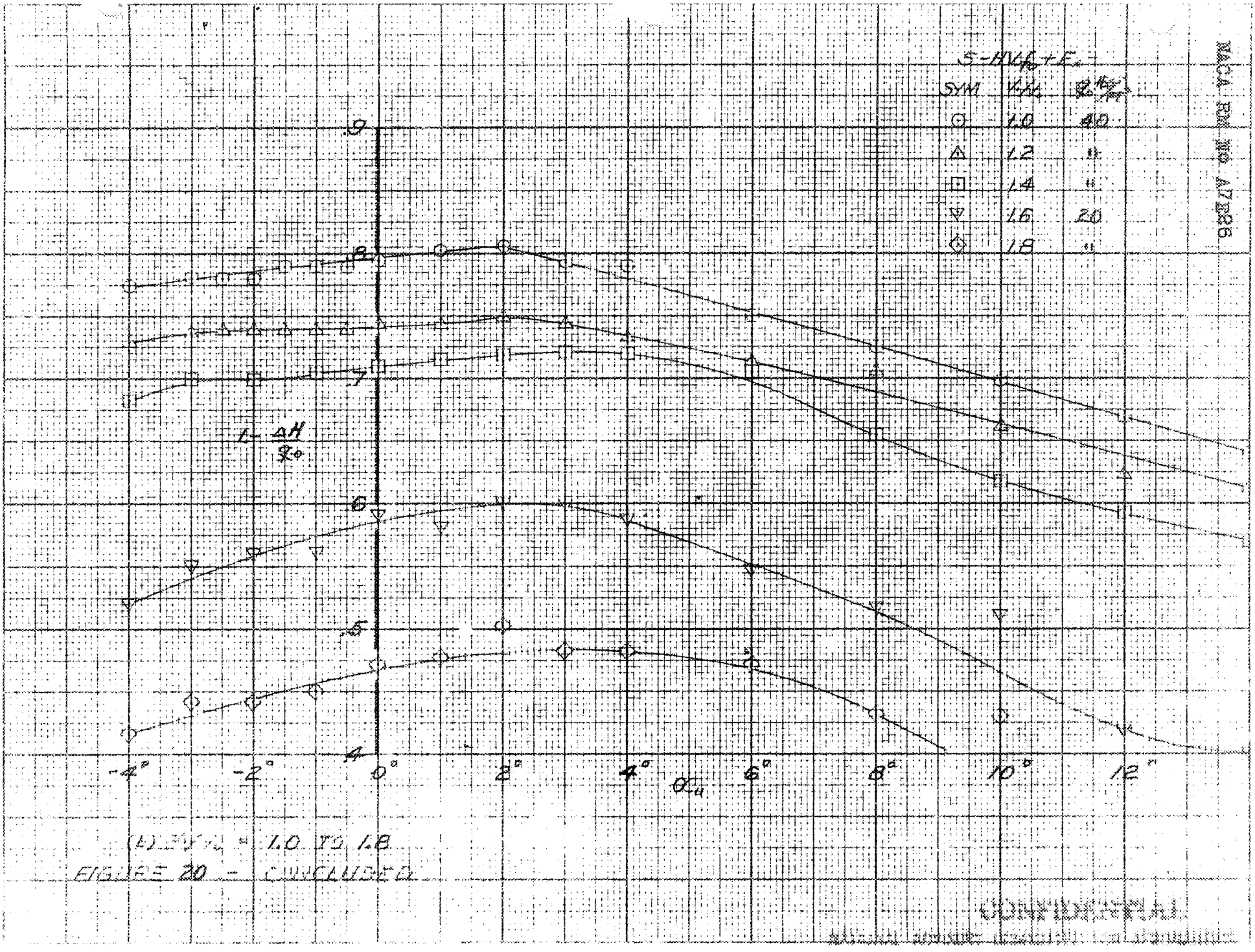
NACA RM No. A7E26
$S = \frac{\Delta M}{q_0}$
SYM $M_{\Delta M}$ $\frac{q_0}{q_\infty}$
1.0 .40
1.2 "
1.4 "
1.6 .20
1.8 "
$C_L - \frac{\Delta M}{q_0}$
.9
.8
.7
.6
.5
-4° -2° 0° 2° 4° α_u 6° 8° 10° 12°
(a) $M_{\Delta M}$ = 1.0 TO 1.8
FIGURE 20 - CONCLUDED
CONFIDENTIAL

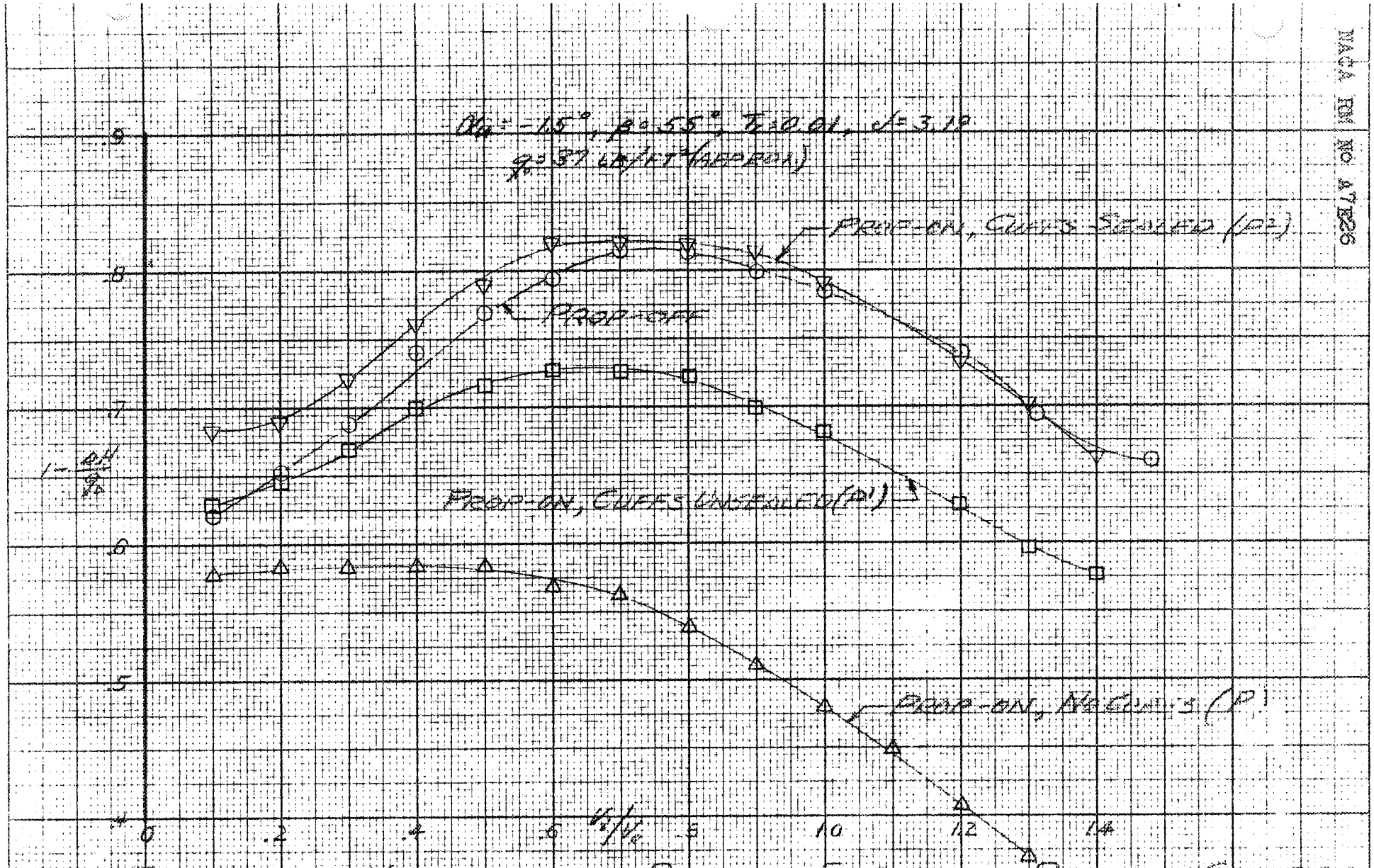

FIGURE 21.- VARIATION OF DYNAMIC-PRESSURE-RATIO CORRECTION FACTOR AT THE ENTRANCE TO THE PROPELLER DISK, $1 - \frac{\alpha_1}{\alpha_2}$, WITH FREE-STREAM VELOCITY RATIO FOR VARIOUS MODIFICATIONS OF THE CUFF AND NACELLE. UNSWEPT HIGH-SPEED CONFIGURATION.

CONFIDENTIAL

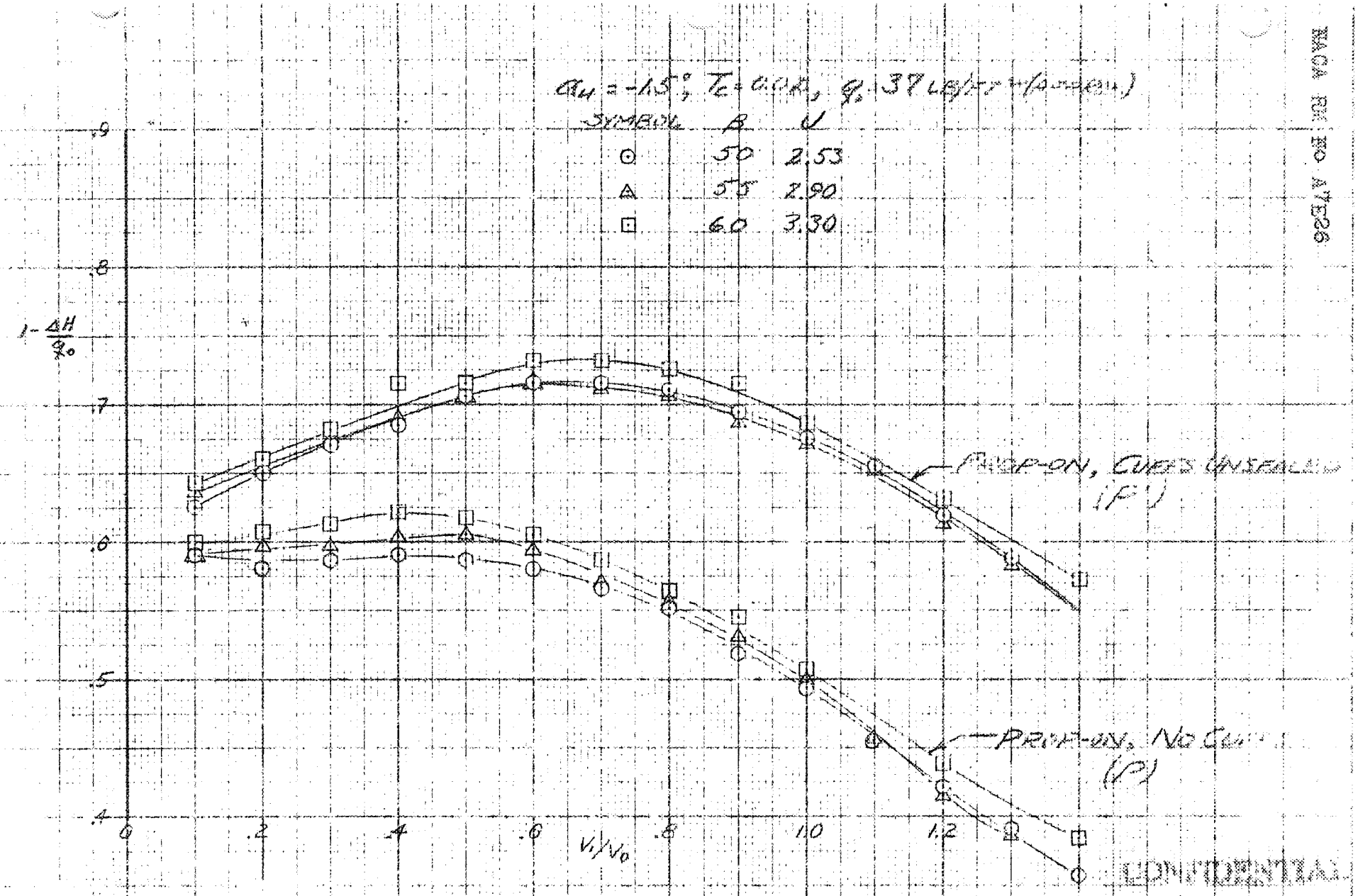

FIGURE 22. - EFFECT OF PROPELLER-BLADE ANGLE ON THE VARIATION OF DYNAMIC-PRESSURE-RECOVERY COEFFICIENT OF THE FUSELAGE TO THE NO UNIT, WITH CONSTANT VELOCITY RATIO FOR VARIOUS PROPELLER MASS FLOWS.

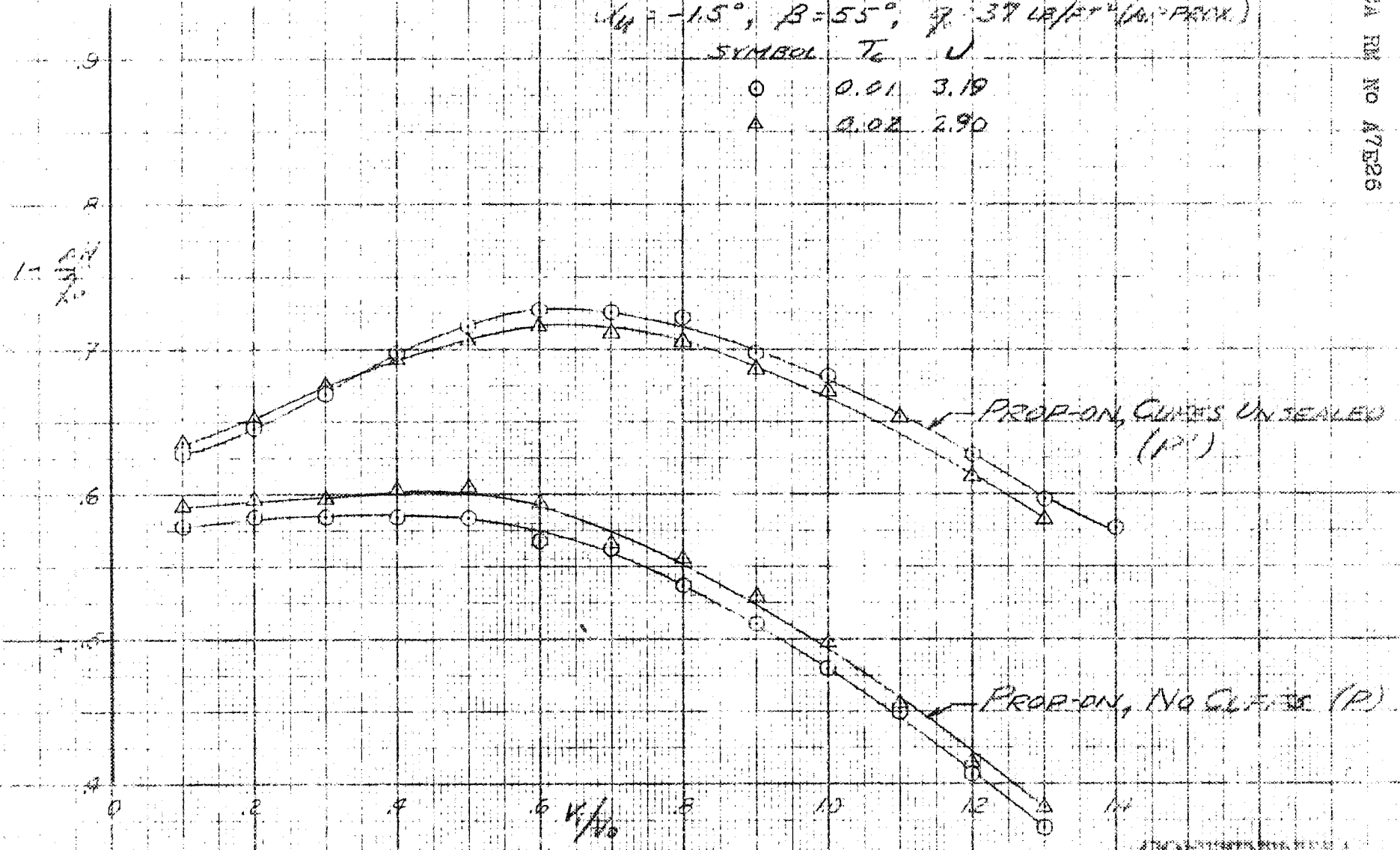

CONFIDENTIAL

FIGURE 23.- EFFECT OF PROPELLER THRUST COEFFICIENT ON ZERO VARIATION OF DOWNWASH-PRESSURE-RECOVERY CORRELATIVE, AT THE CG BALANCE AIR PORT AT THE UNIT, WITH CONE-INLET-VELOCITY RATIO FOR VARIOUS PROPELLER MODIFICATIONS.

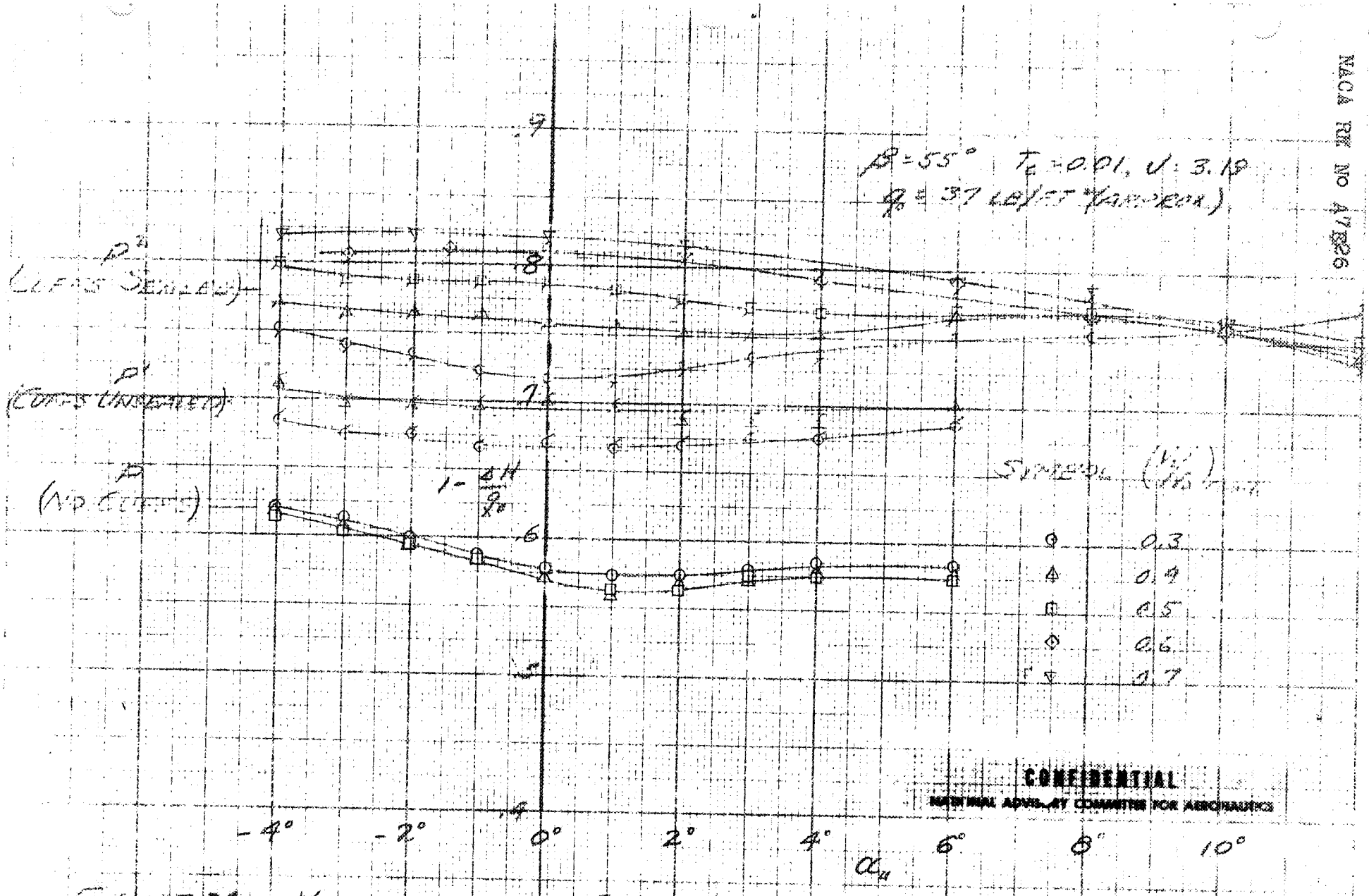

CONFIDENTIAL
NATIONAL ADVISORY COMMITTEE FOR AERONAUTICS

FIGURE 24. - VARIATION OF DIMENSIONLESS PRESSURE GRADIENT CONSTANT, OF THE CROSS-FLOW PLANE, WITH ANGLE OF ATTACK FOR VARIOUS VALUES OF DISTANCE FROM LEADING EDGE. WEDGE-CONE COMBINATION; MACH NUMBER, 3.18; STAGNATION TEMPERATURE, 530° R.

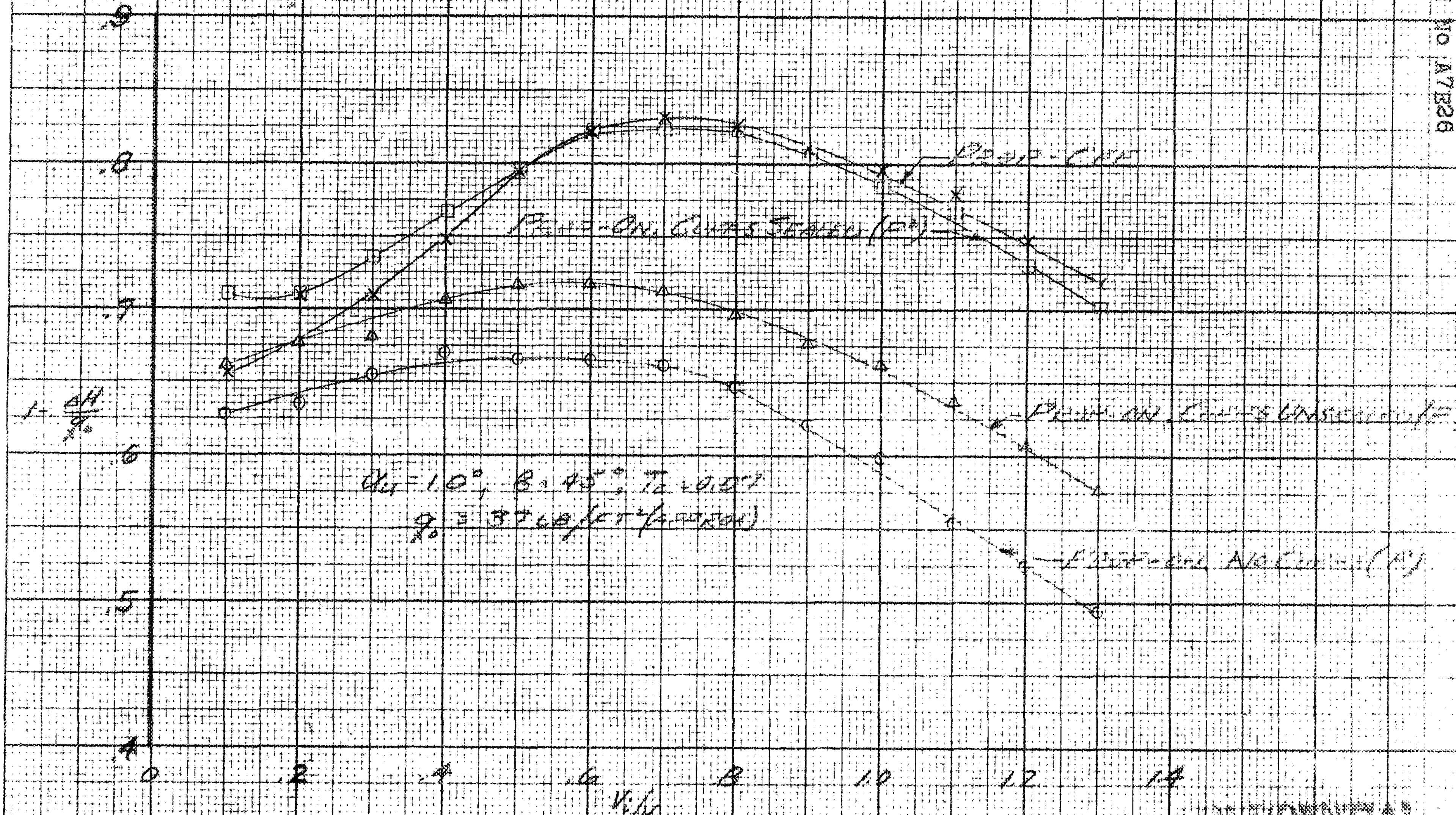

Figure 25.– Variation of [illegible] [illegible]

CONFIDENTIAL

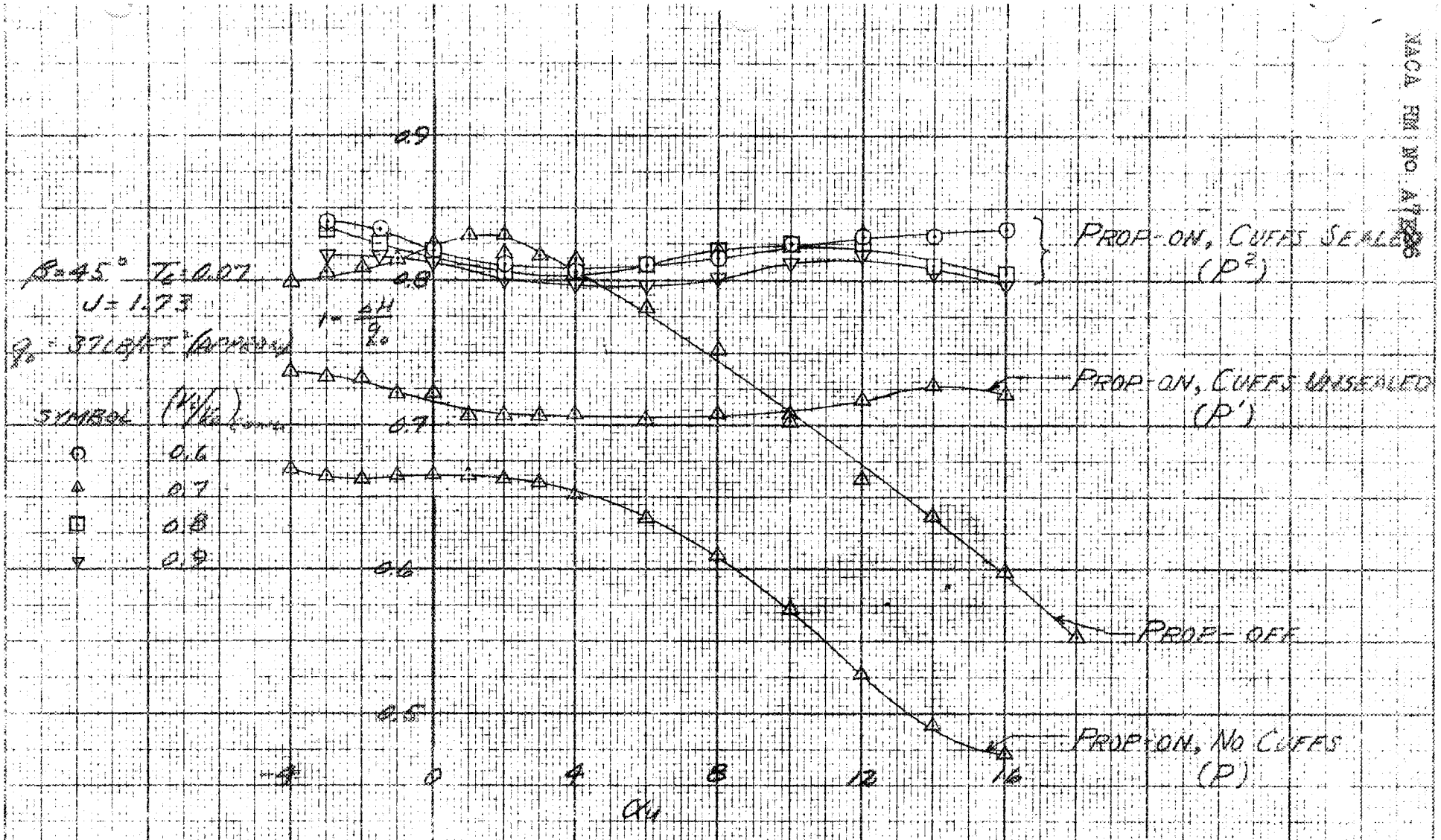

FIGURE 26.- VARIATION OF DYNAMIC-PRESSURE-RECOVERY COEFFICIENTS AT THE ENTRANCE TO THE TG-100 UNIT, WITH ANGLE OF ATTACK FOR VARIOUS PROPELLER MODIFICATIONS. SIMULATED CLIMB CONDITION.

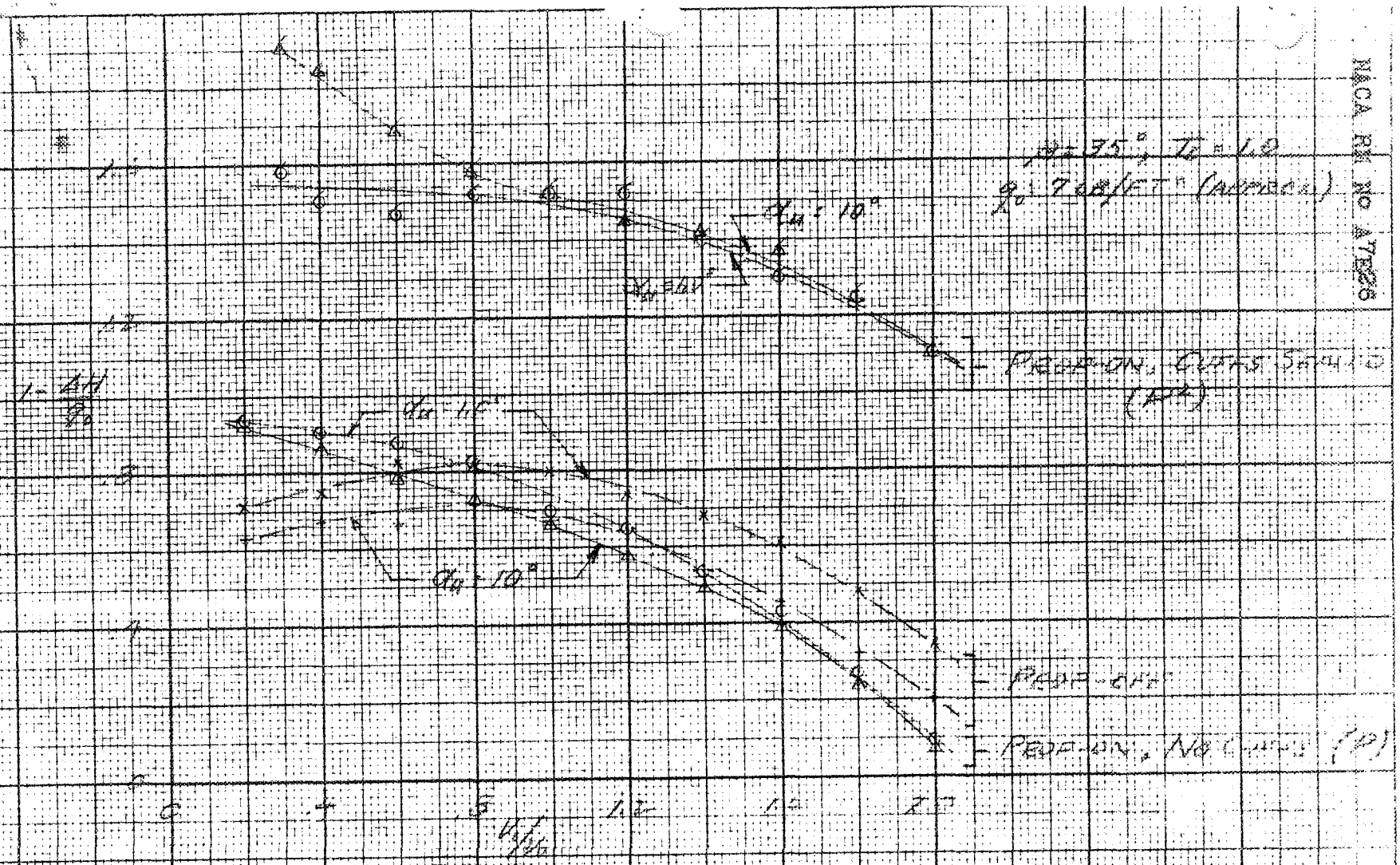

FIGURE 27. - VARIATION OF PRESSURE-AREA-PRODUCT COEFFICIENT, $\frac{L - L_{\alpha=0}}{q_0}$, WITH ANGLE OF YAW FOR TAPERED WING, WITH CASE-TWO VELOCITY AREAS FOR VARIOUS PRESSURE-AREA-PRODUCT COEFFICIENTS FOR UNTAPERED TAPE-CUT CASE-TWO

FIGURE 28.- VARIATION OF LOCAL-TO-FREE-STREAM PRESSURE-RECOVERY COEFFICIENT AT THE ENTRANCE TO THE 75-MM DUCT WITH ANGLE OF ATTACK FOR VARIOUS CONE-INLET-VELOCITY RATIOS AND PRESSURE MEASUREMENTS. SMOOTH-SURFACE CONE-CYLINDER COMBINATION.

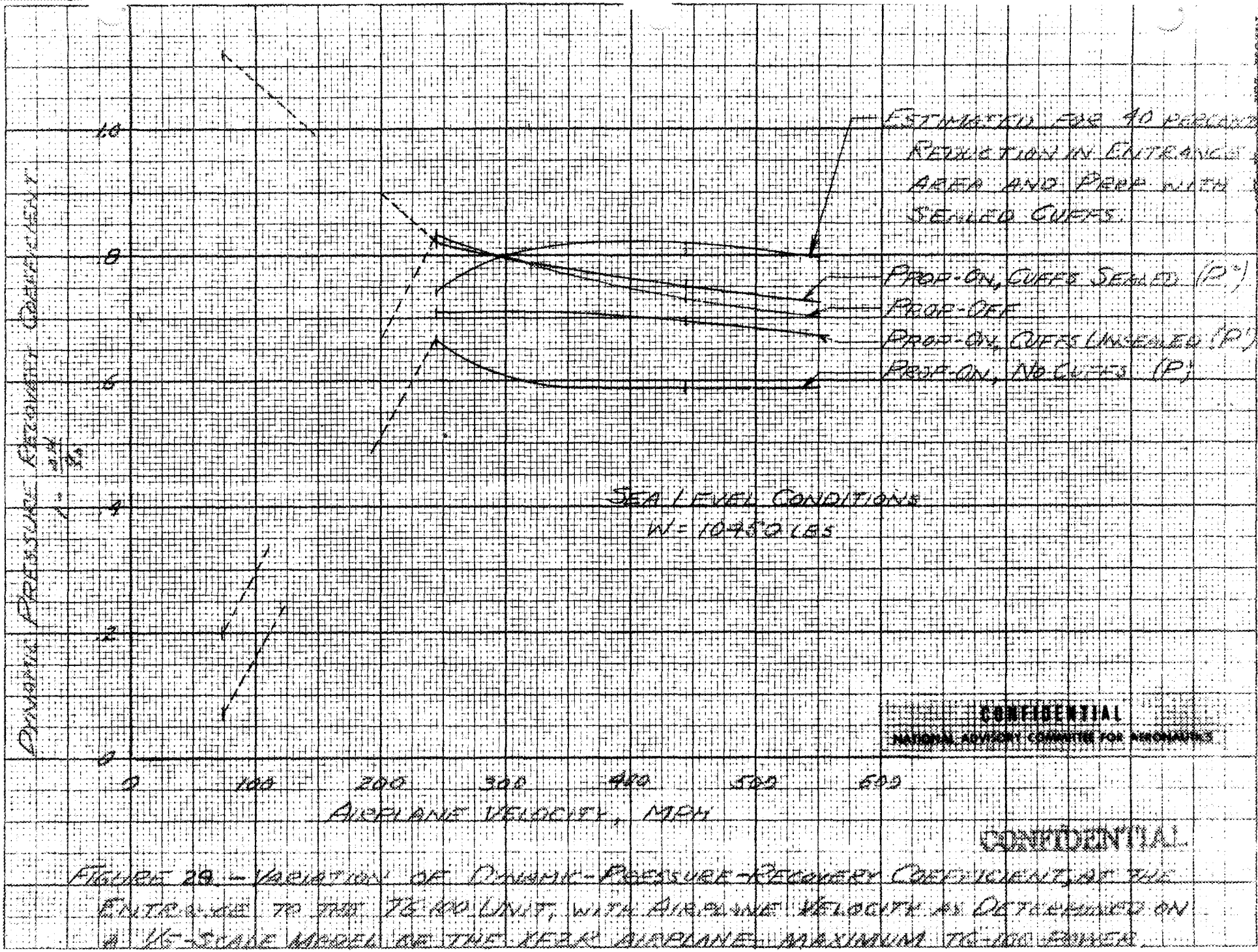

CONFIDENTIAL

FIGURE 28 — VARIATION OF DYNAMIC-PRESSURE-RECOVERY COEFFICIENT AT THE ENTRANCE TO THE J2 AN UNIT, WITH AIRPLANE VELOCITY AS DETERMINED ON A 1/6-SCALE MODEL OF THE XF2R AIRPLANE, MAXIMUM TO-100 ENGINE

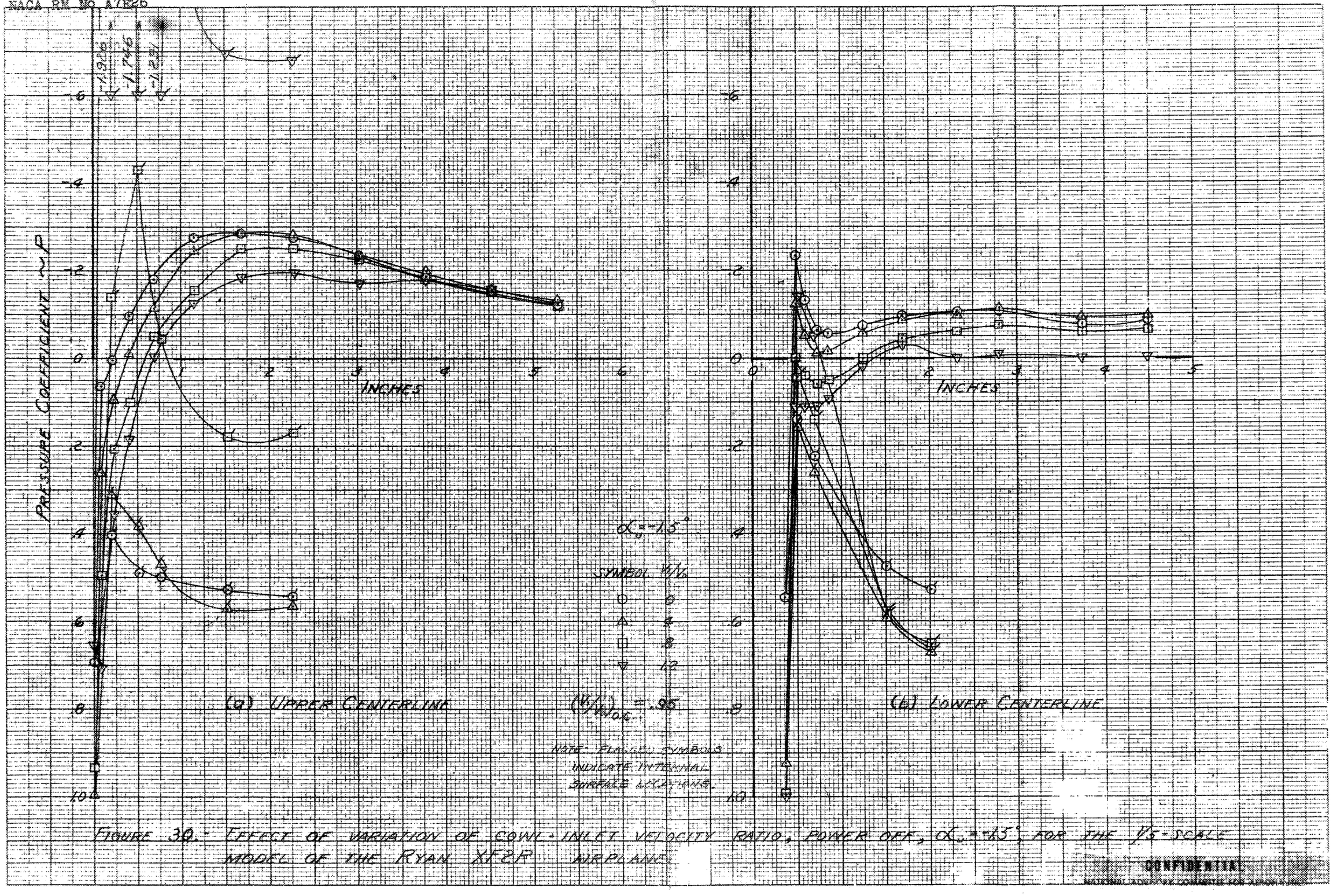

FIGURE 30.- EFFECT OF VARIATION OF CONE-INLET VELOCITY RATIO, POWER OFF, $\alpha_s = -15°$, FOR THE 1/5-SCALE MODEL OF THE RYAN XF2R AIRPLANE.

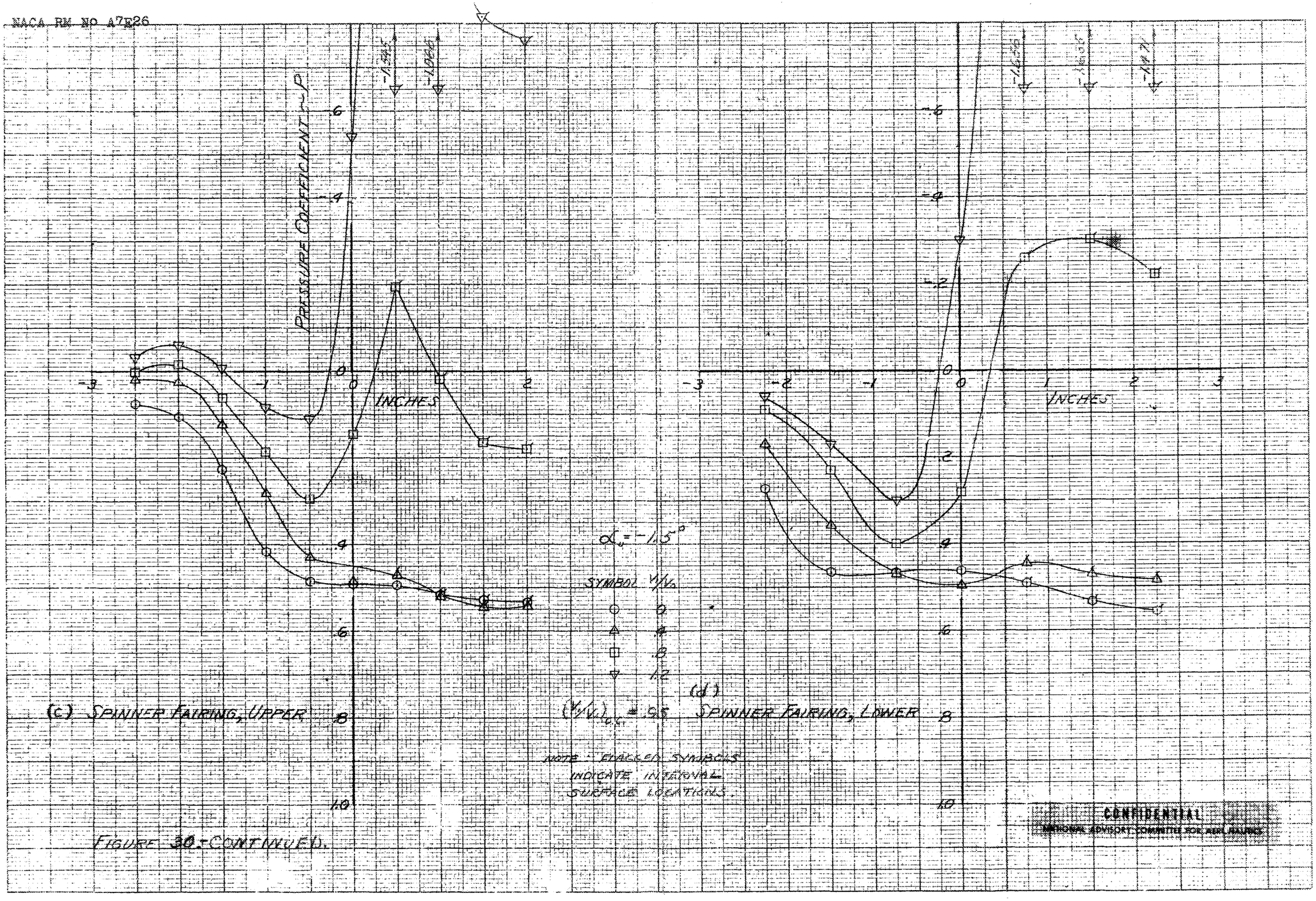

(c) Spinner fairing, upper

(d) Spinner fairing, lower

FIGURE 30.- CONTINUED.

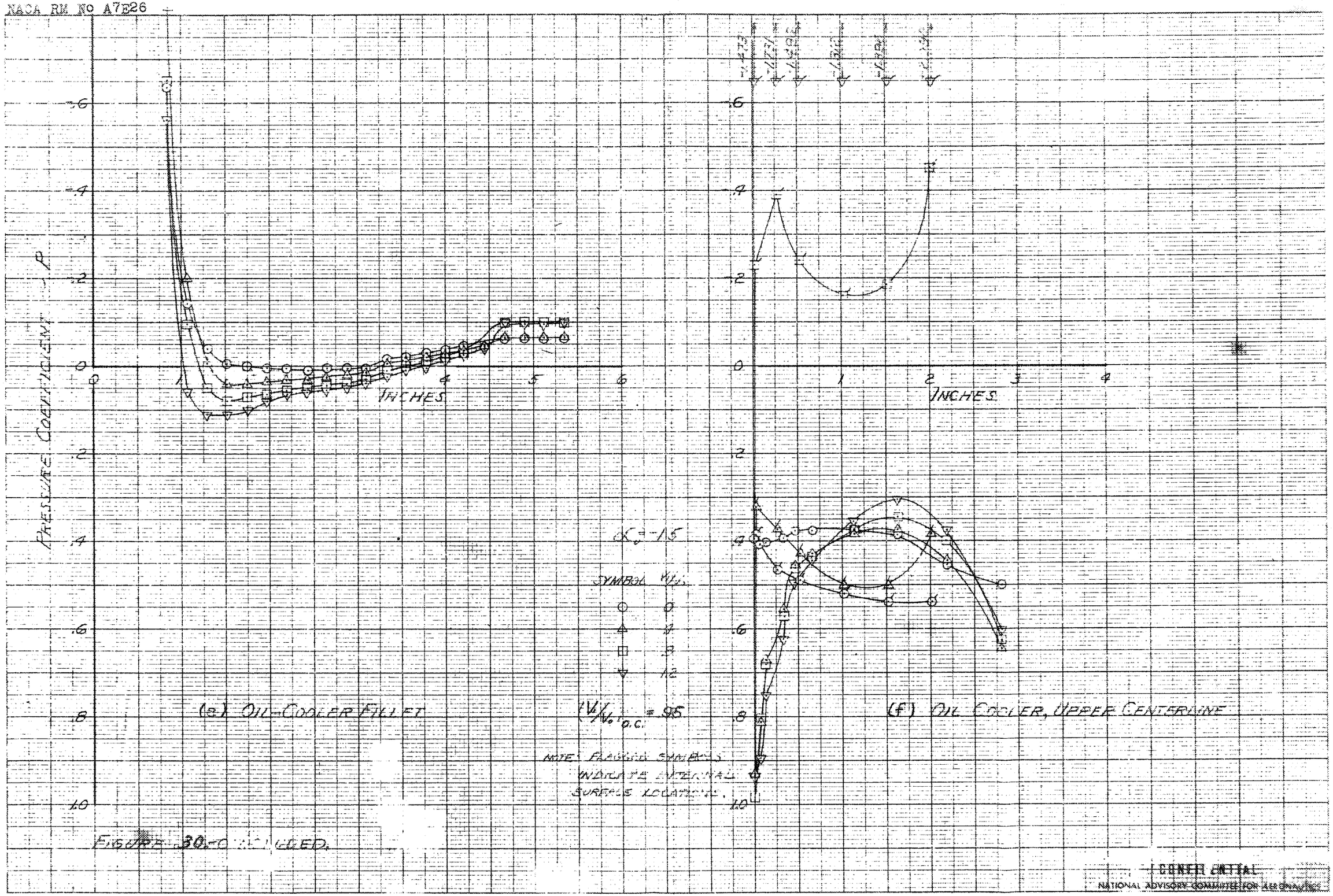

FIGURE 30.- CONCLUDED.

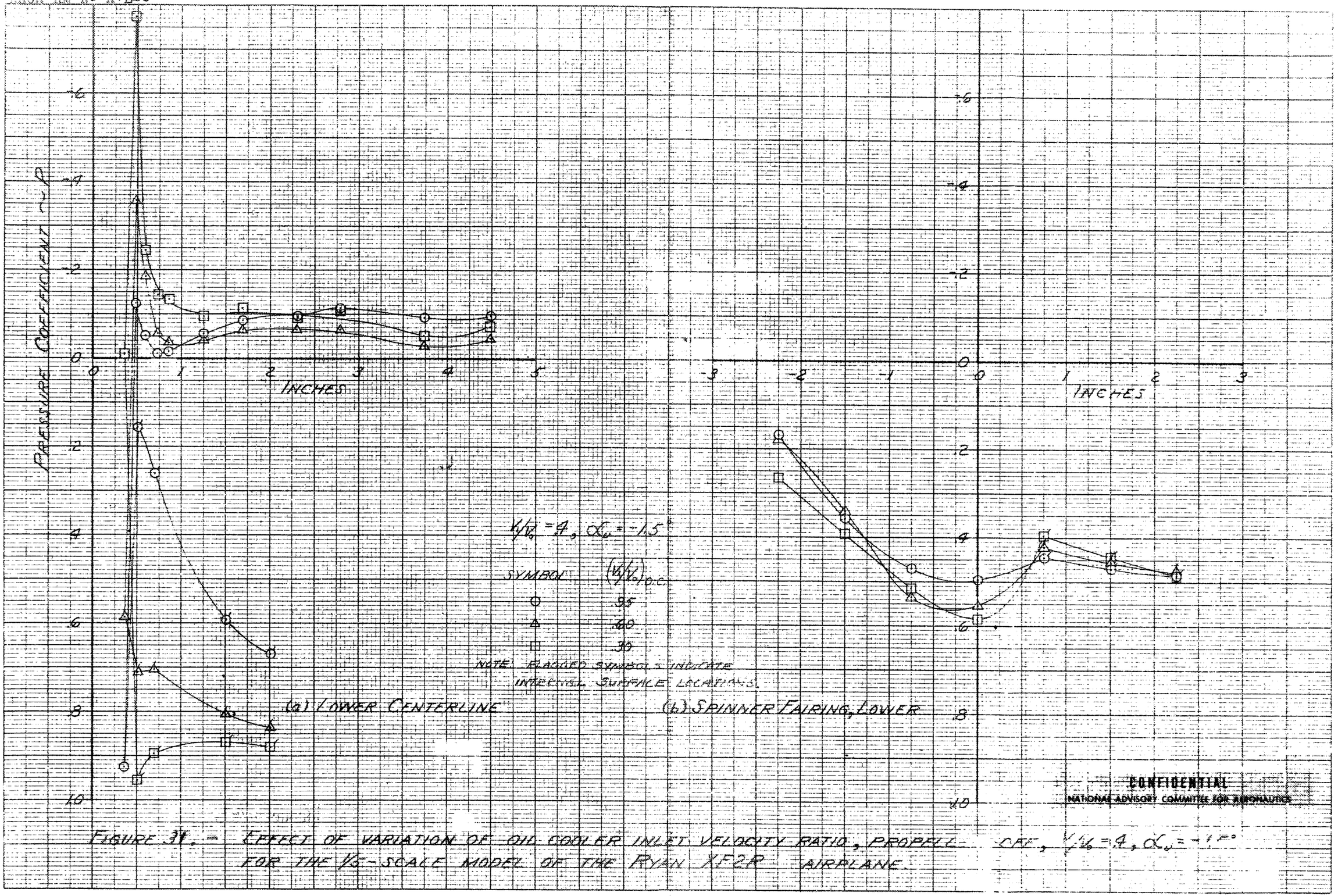

FIGURE 31. - EFFECT OF VARIATION OF OIL COOLER INLET VELOCITY RATIO, PROPELLER OFF, $V/V_0 = .4$, $\alpha_c = -1.5°$ FOR THE 1/5-SCALE MODEL OF THE RYAN XF2R AIRPLANE.

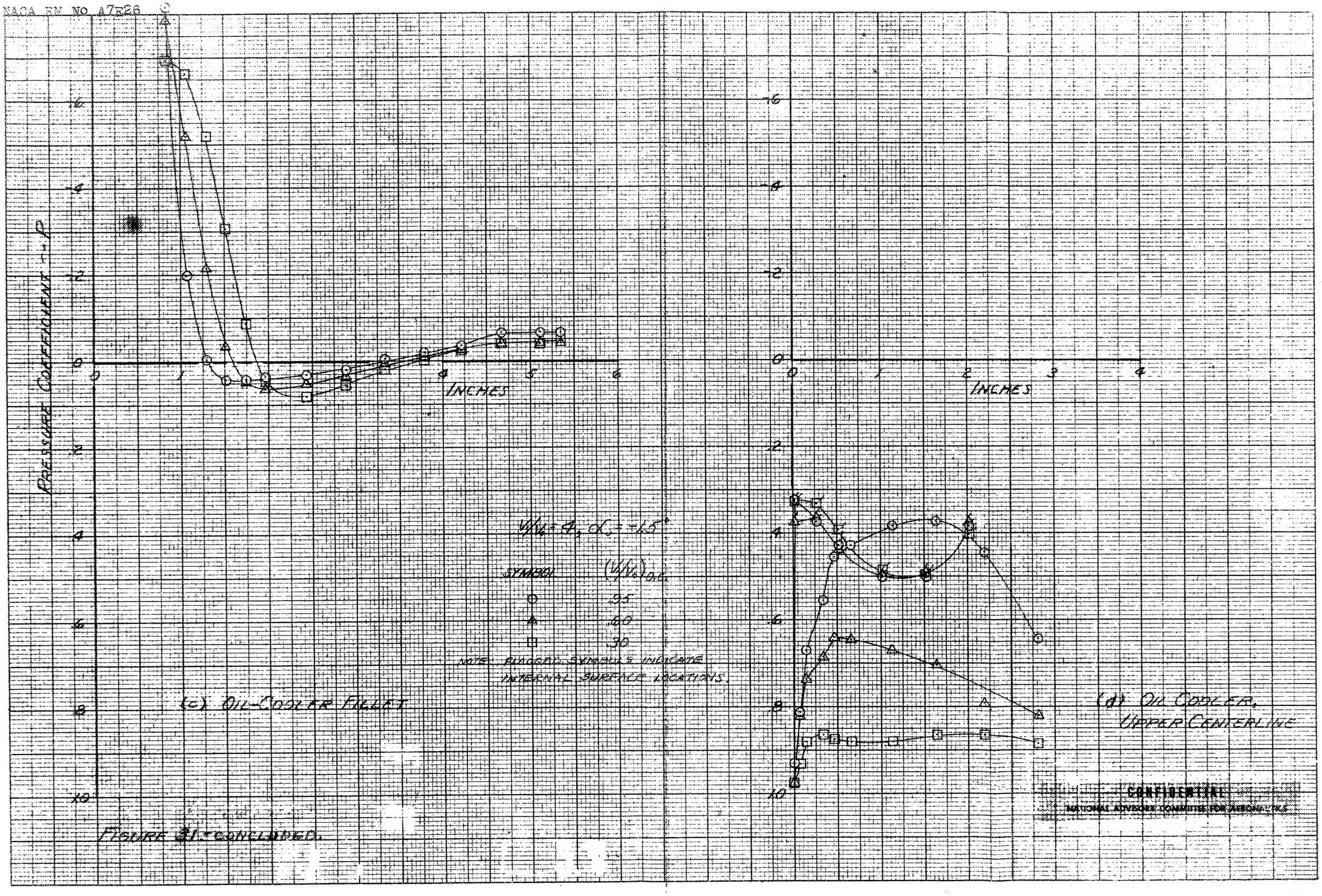

Figure 31.- Concluded.

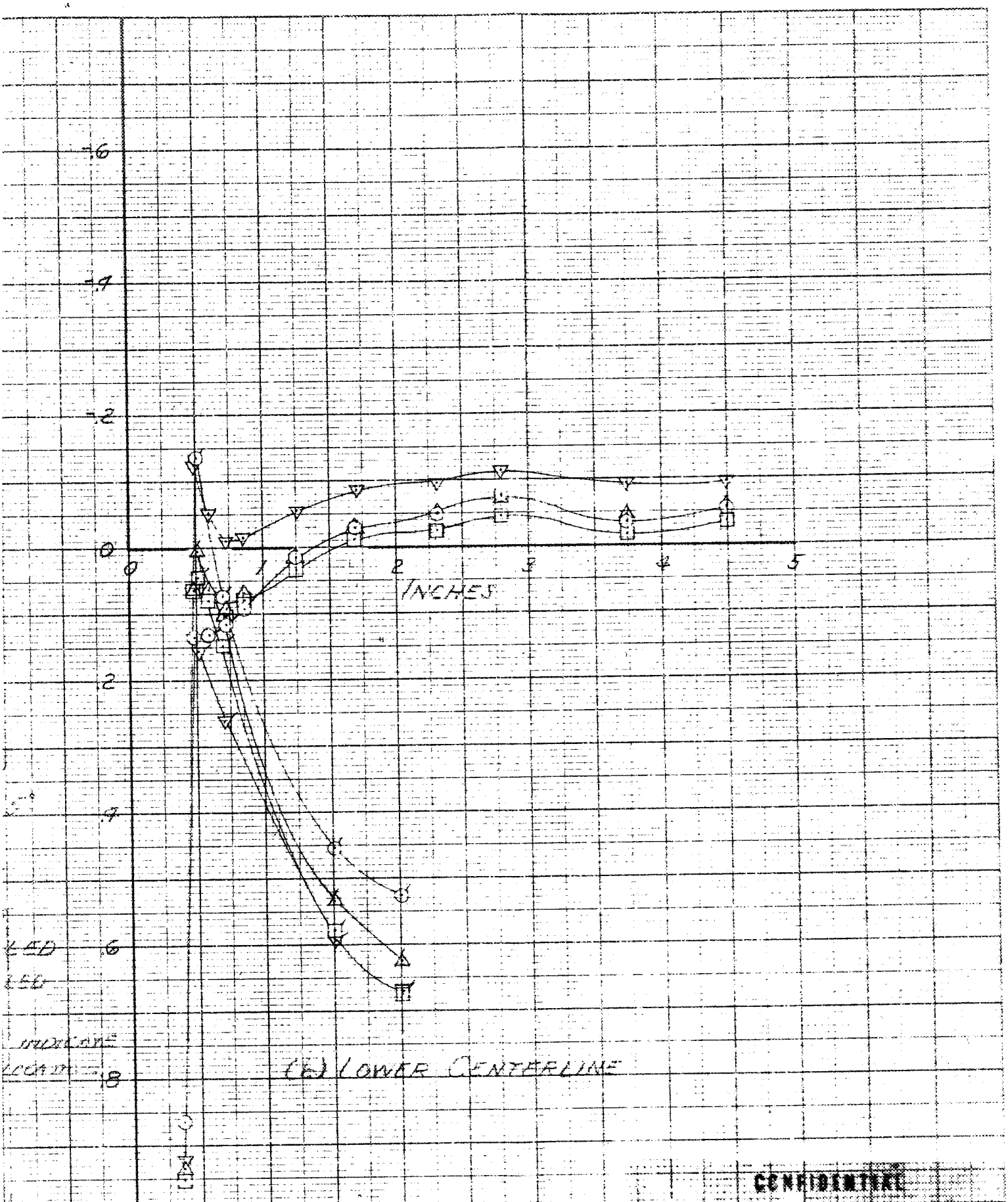

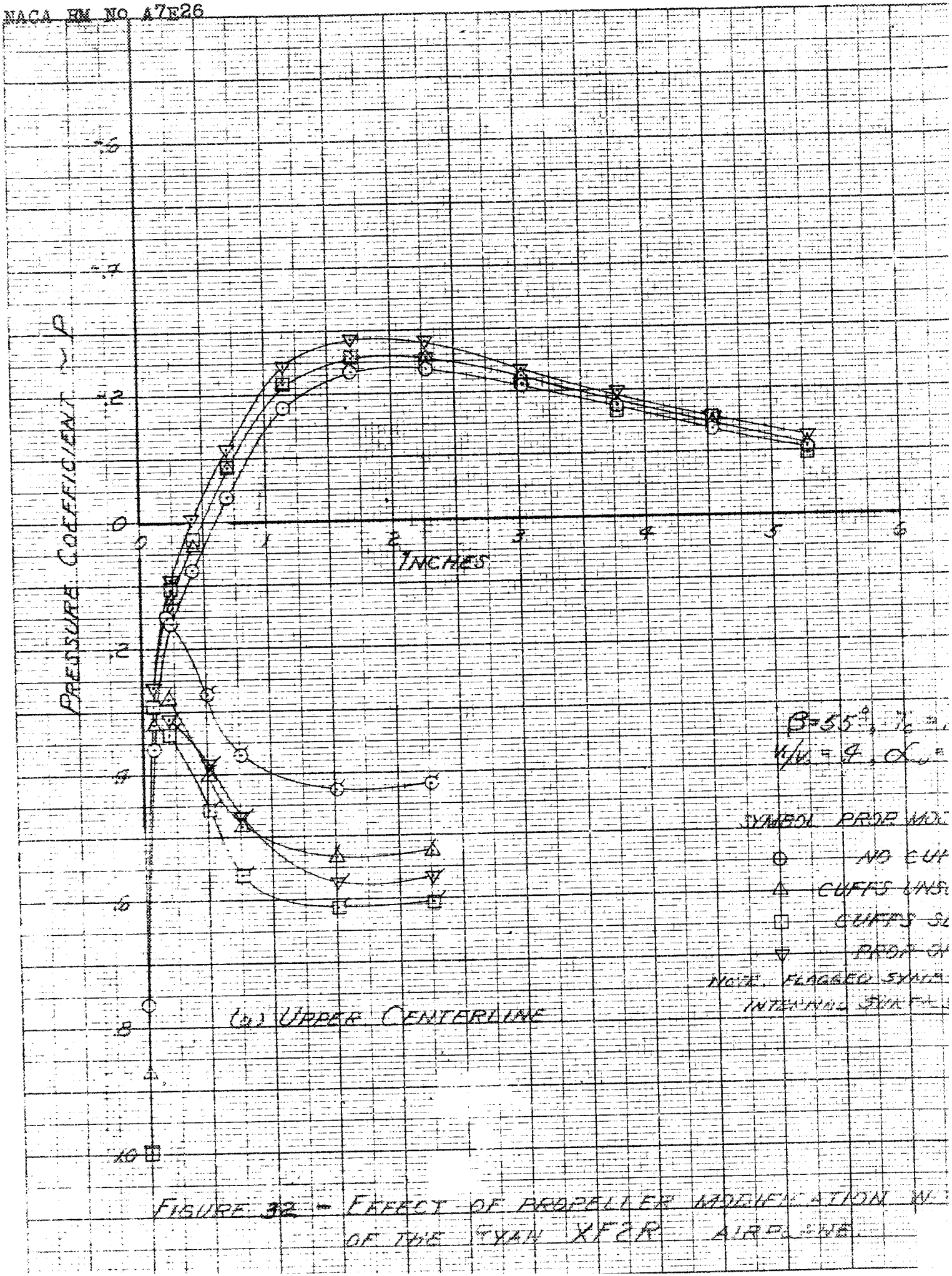

FIGURE 32 - EFFECT OF PROPELLER MODIFICATION ON
OF THE TYPE XF2R AIRPLANE

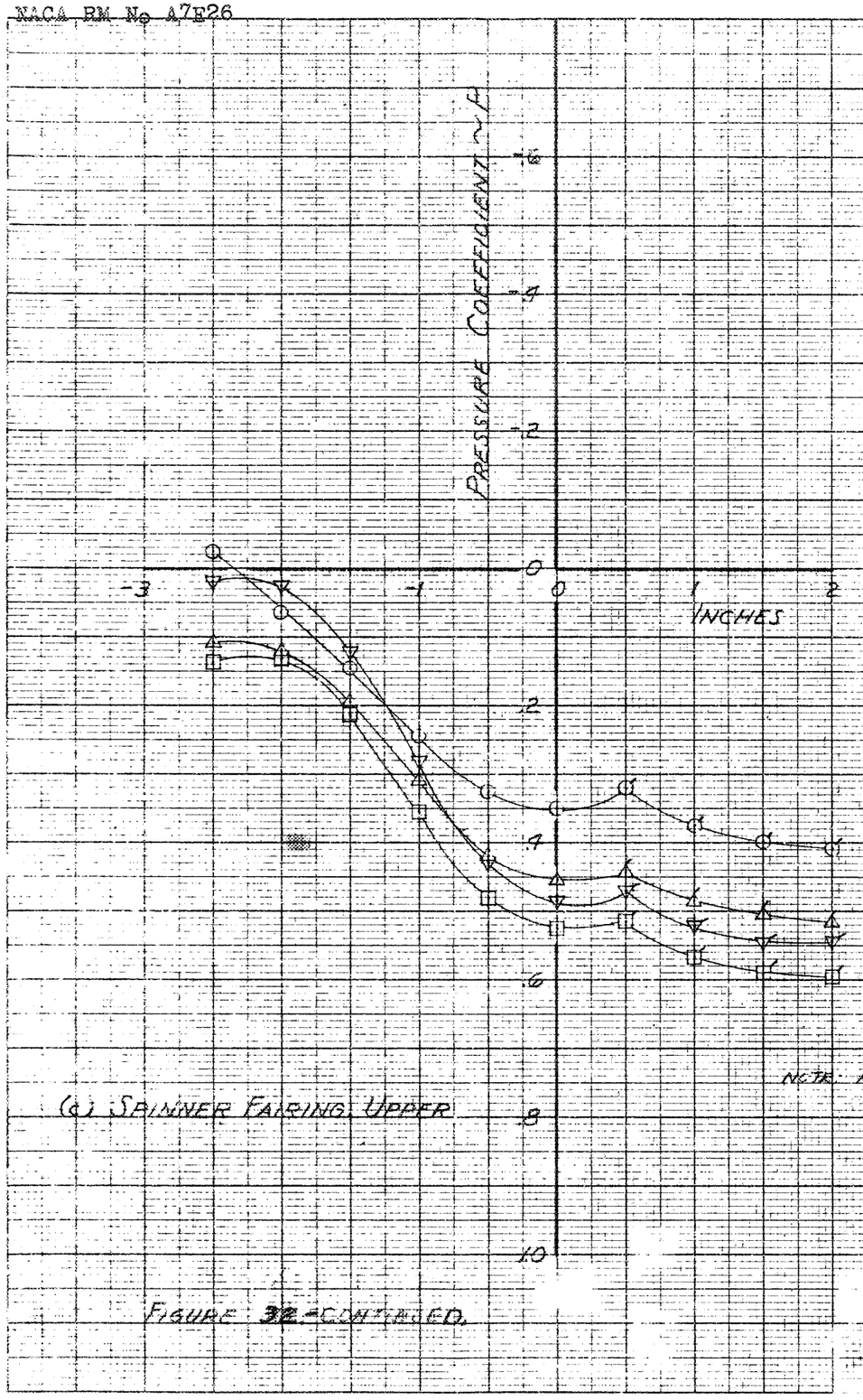

(c) SPINNER FAIRING, UPPER

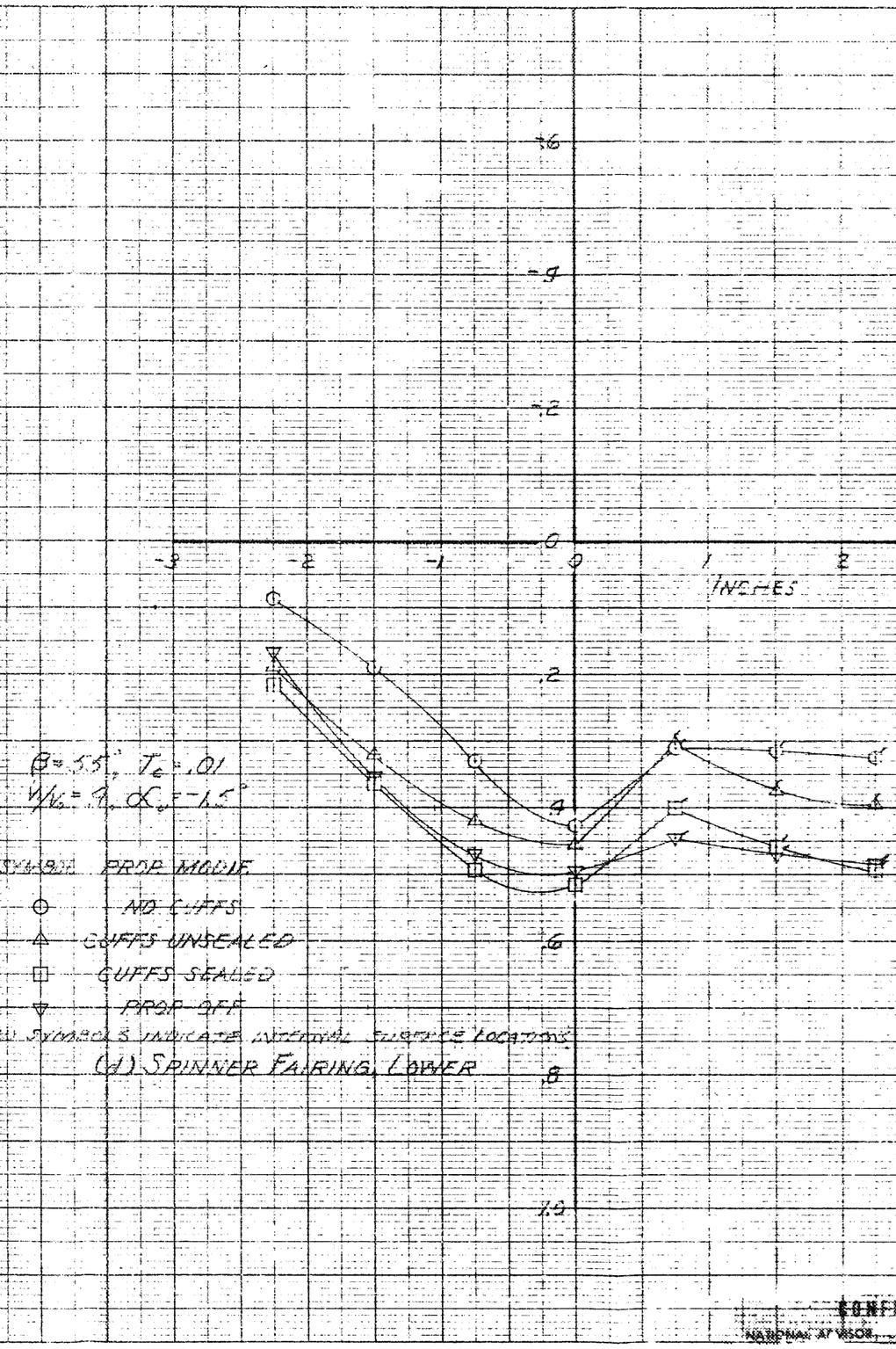

(d) SPINNER FAIRING, LOWER

FIGURE 32.- CONTINUED.

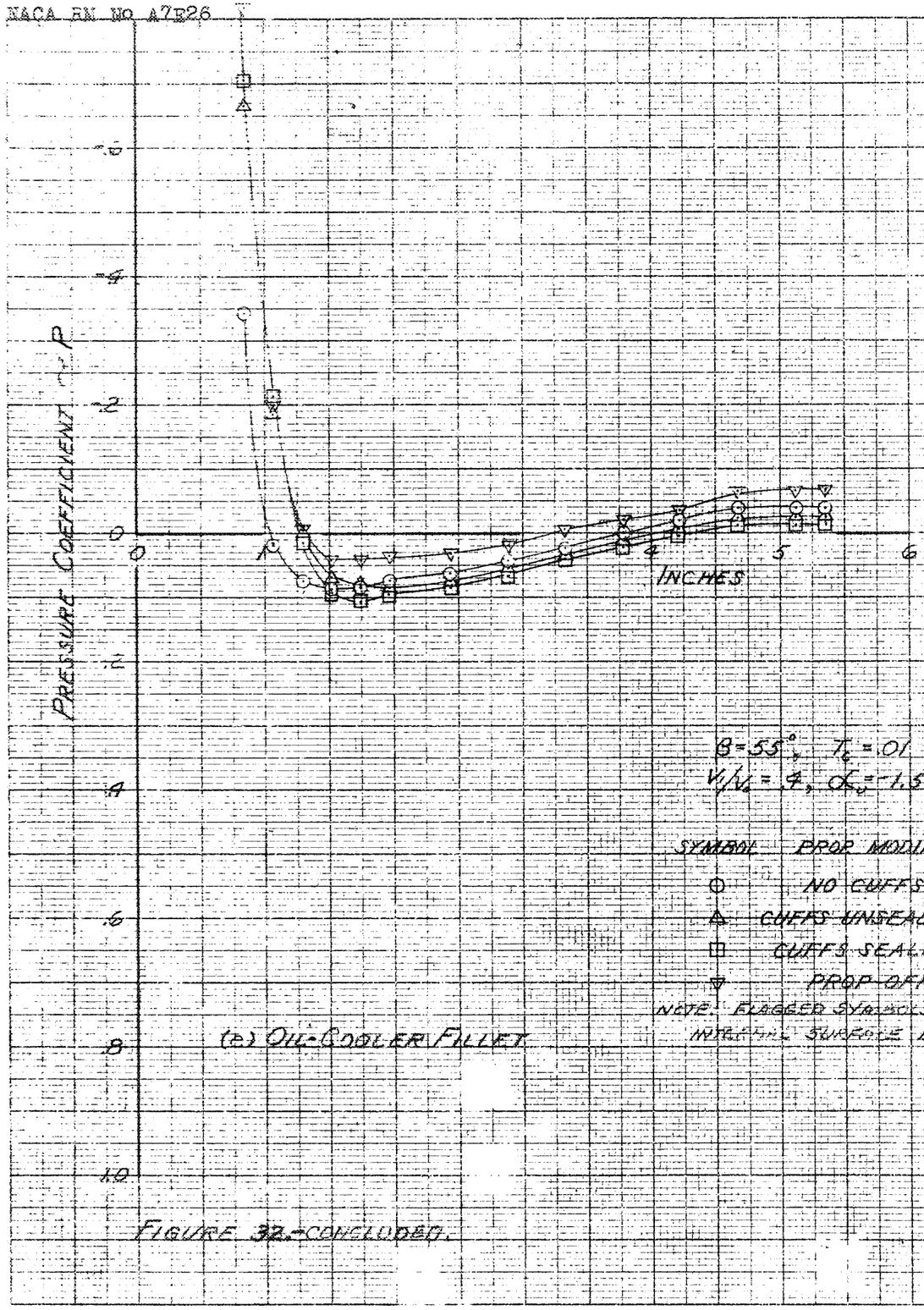

(b) Oil-Cooler Fillet

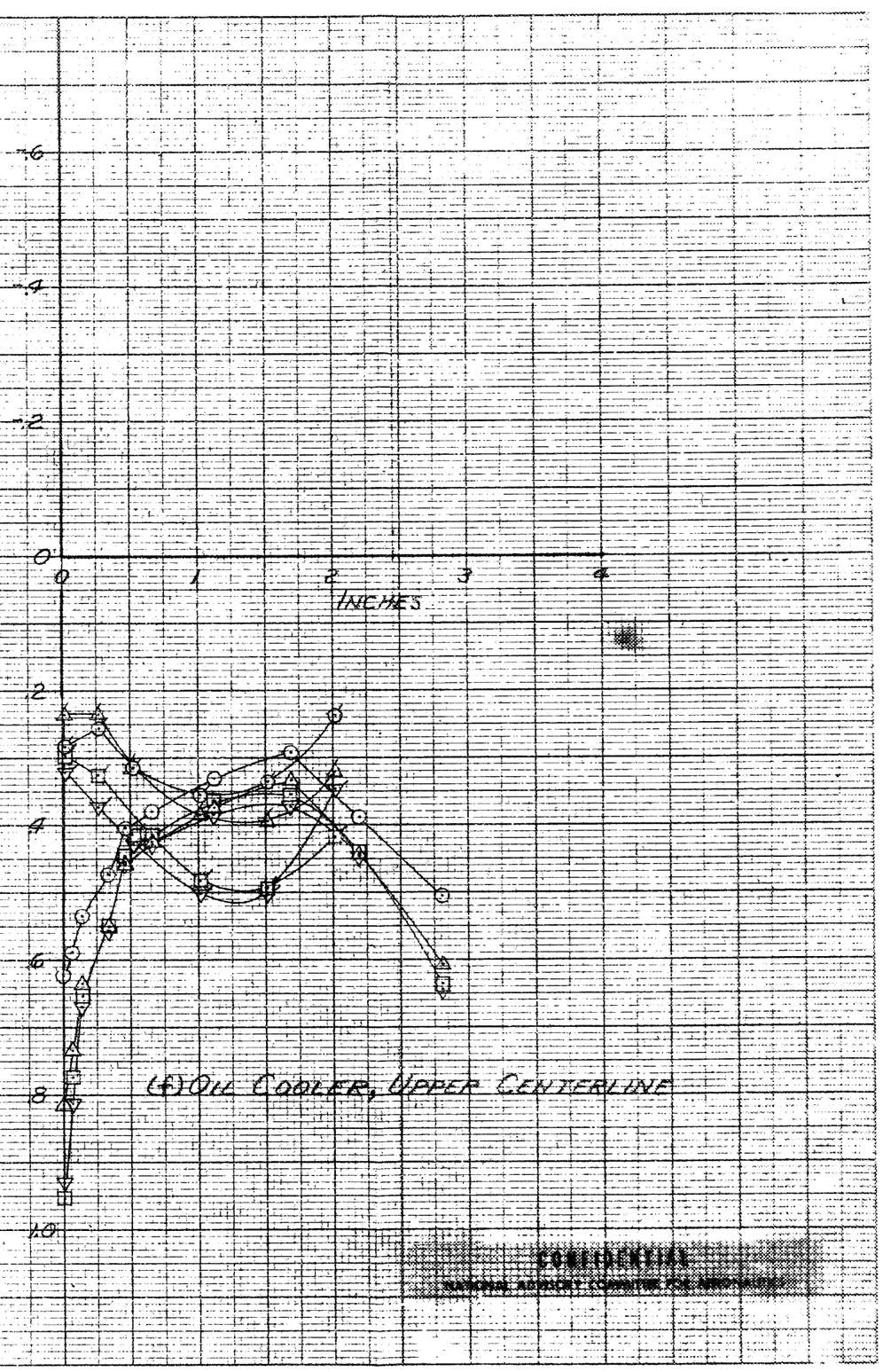

(f) Oil Cooler, Upper Centerline

FIGURE 32.- CONCLUDED.

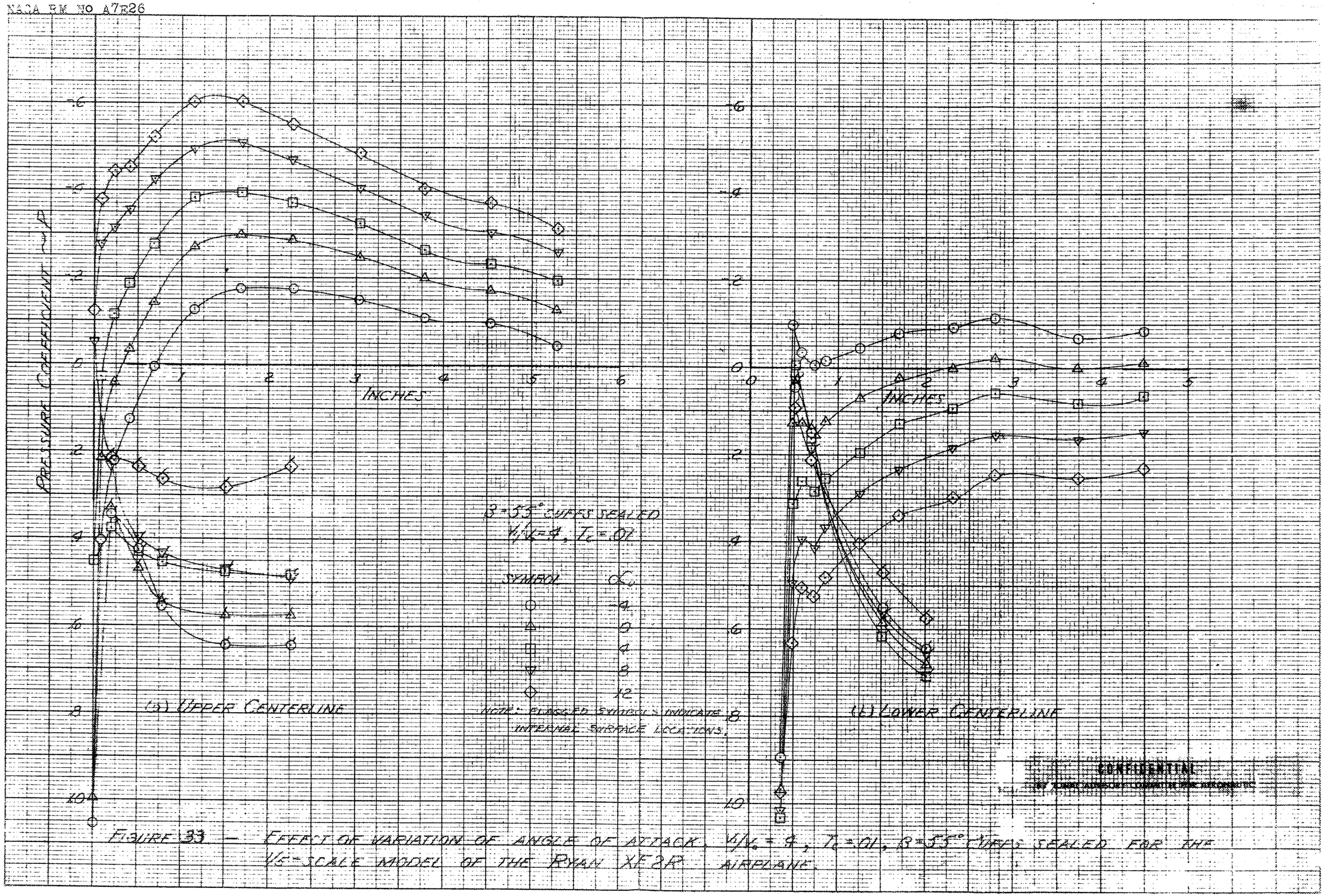

FIGURE 33 — EFFECT OF VARIATION OF ANGLE OF ATTACK, V_j/V_∞ = 4, T_c = .01, β = 55° FLAPS SEALED FOR THE 1/6-SCALE MODEL OF THE RYAN XFR AIRPLANE.

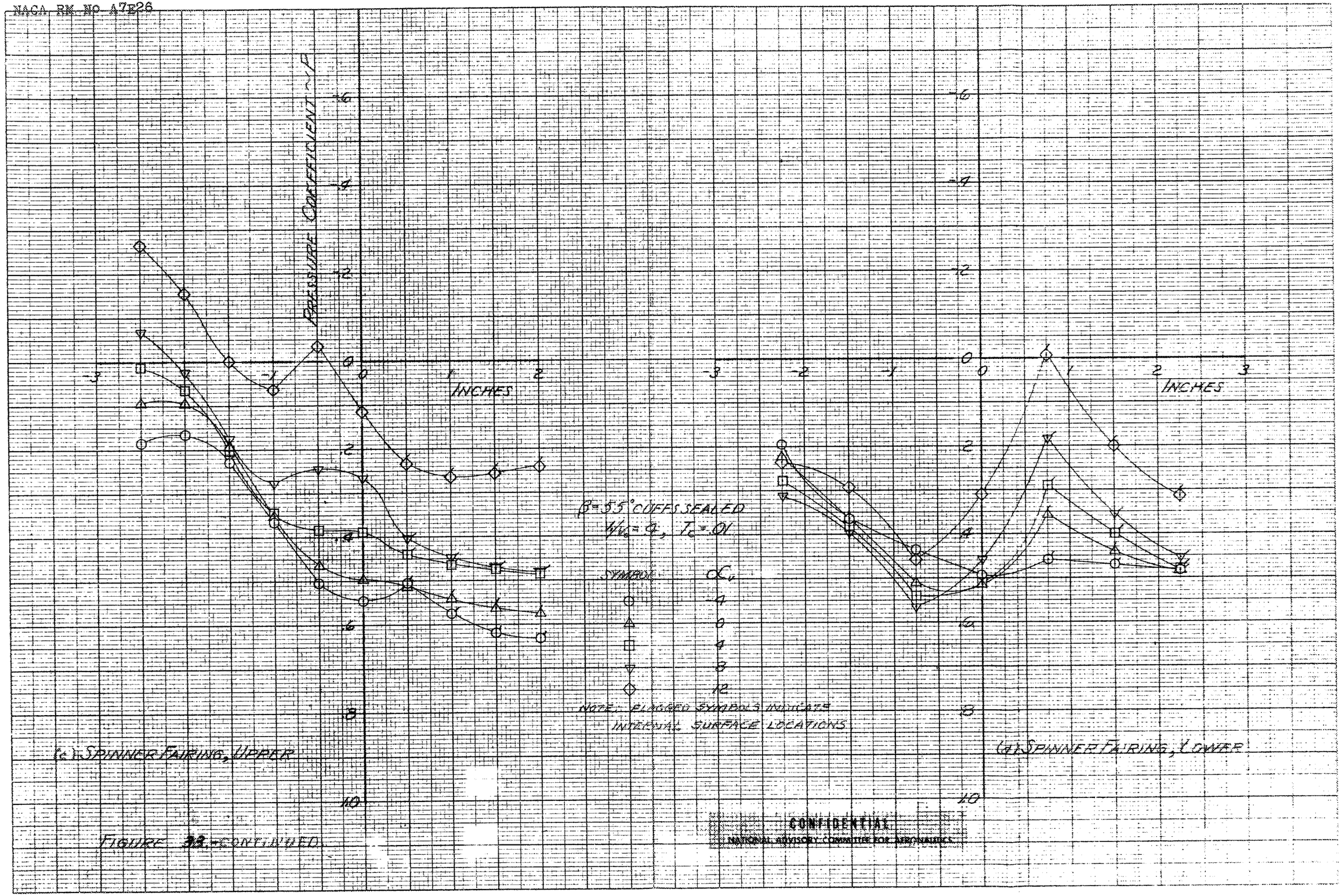

(c) Spinner Fairing, Upper

(d) Spinner Fairing, Lower

FIGURE 32.- CONTINUED.

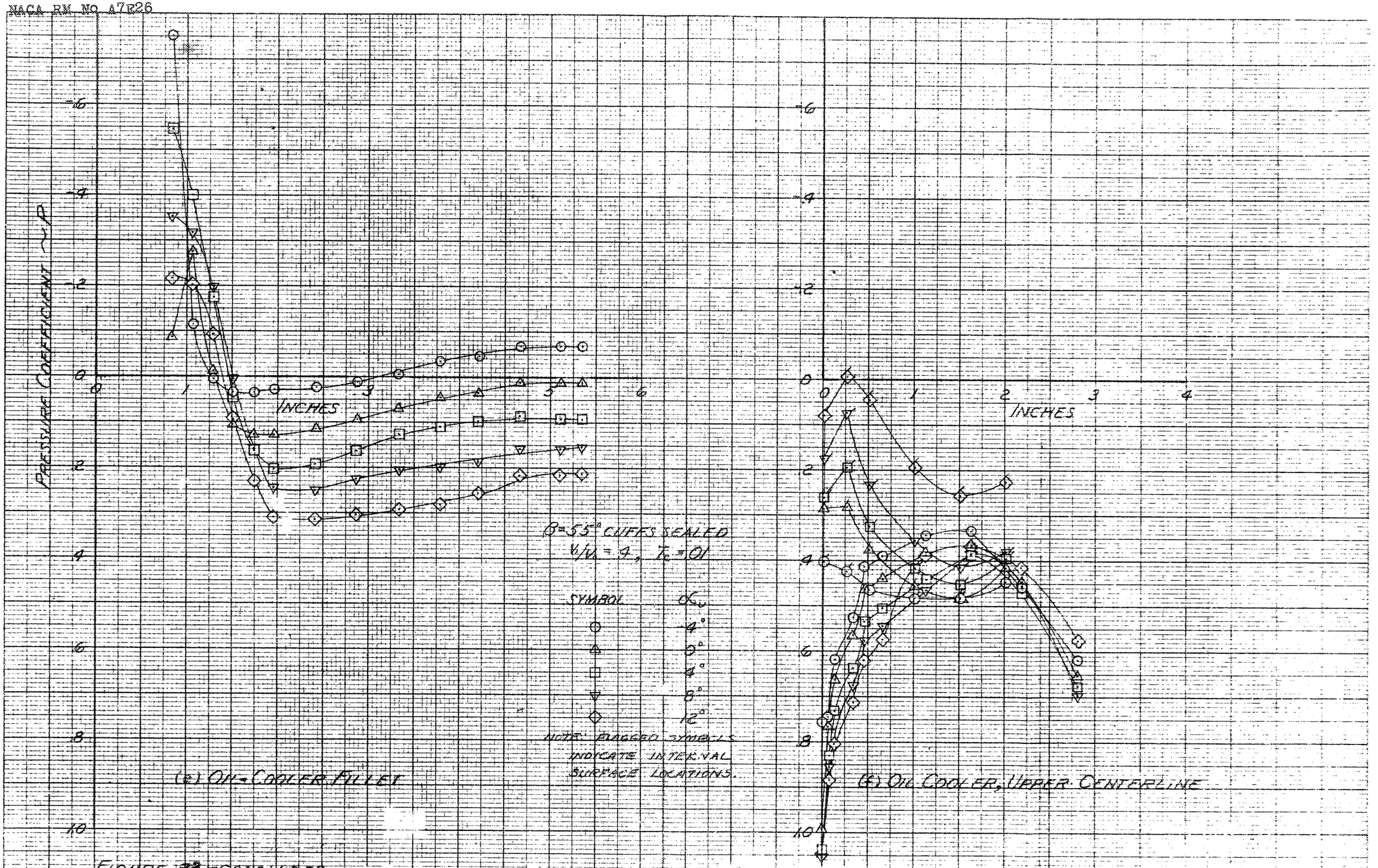

FIGURE 23.- CONCLUDED.

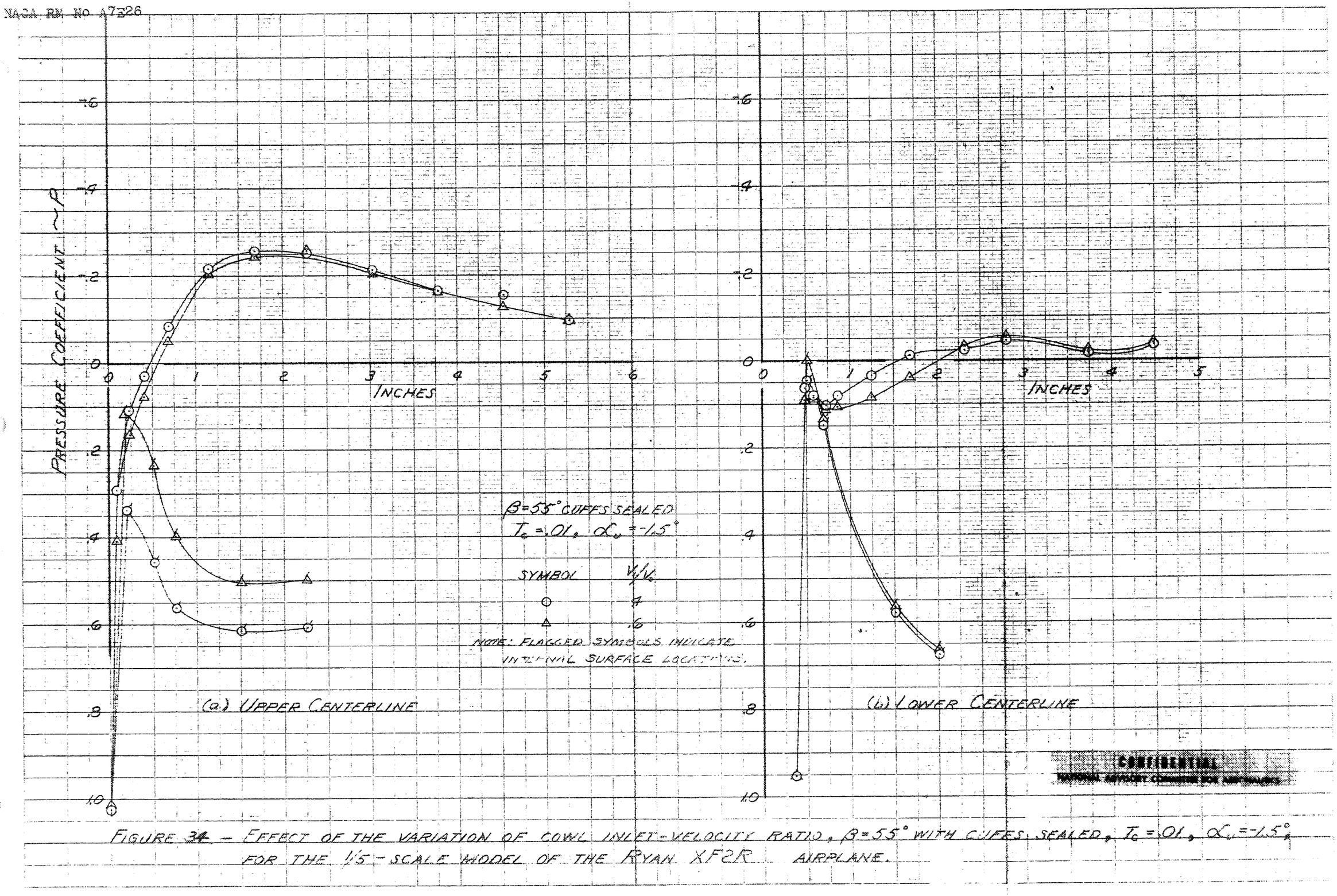

FIGURE 34 – EFFECT OF THE VARIATION OF COWL INLET-VELOCITY RATIO, $\beta = 55°$ WITH CUFFS SEALED, $T_c = .01$, $\alpha_c = -1.5°$, FOR THE 1/5-SCALE MODEL OF THE RYAN XF2R AIRPLANE.

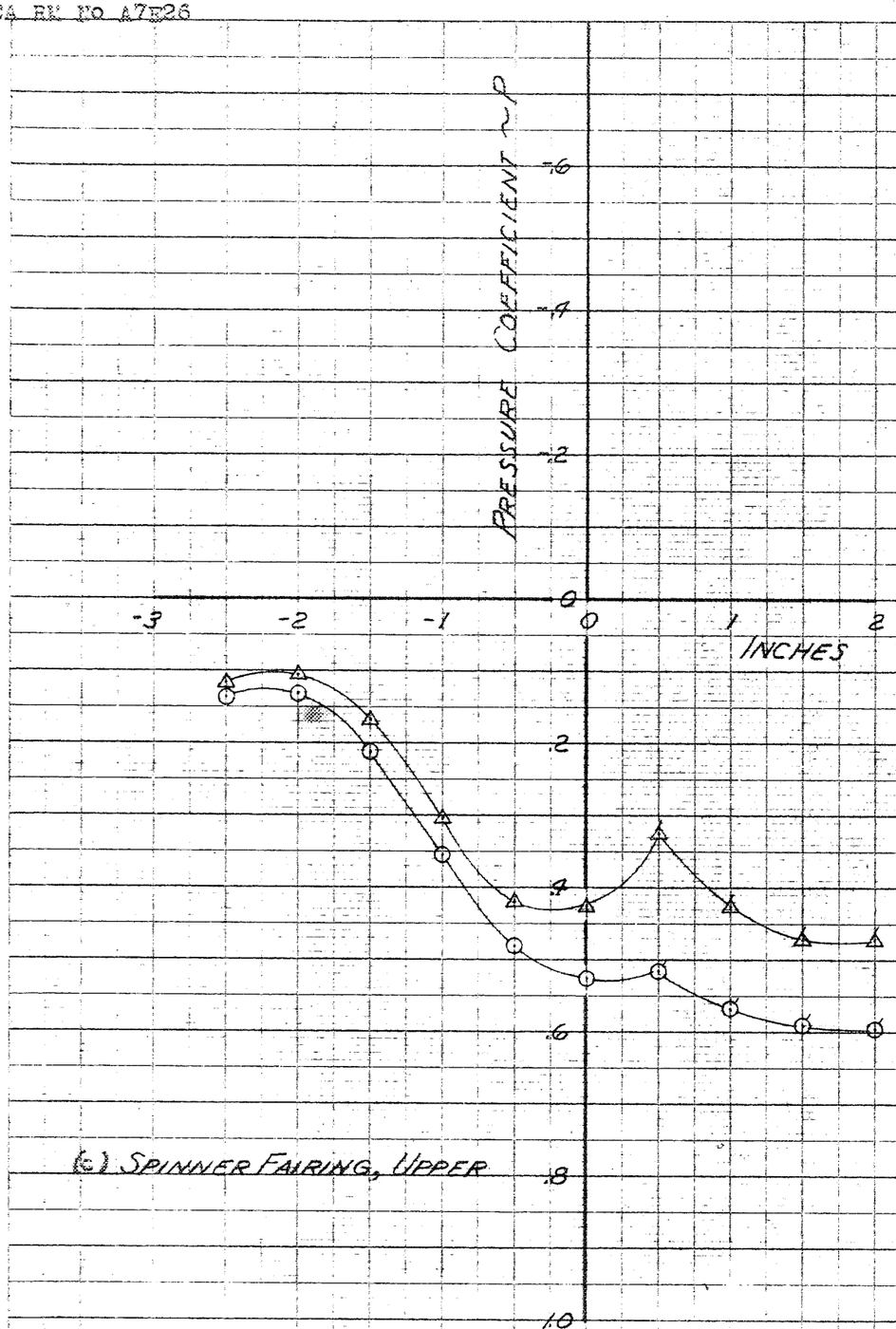

(c) SPINNER FAIRING, UPPER

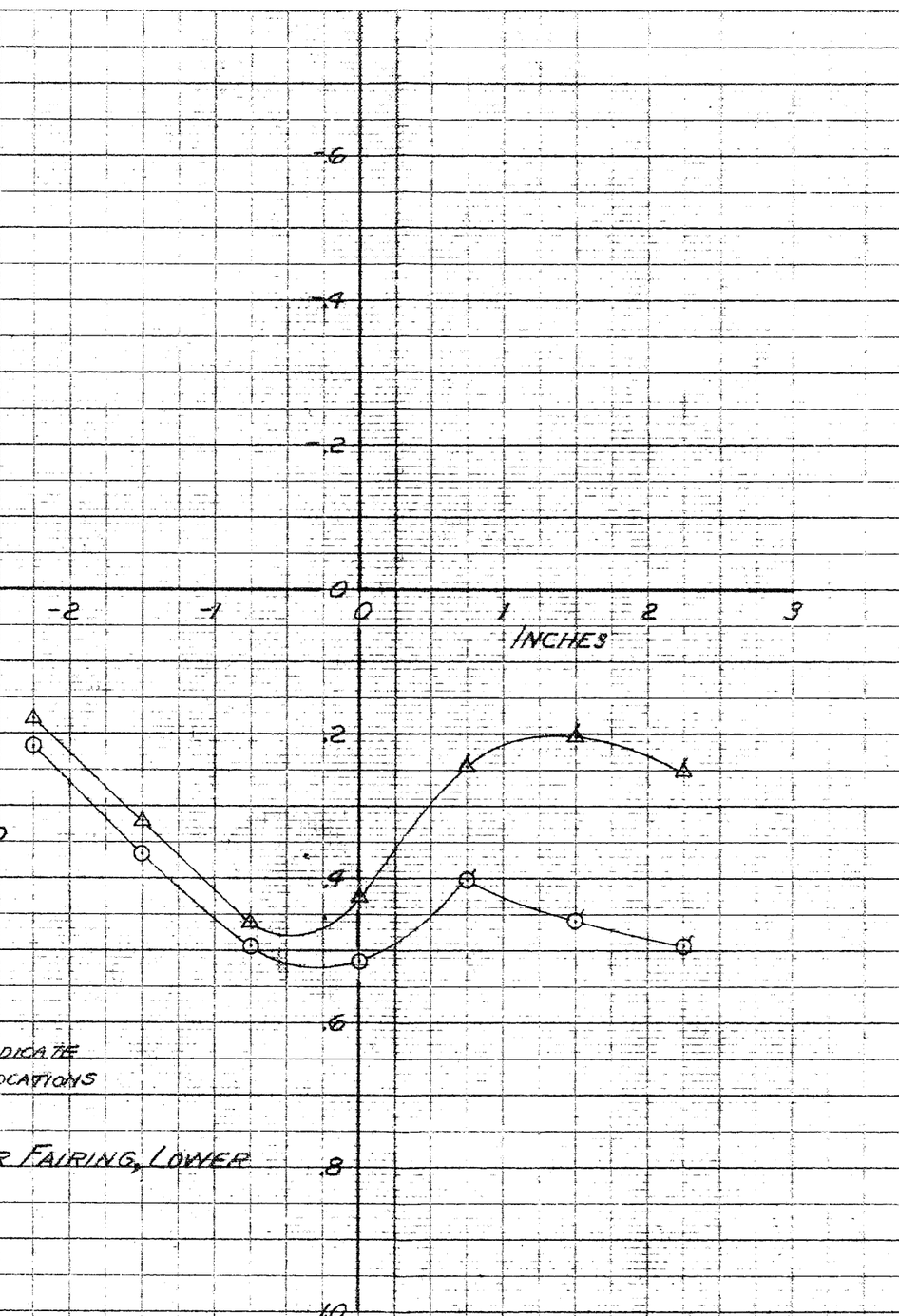

(d) SPINNER FAIRING, LOWER

$\beta = 35°$ CUFFS SEALED
$T_c = .01$, $\alpha_c = -1.5°$

SYMBOL	V_j/V_o
○	4
△	6

NOTE: FLAGGED SYMBOLS INDICATE INTERNAL SURFACE LOCATIONS

FIGURE 34.- CONTINUED.

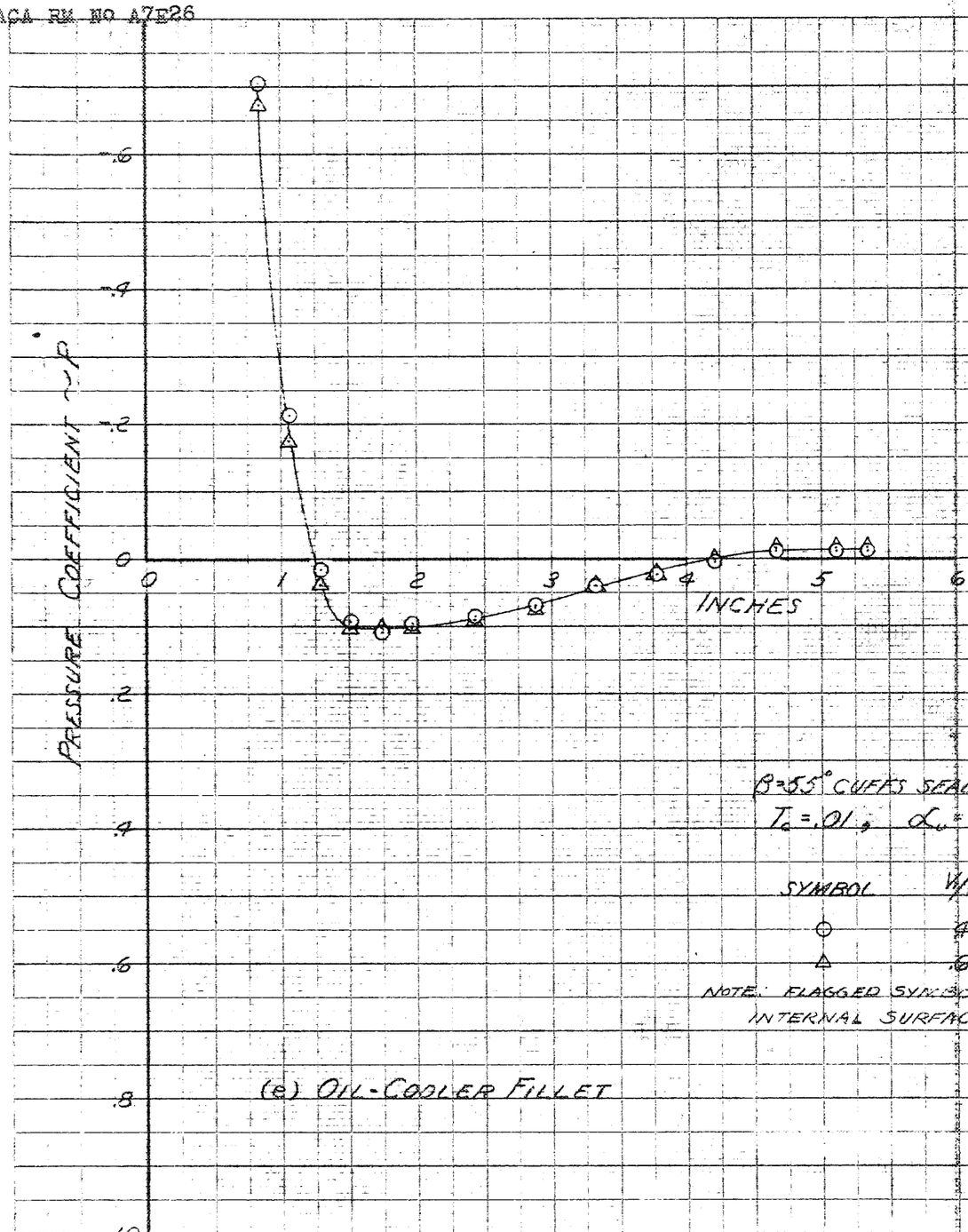

(e) Oil-Cooler Fillet

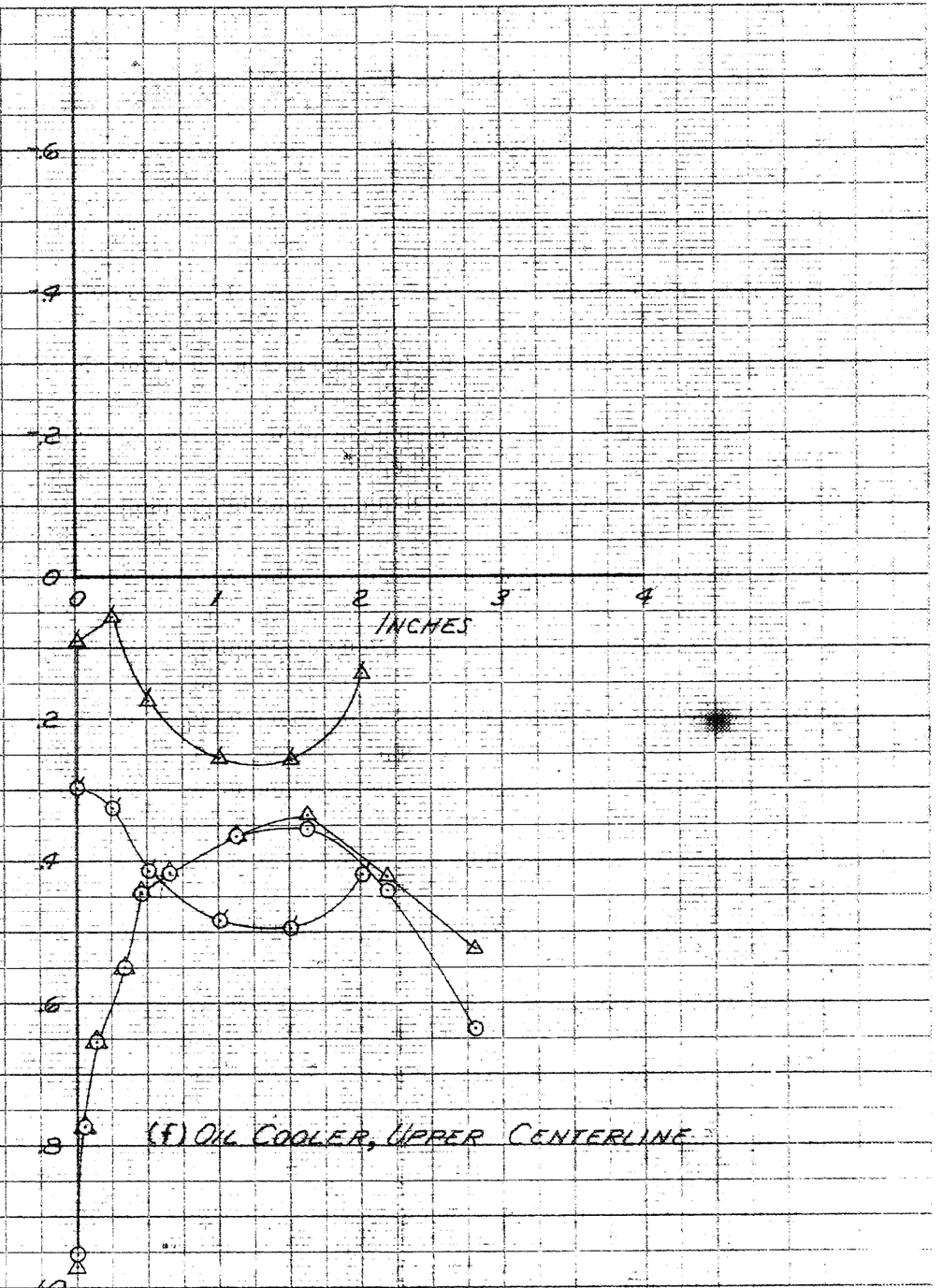

(f) Oil Cooler, Upper Centerline

FIGURE 34.- CONCLUDED.

SYM.	CONDITION	β	T_c	V/V_∞	α_a
⊙	HIGH SPEED	55	.01	.4	-1.5
△	CLIMB	45	.07	.7	2
⊞	TAKE-OFF	35	1.0	2.0	10

NOTE: FLAGGED SYMBOLS INDICATE INTERNAL SURFACE ACCELERATION.

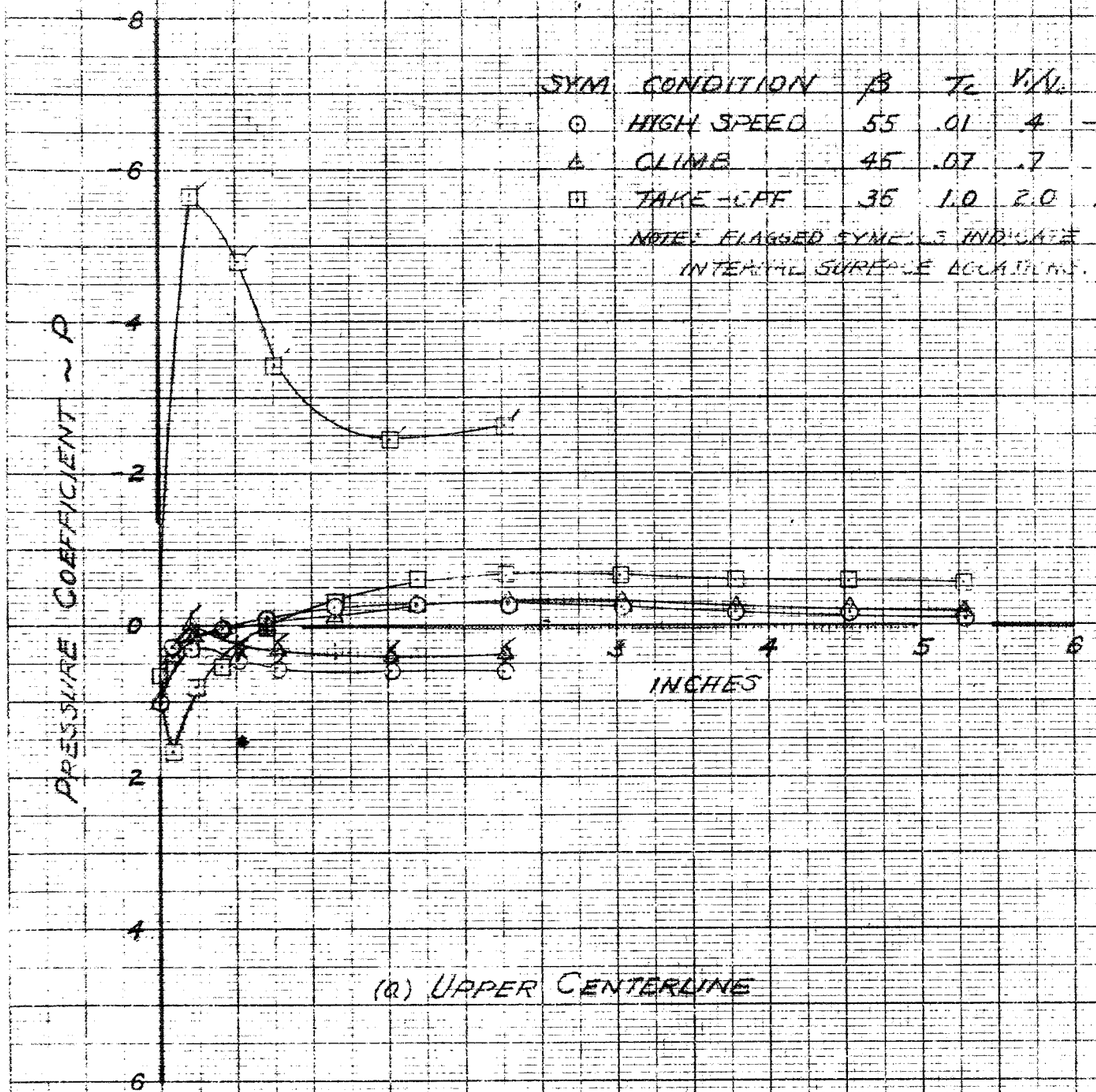

(a) UPPER CENTERLINE

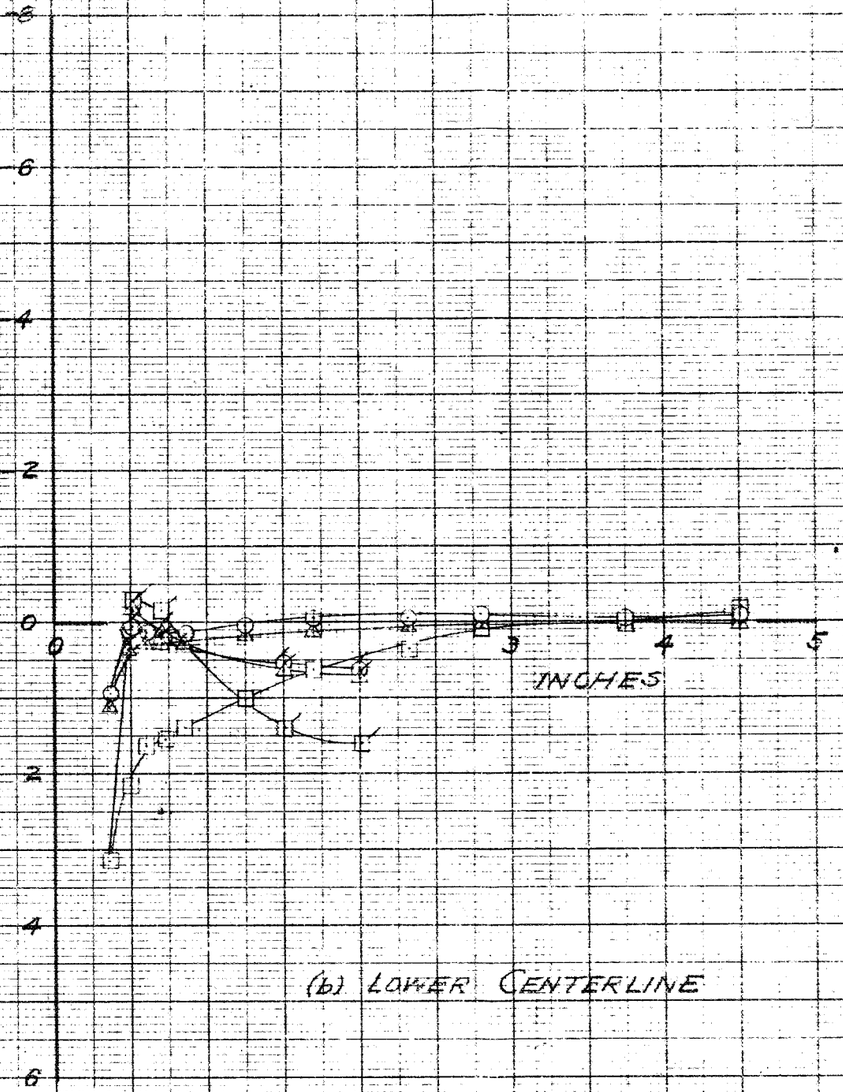

(b) LOWER CENTERLINE

FIGURE 35. - PRESSURE DISTRIBUTION FOR THE HIGH SPEED, CLIMB, AND TAKE-OFF CONDITIONS WITH THE PROPELLER WITH SEALED CUFFS. 1/5-SCALE MODEL OF THE RYAN XFR-1 AIRPLANE.

SYM	CONDITION	β	T_c	V_1/V_0	α_u
○	HIGH SPEED	55	.01	.4	-1.5
△	CLIMB	45	.07	.7	2
□	TAKE-OFF	35	1.0	2.0	10

NOTE: FLAGGED SYMBOLS INDICATE INTERNAL SURFACE LOCATIONS.

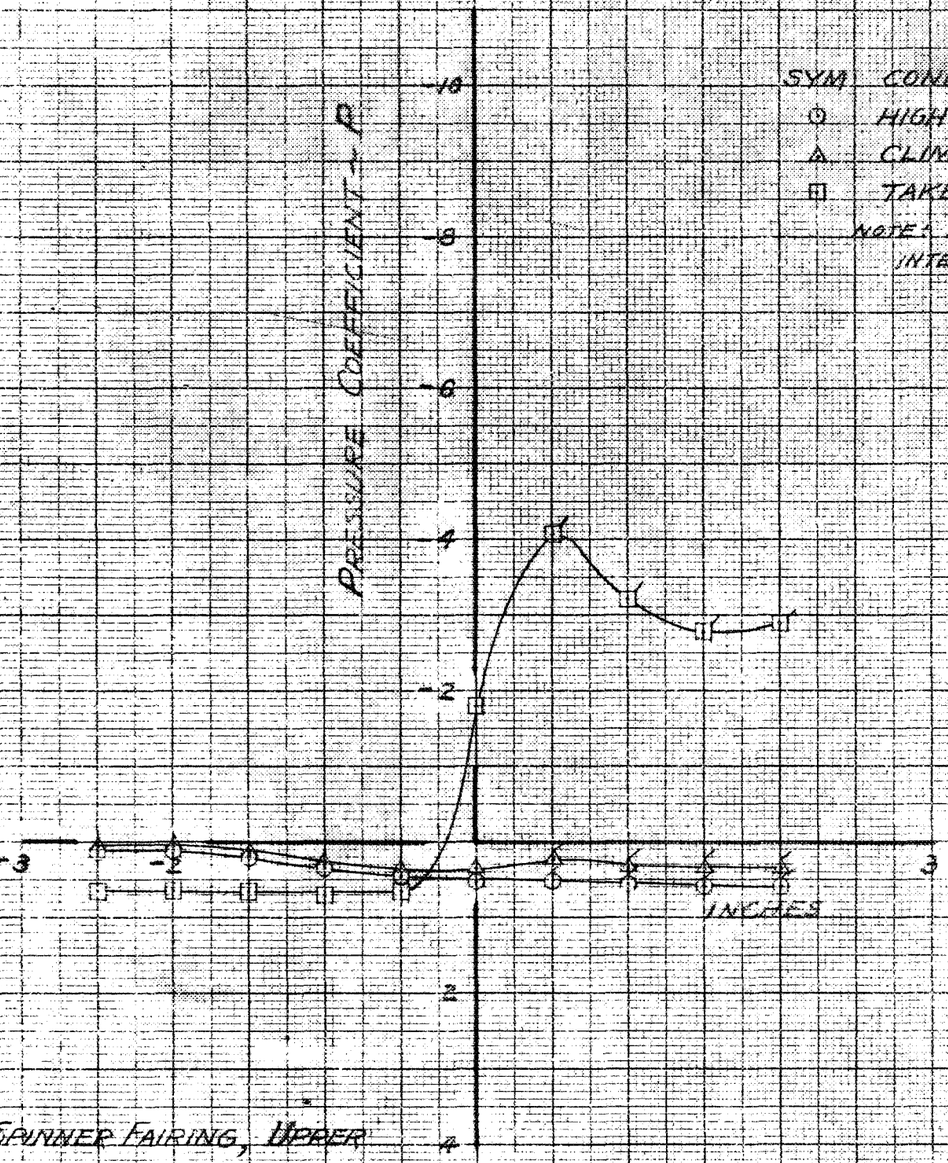

(c) SPINNER FAIRING, UPPER

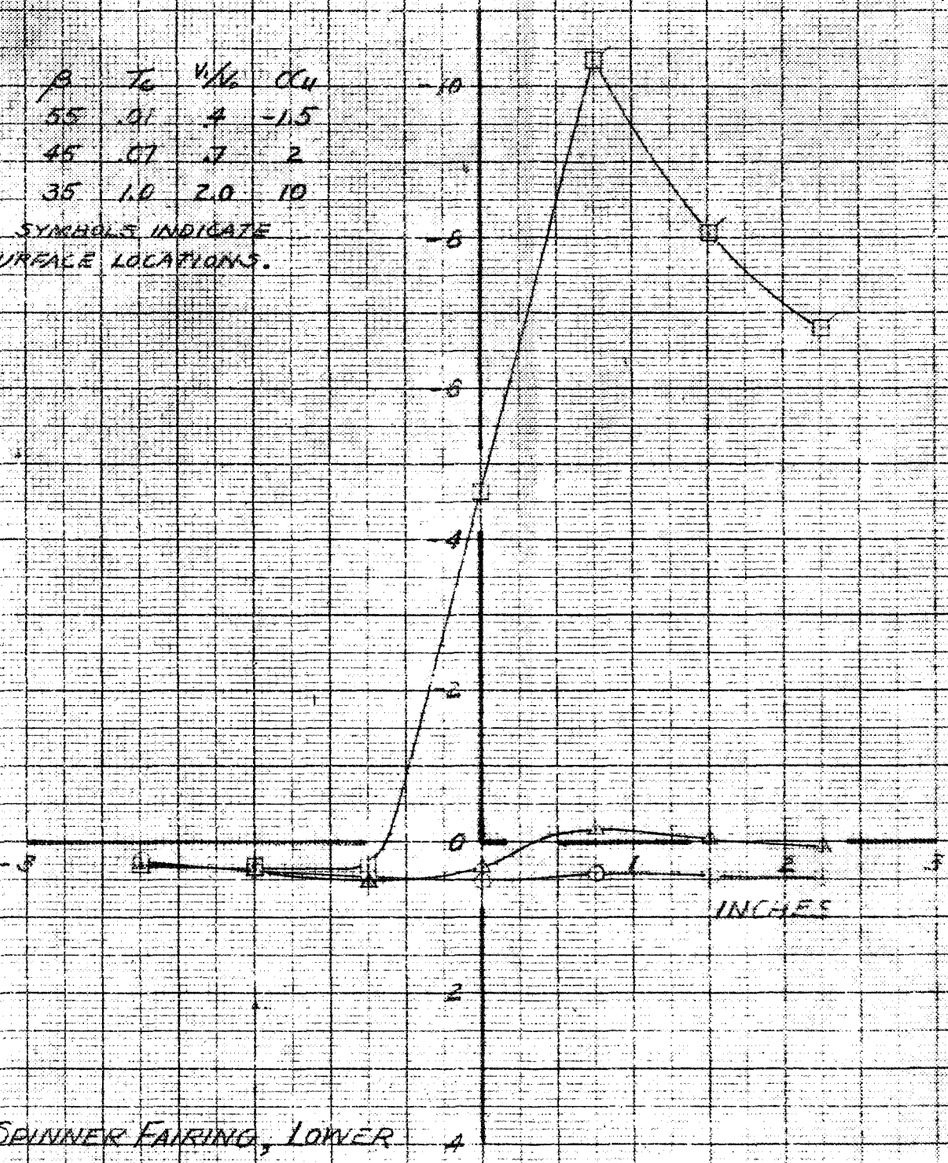

(d) SPINNER FAIRING, LOWER

FIGURE 35 - CONTINUED. 1/5-SCALE MODEL OF THE RYAN XF2R AIRPLANE.

SYM	CONDITION	β	T_c	V/V_∞	$\delta\alpha_u$
○	HIGH SPEED	55	.01	.4	-1.5
△	CLIMB	45	.07	.7	2
□	TAKE-OFF	35	1.0	2.0	10

NOTE: FLAGGED SYMBOLS INDICATE INTERNAL SURFACE LOCATIONS.

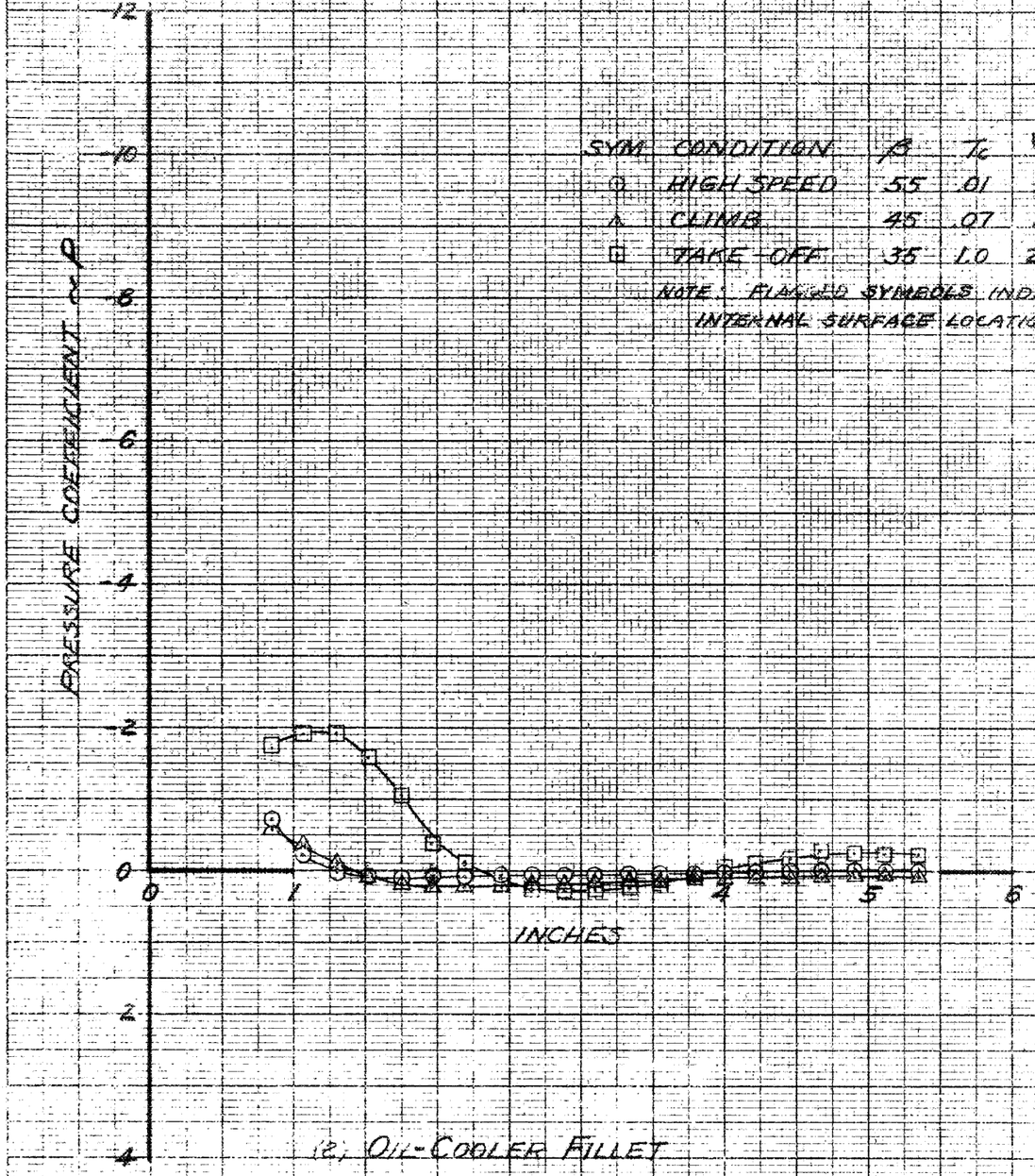

(e) OIL-COOLER FILLET

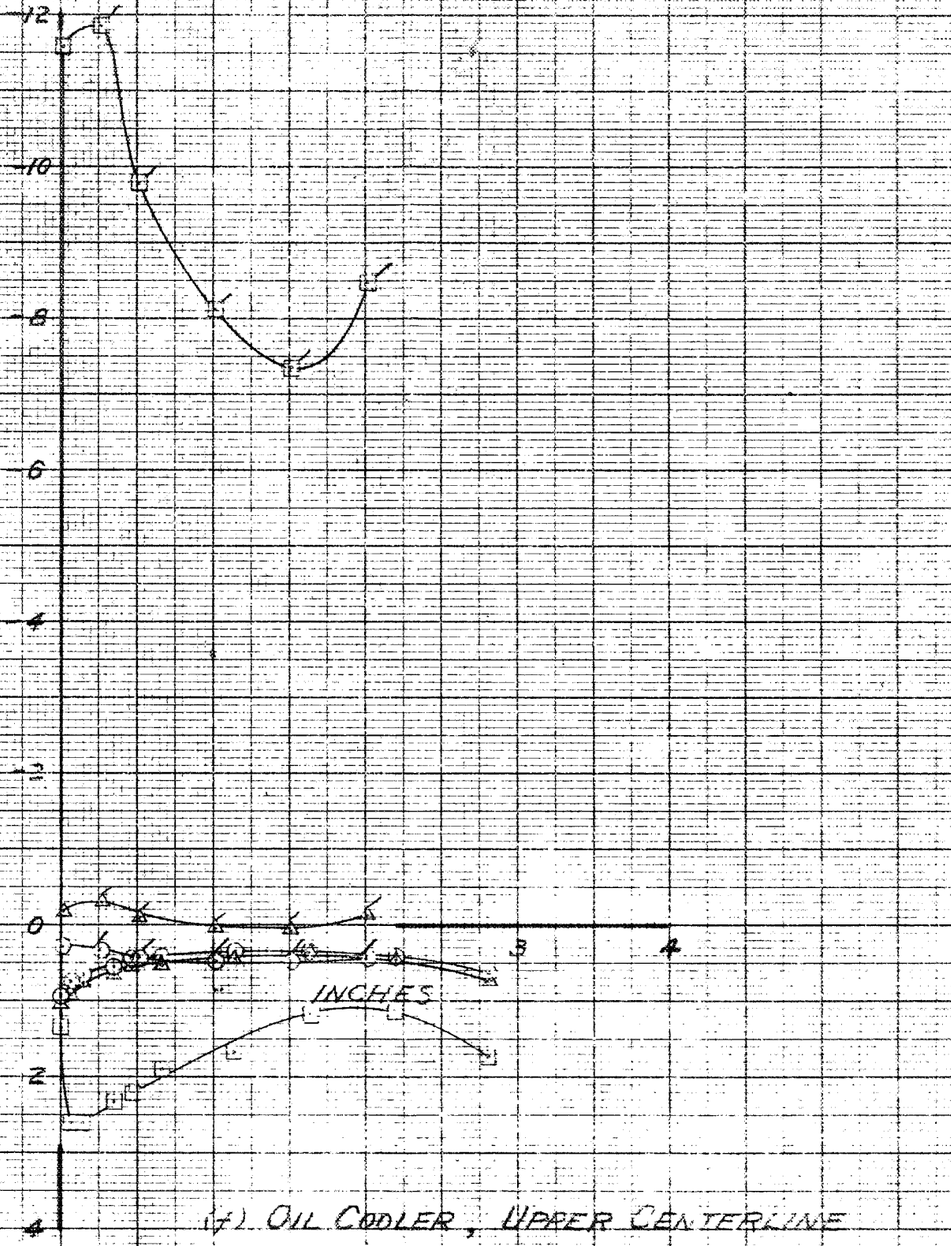

(f) OIL COOLER, UPPER CENTERLINE

CONFIDENTIAL

NATIONAL ADVISORY COMMITTEE FOR AERONAUTICS

FIGURE 35.- CONCLUDED. 1/5-SCALE MODEL OF THE F-80A XF2R AIRPLANE

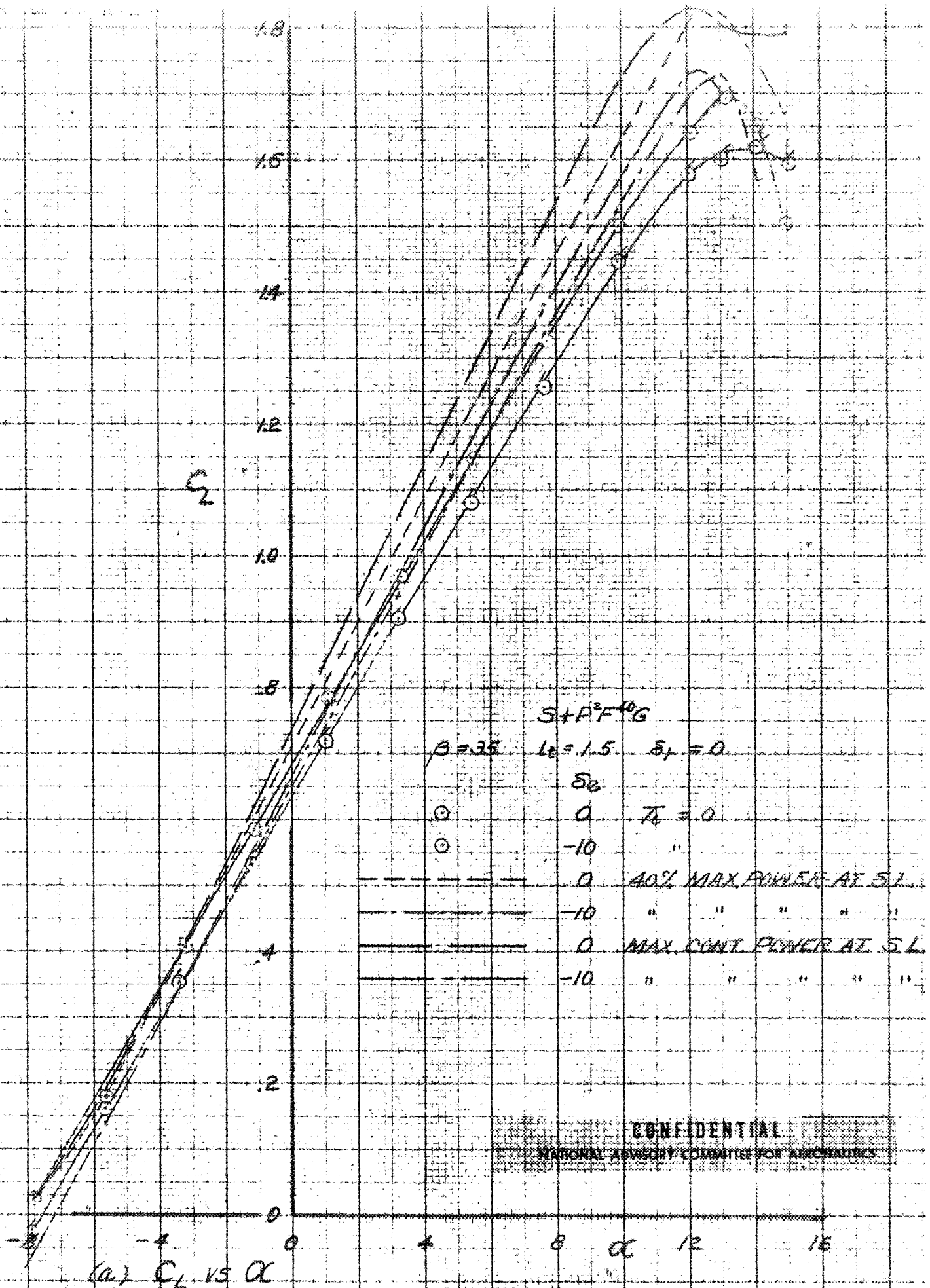

(a) C_L vs α

FIGURE 36.—EFFECT OF POWER ON THE AERODYNAMIC CHARACTERISTICS OF THE 1/5-SCALE MODEL OF THE RYAN XF2R AIRPLANE. FLAPS 40°

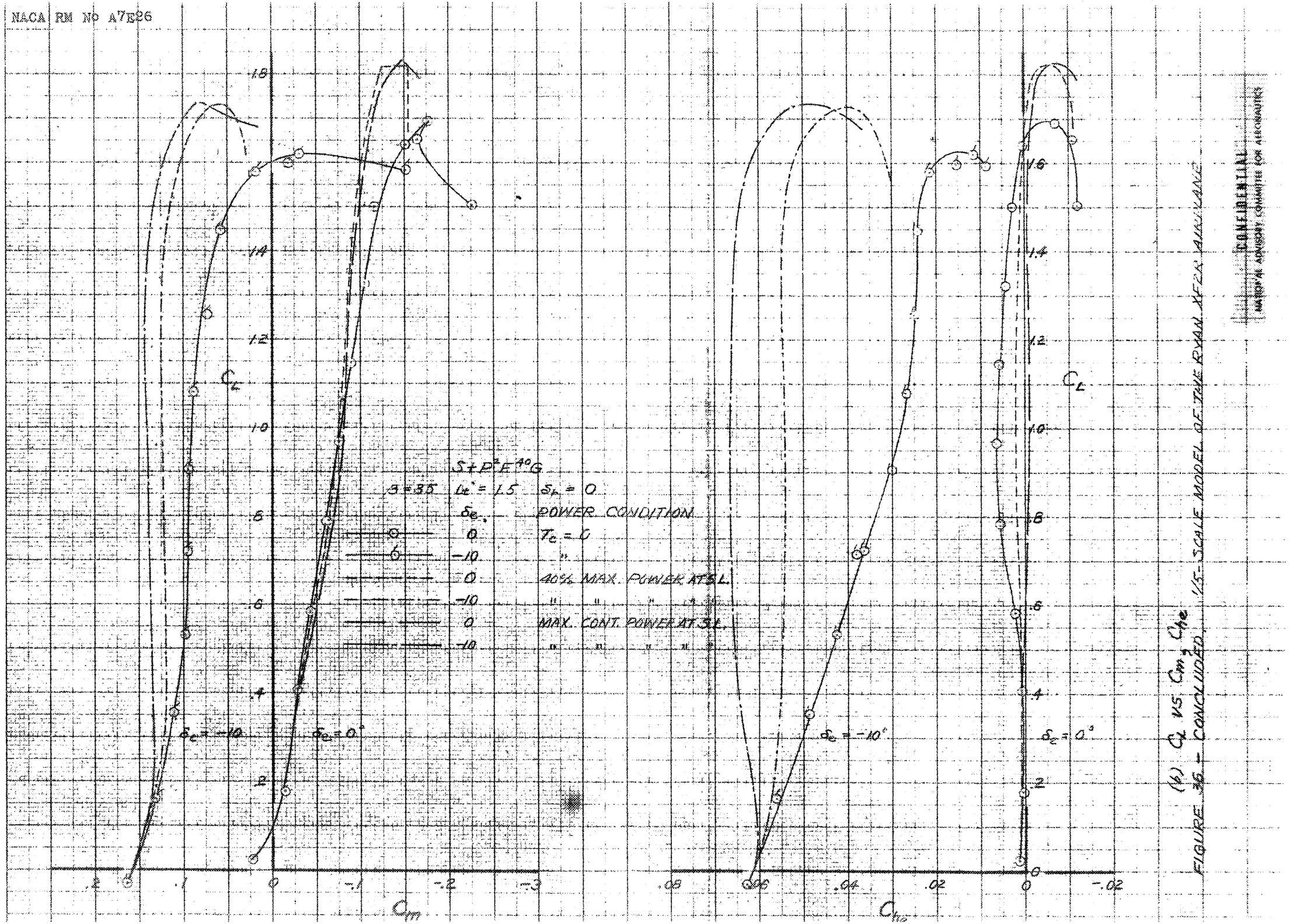

CONFIDENTIAL
NATIONAL ADVISORY COMMITTEE FOR AERONAUTICS

FIGURE 36 - CONCLUDED. 1/5-SCALE MODEL OF THE RYAN XF2R AIRPLANE

(b) C_L vs C_m, C_{m_c}

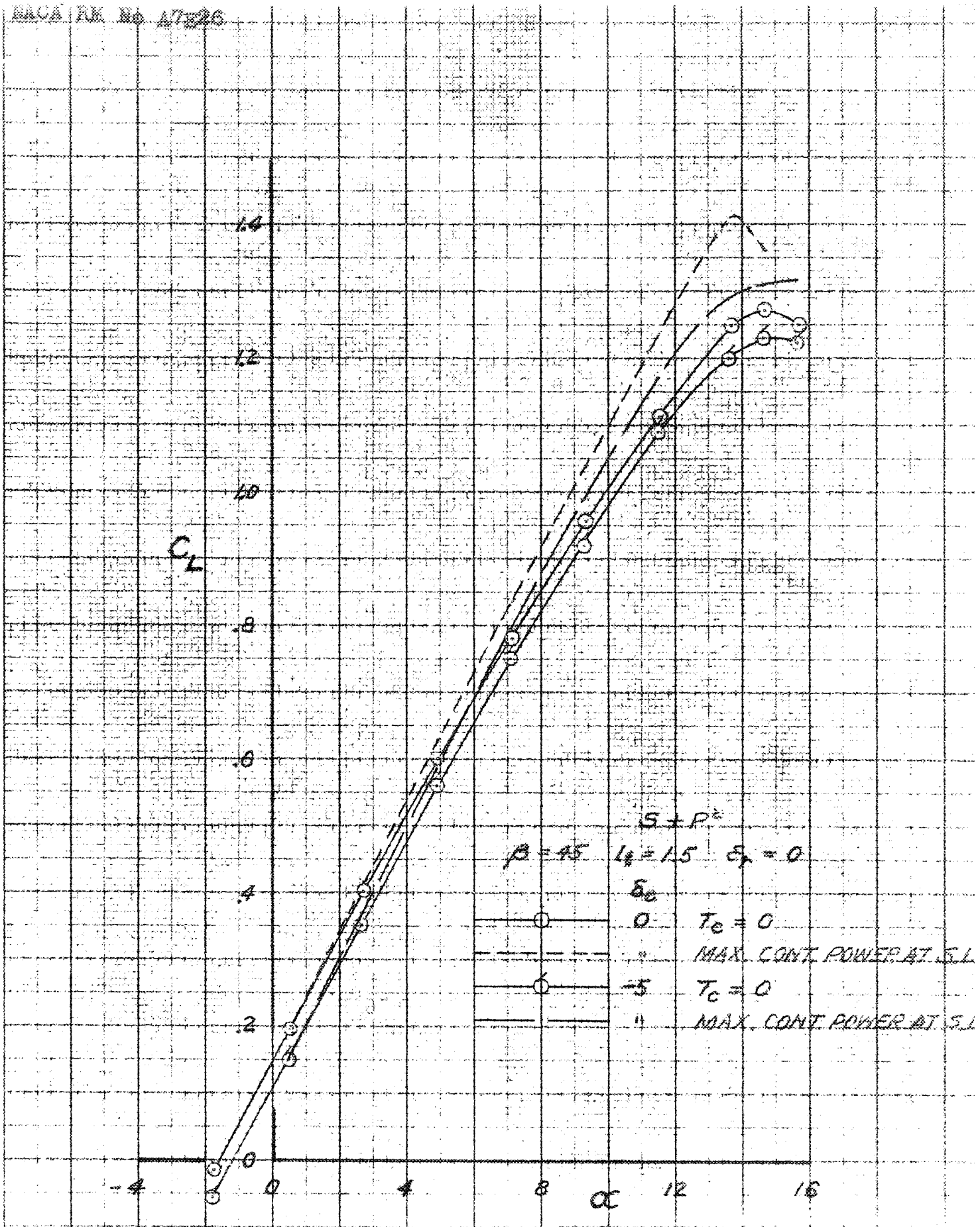

CONFIDENTIAL
NATIONAL ADVISORY COMMITTEE FOR AERONAUTICS

(a) C_L vs. α

FIGURE 37.- EFFECT OF POWER ON THE AERODYNAMIC CHARACTERISTICS OF THE 1/5-SCALE MODEL OF THE RYAN XFZR AIRPLANE. FLAPS

FIGURE 37 - CONCLUDED. (b) C_L VS C_m, $C_{m_{tc}}$. 1/15-SCALE MODEL OF THE RYAN XF2R AIRPLANE.

$S + P^2$

$\beta = 45$ $i_t = 1.5$ $\xi_r = 0$

	δ_e	
——o——	0	$T_c = 0$
- - - - -	"	MAX. CONT. POWER @ S.L.
——o——	-5	$T_c = 0$
———	"	MAX. CONT. POWER @ S.L.

NACA RM No A7E26

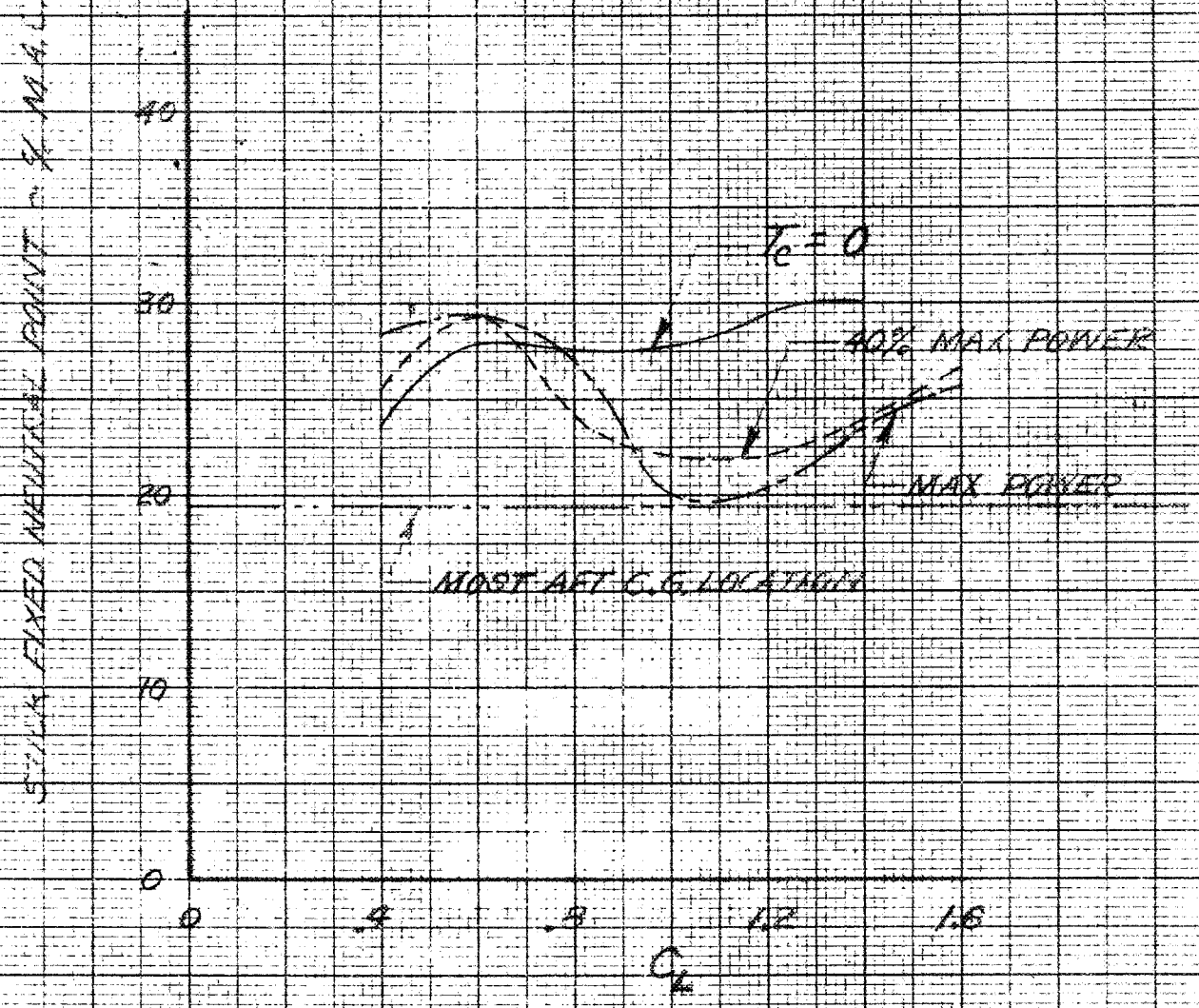

FIGURE 38 - PREDICTED VARIATION OF STICK-FIXED NEUTRAL POINT LOCATION WITH LIFT COEFFICIENT, RYAN XFZR AIRPLANE WITH FLAPS AT 40° AND GEAR EXTENDED.

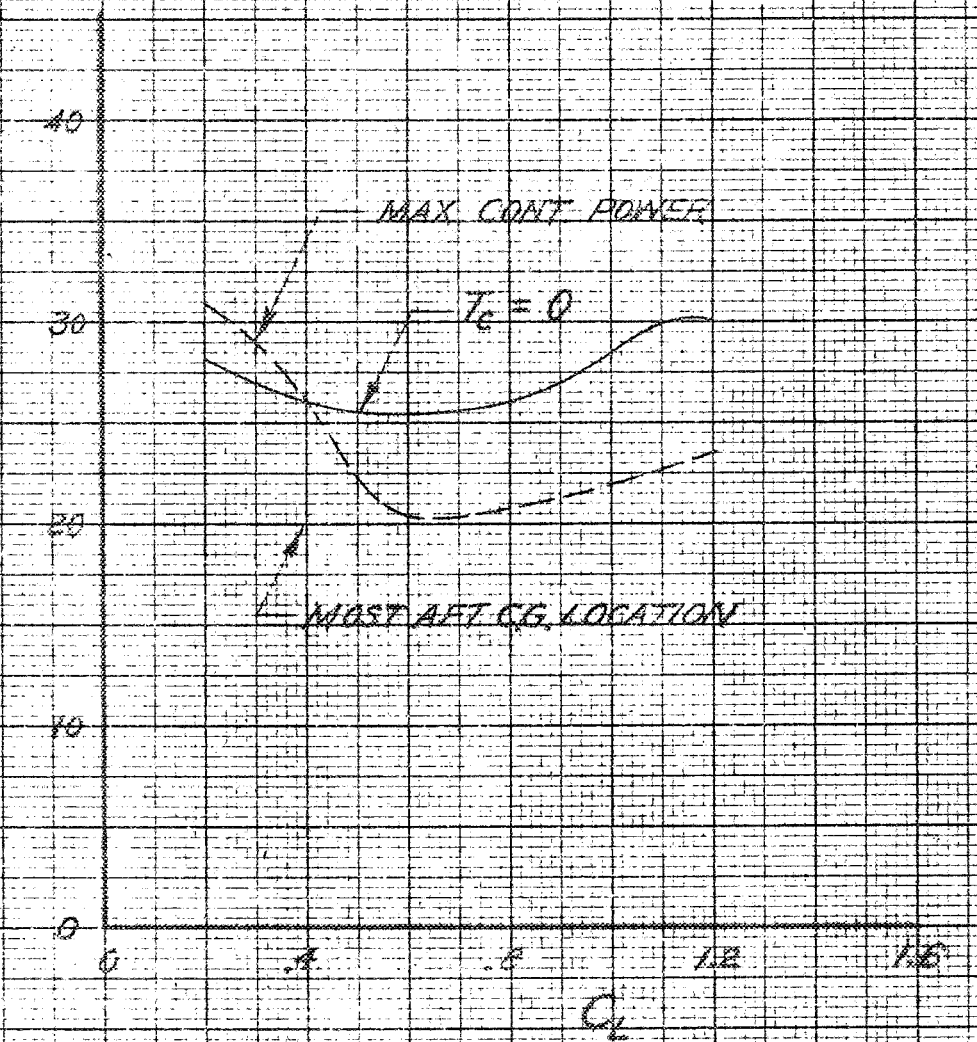

FIGURE 39 — PREDICTED VARIATION OF STICK-FIXED NEUTRAL POINT LOCATION WITH LIFT COEFFICIENT. RYAN XV-5A AIRPLANE WITH FLAP AND GEAR RETRACTED.

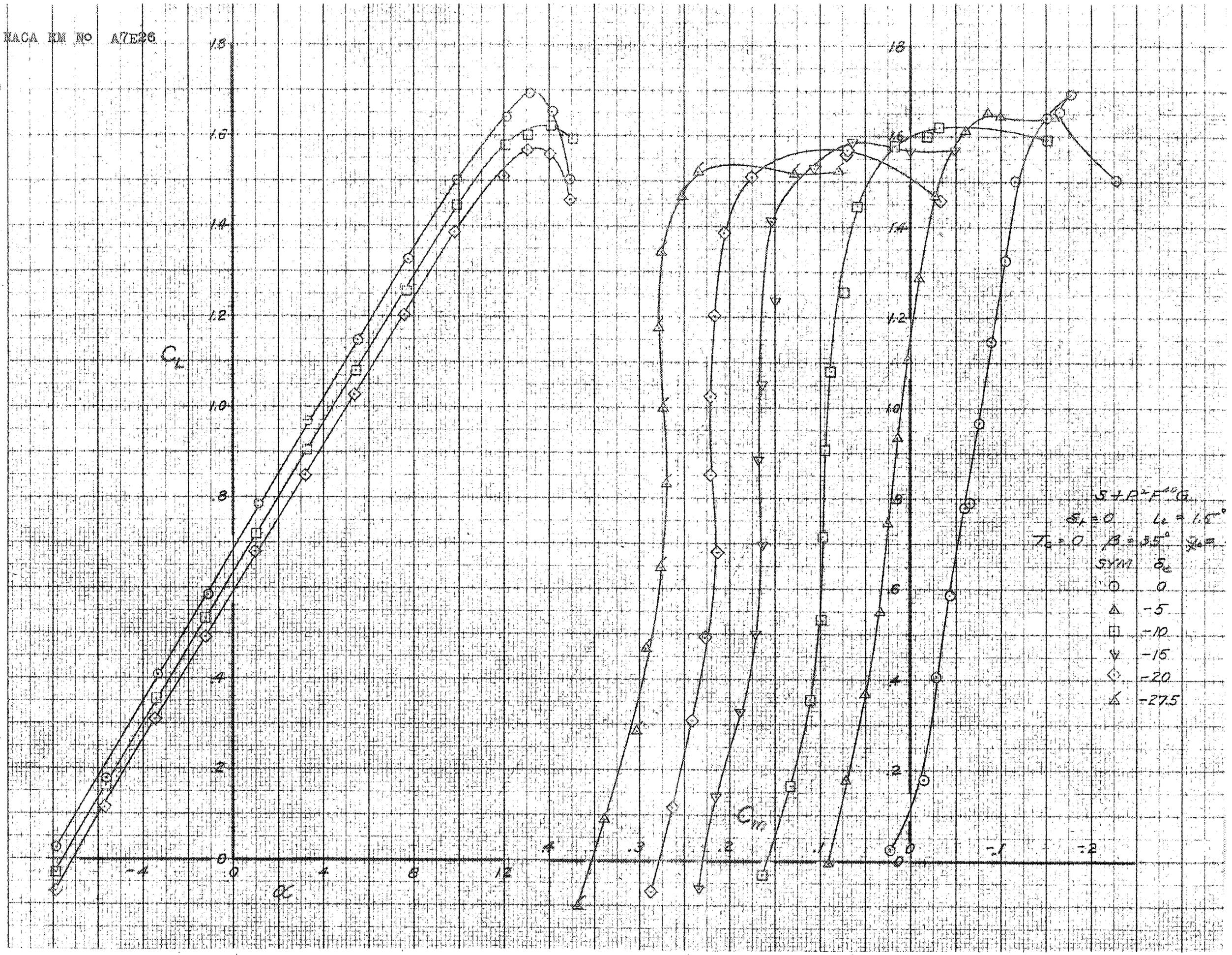
C_L
1.8
1.6
1.4
1.2
1.0
.8
.6
.4
.2
0
-4
0
4
8
12
α
C_m
.4
.3
.2
.1
0
-.1
-.2
$\delta_f + \beta = F^{40}G$
$\delta_f = 0$ $i_t = 1.6°$
$T_c = 0$ $\beta = 35°$ $\frac{x_{cg}}{c} =$
SYM δ_e
0
-5
-10
-15
-20
-27.5

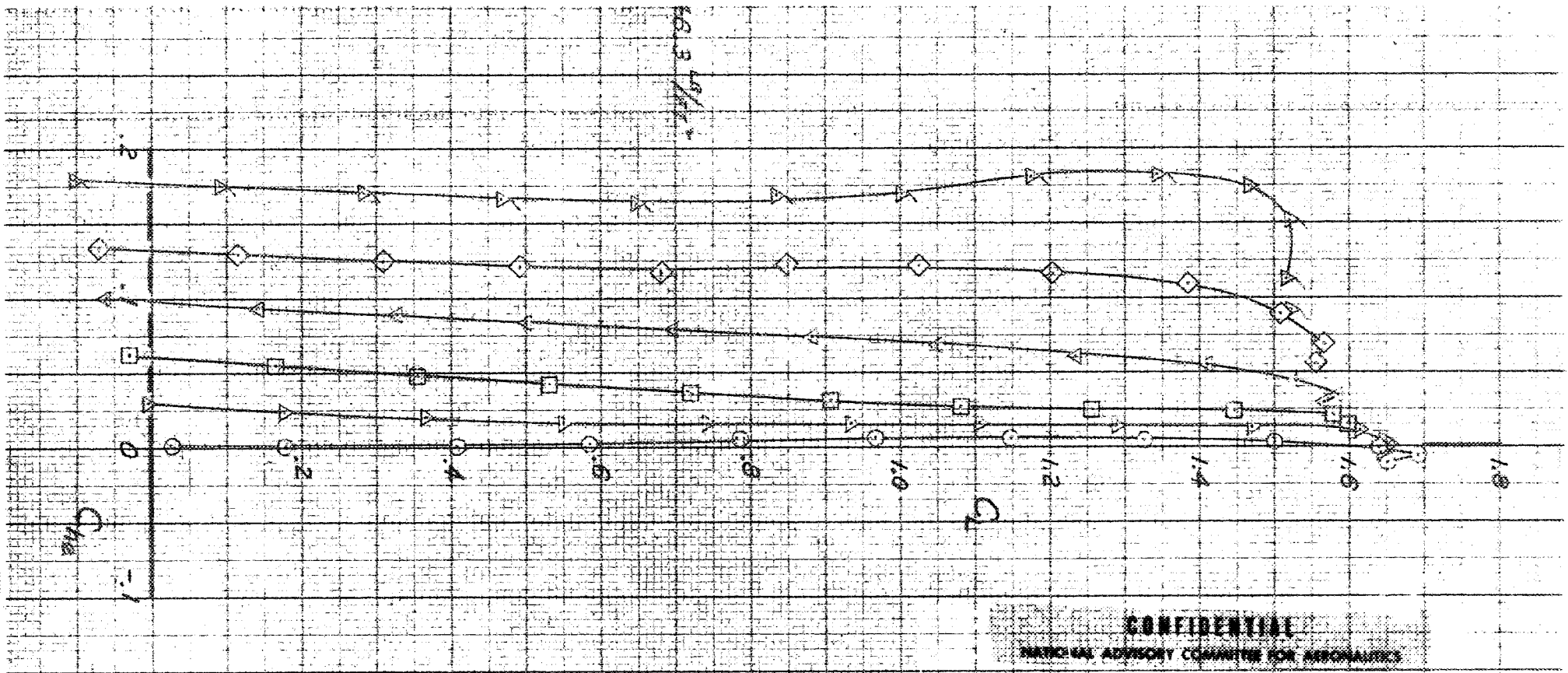

FIGURE 48 - EFFECT OF ELEVATOR DEFLECTION ON THE AERODYNAMIC CHARACTERISTICS OF THE 1/5-SCALE MODEL OF THE RYAN XFR AIRPLANE. FLAPS DEFLECTED 40° AND GEAR EXTENDED. HORIZONTAL-TAIL INCIDENCE = 1.5° i_t = 0

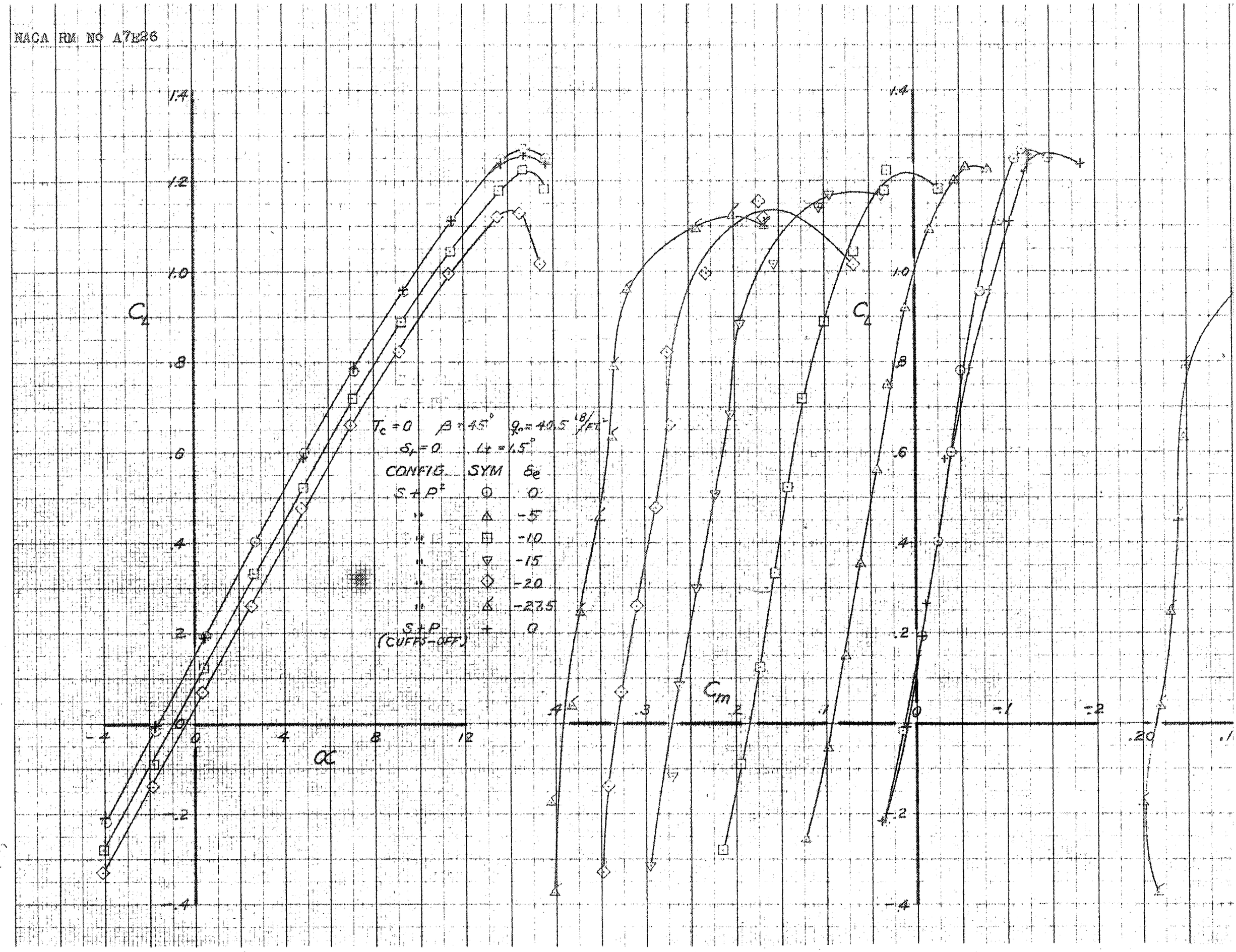
C_L
1.4
1.2
1.0
.8
.6
.4
.2
-.2
-.4
-4
0
4
8
12
α
$T_c = 0$ $\beta = 4.5°$ $q_\infty = 40.5$ lb/ft²
$\delta_f = 0$ $i_t = 1.5°$
CONFIG. SYM δ_e
S + P² ○ 0
" △ -5
" □ -10
" ▽ -15
" ◇ -20
" ◁ -22.5
S + P (CUFFS-OFF) + 0
C_m
.4
.3
.2
.1
0
-.1
-.2
-.20
-.1

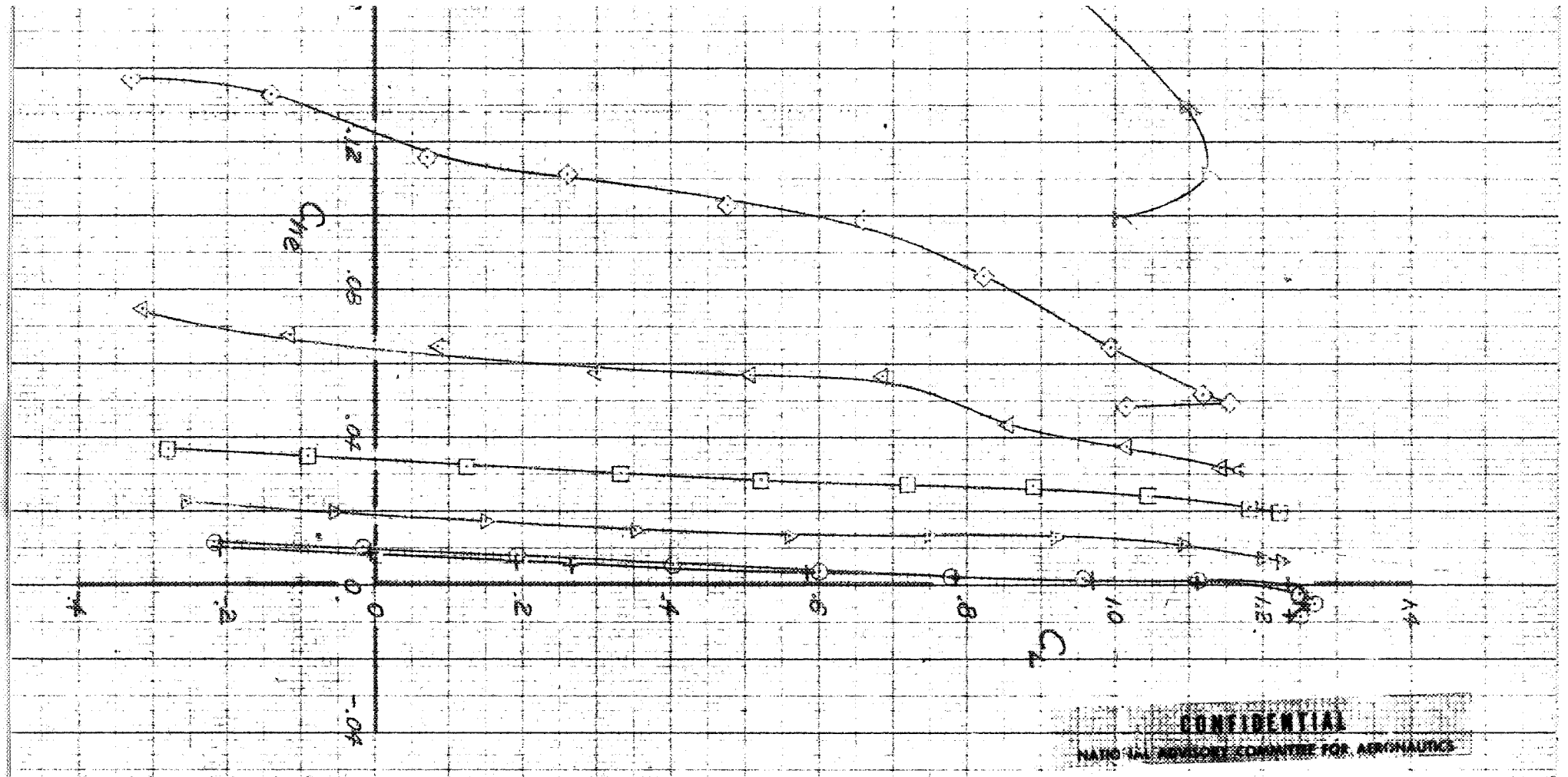

FIGURE 41 - EFFECT OF ELEVATOR DEFLECTION ON THE AERODYNAMIC CHARACTERISTICS OF THE 1/5-SCALE MODEL OF THE RYAN XF2R AIRPLANE. FLAPS AND GEAR RETRACTED. HORIZONTAL-TAIL INCIDENCE = 1.5° $T_c = 0$

NACA RM NO A7B26

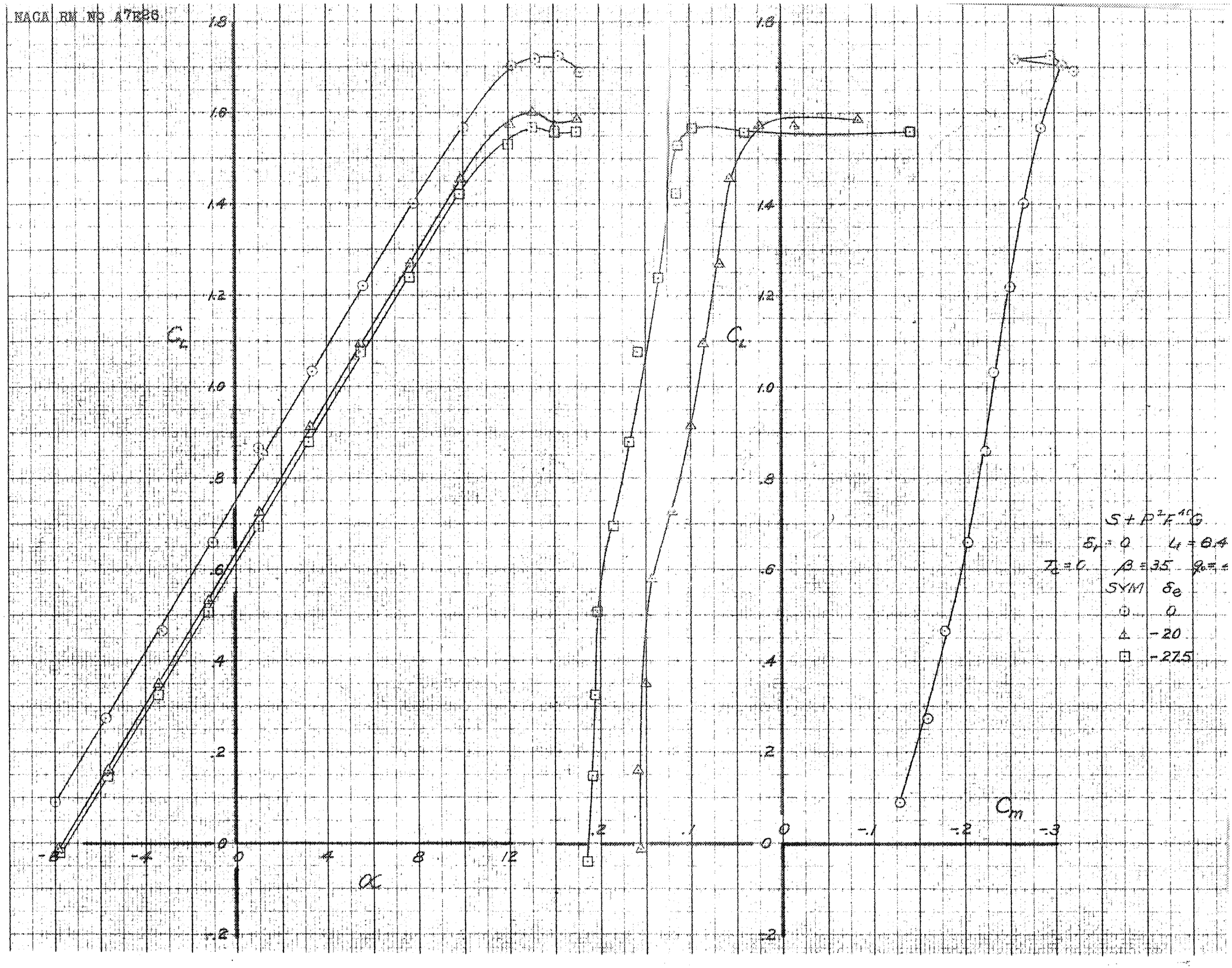

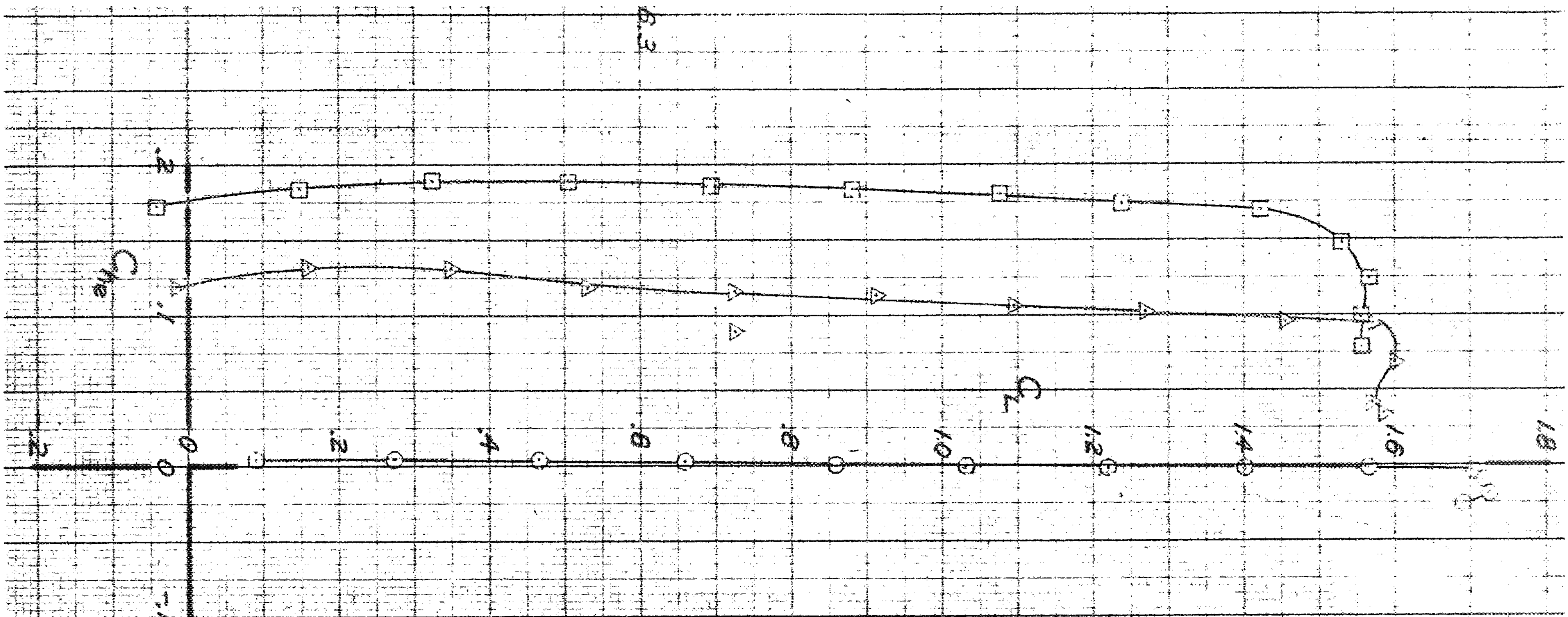

FIGURE 42 - EFFECT OF ELEVATOR DEFLECTION ON THE AERODYNAMIC CHARACTERISTIC
OF THE 1/5-SCALE MODEL OF THE RYAN XF2R AIRPLANE. FLAPS DEFLECTE
40° AND GEAR EXTENDED. HORIZONTAL-TAIL INCIDENCE = 6.4°. $T_c = 0$

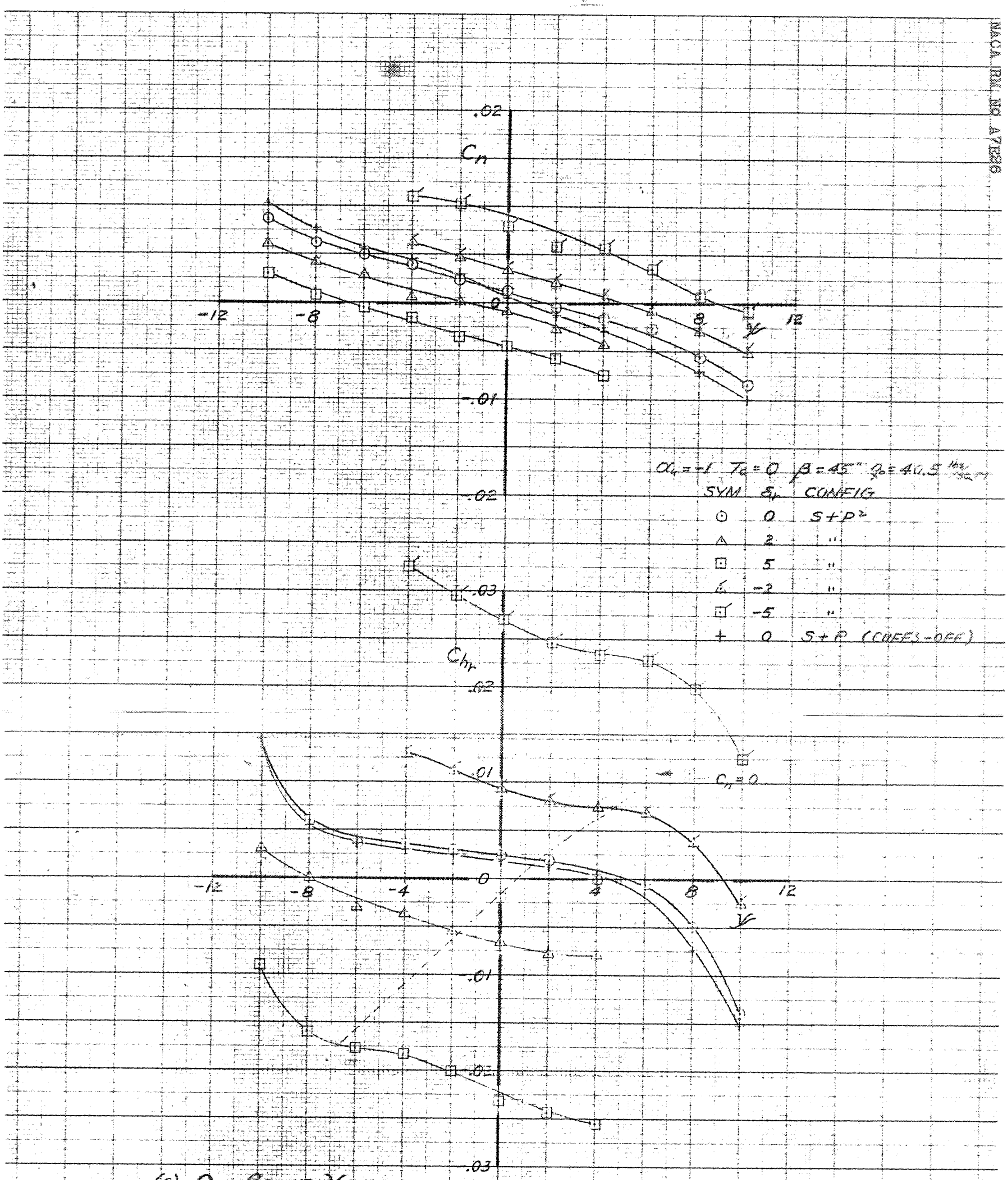

(a) C_n, C_{h_r} vs χ_c

FIGURE 43 - AERODYNAMIC CHARACTERISTICS OF THE 1/5-SCALE MODEL OF THE RYAN XF2R AIRPLANE IN YAW. HIGH-SPEED CONDITION WITH FLAPS AND G.F. RETRACTED.

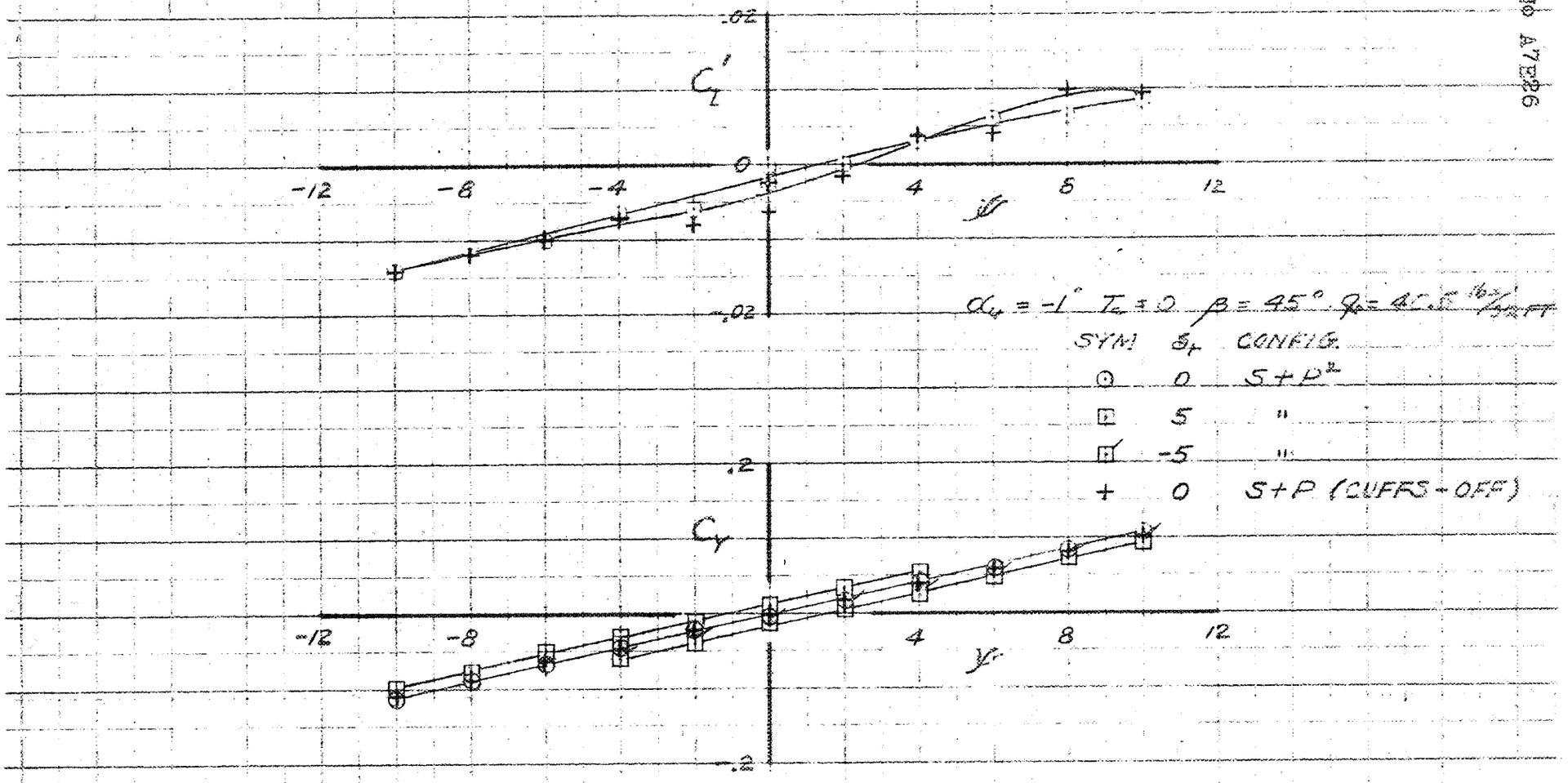

(b) C_l', C_Y vs β

FIGURE 43 - CONTINUED. 1/5-SCALE MODEL OF THE RYAN XFZR AIRPLANE.

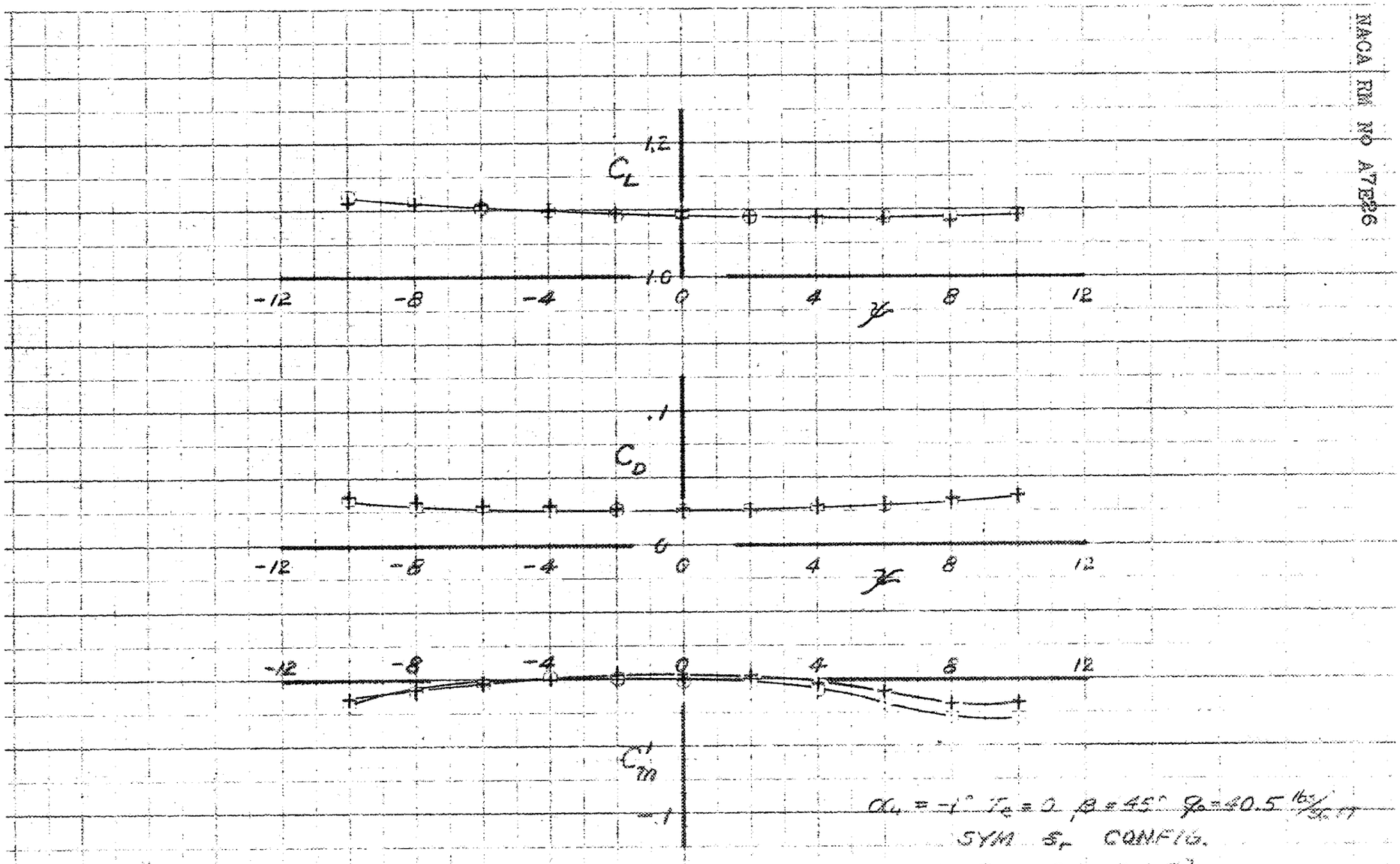

(c) C_L, C_D, C'_m vs α

FIGURE 43 - CONCLUDED. 1/5-SCALE MODEL OF THE F-104 AIRPLANE

C_m

.04
.02
0
-.02
-.04

-30 -20 -10 0 10 20

C_{l_t}

.4
.3
.2
.1
0
-.1

$C_l = 0$

-30 -20 -10 0 10 20 30

α

$S + P^2$

$\alpha_a = .5$ $T_c = 0.22$ $\beta = 45°$ $\eta_c = 33\%$

SYM	δ_f
○	0
△	10
□	20
▽	30
◇	-10
▽	-30
◇	-35

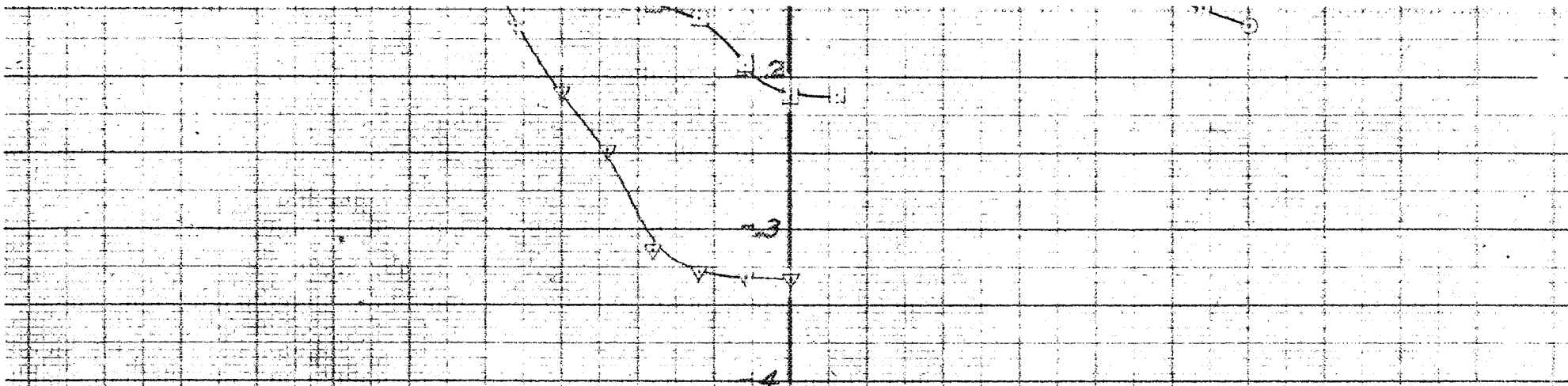

(a) C_n, C_{h_r} vs ψ

FIGURE 44 - AERODYNAMIC CHARACTERISTICS OF THE 1/5 - SCALE MODEL OF THE F[illegible] XF2R AIRPLANE IN YAW CLIMB CONDITION WITH FLAPS AND GEAR RETRACTED

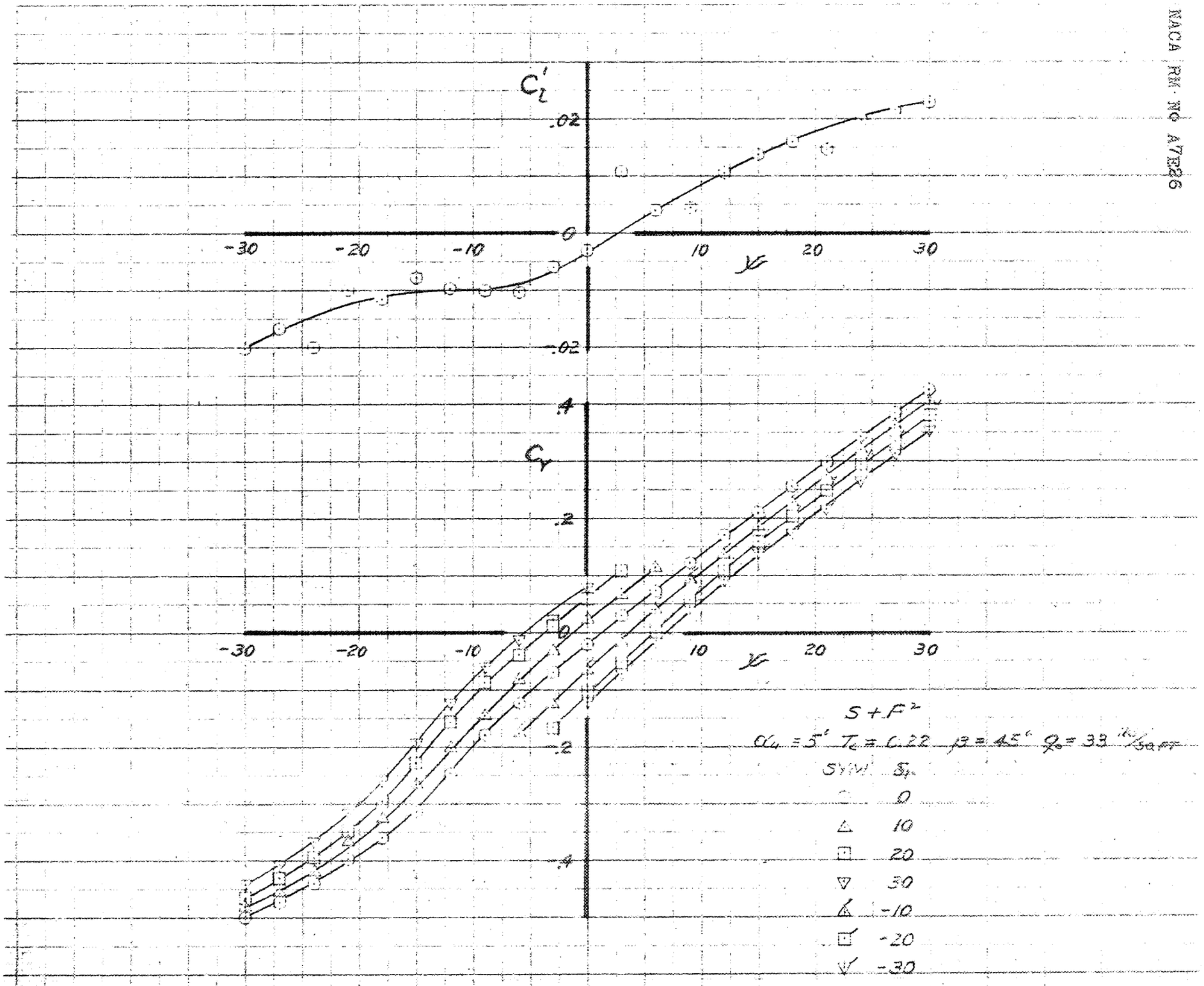

(b) C_l', C_Y vs γ_c

FIGURE 44 - CONTINUED. 1/6-SCALE MODEL OF THE RYAN XF2R AIRPLANE.

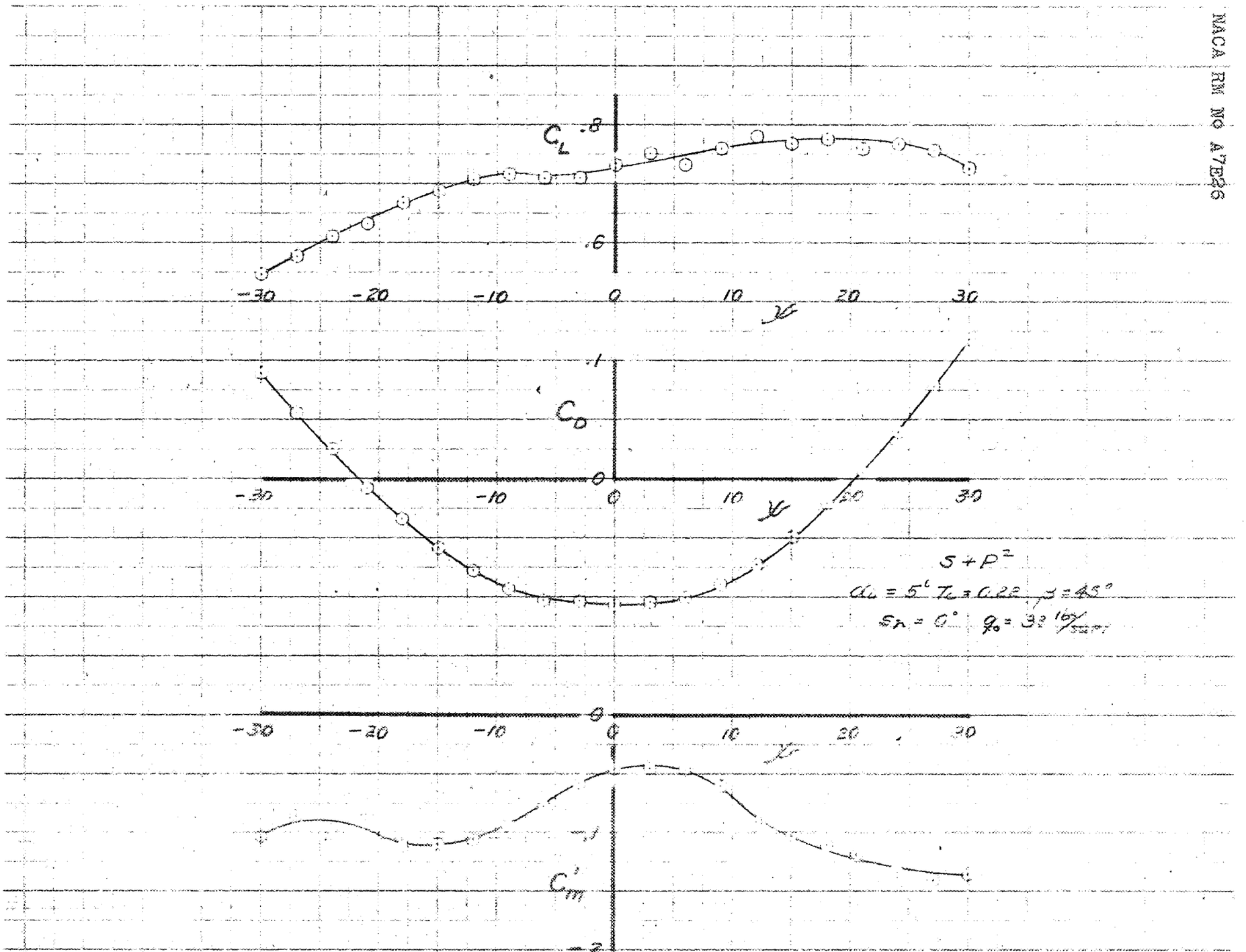

(c) C_L, C_D, C_m' vs α_c

CONFIDENTIAL
NATIONAL ADVISORY COMMITTEE FOR AERONAUTICS

FIGURE 44 - CONCLUDED. 1/6-SCALE MODEL OF THE [illegible] AIRPLANE

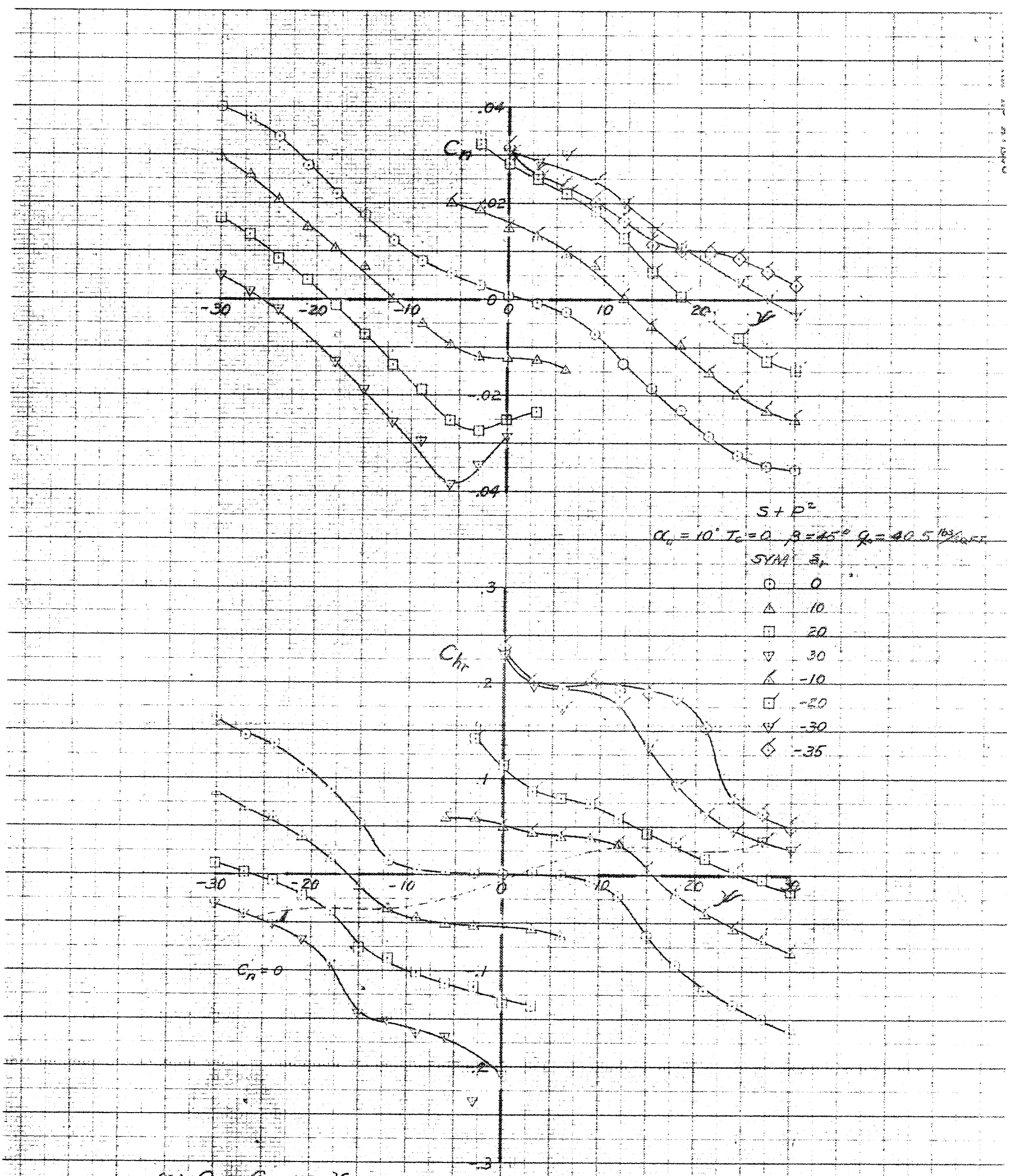

(a) C_n, C_{l_r} vs γ

FIGURE 45 - AERODYNAMIC CHARACTERISTICS OF THE 1/5-SCALE MODEL OF THE RYAN XF2R-1 AIRPLANE IN YAW. GLIDE CONDITION WITH FLAPS AND GEAR RETRACTED.

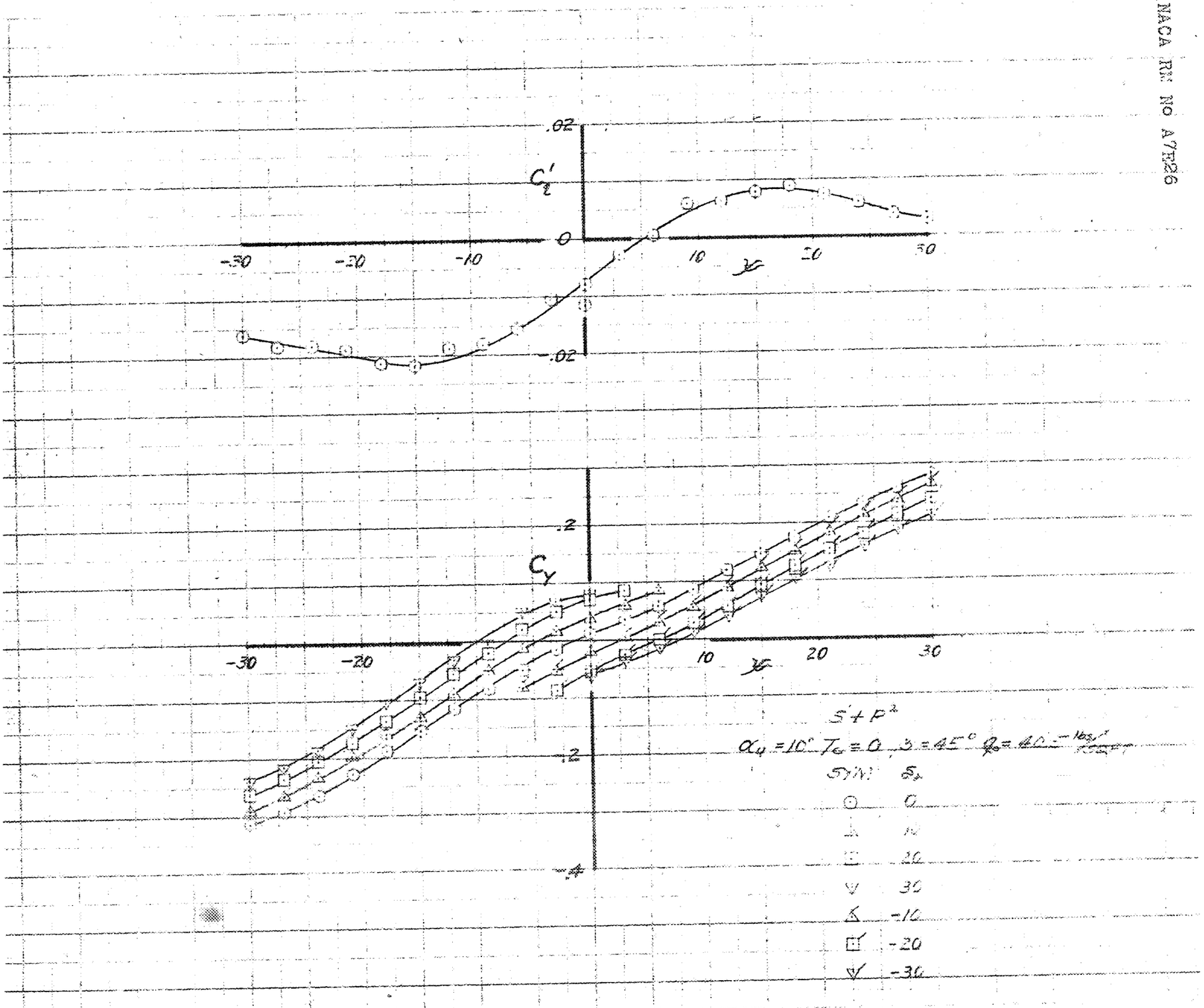

(b) $C_{l'}$, C_Y vs β

FIGURE 45.- CONTINUED. 1/5-SCALE MODEL OF THE RYAN XFR-1 AIRPLANE.

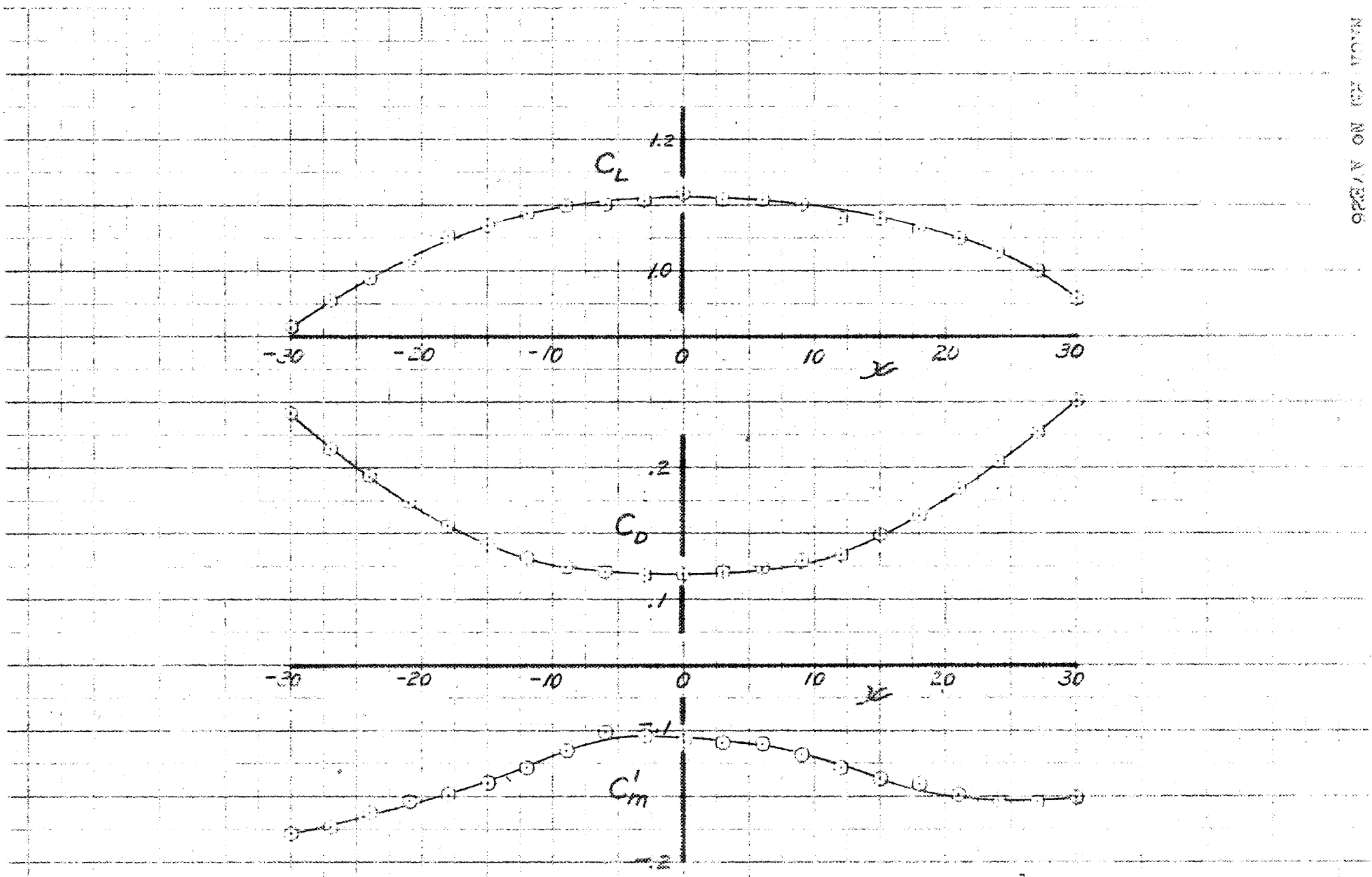

$S + P^2$

$\omega_{l_0} = 10$ $\quad Z_0 = 0$ $\quad \alpha_c = \alpha_{c_0}$

$\delta_r = 0$ $\quad g_0 = 32.2$ ft/sec^2

(c) C_L, C_D, C'_m vs α_c

FIGURE 45. - CONCLUDED. 1/3-SCALE MODEL OF THE RYAN XF2R AIRPLANE.

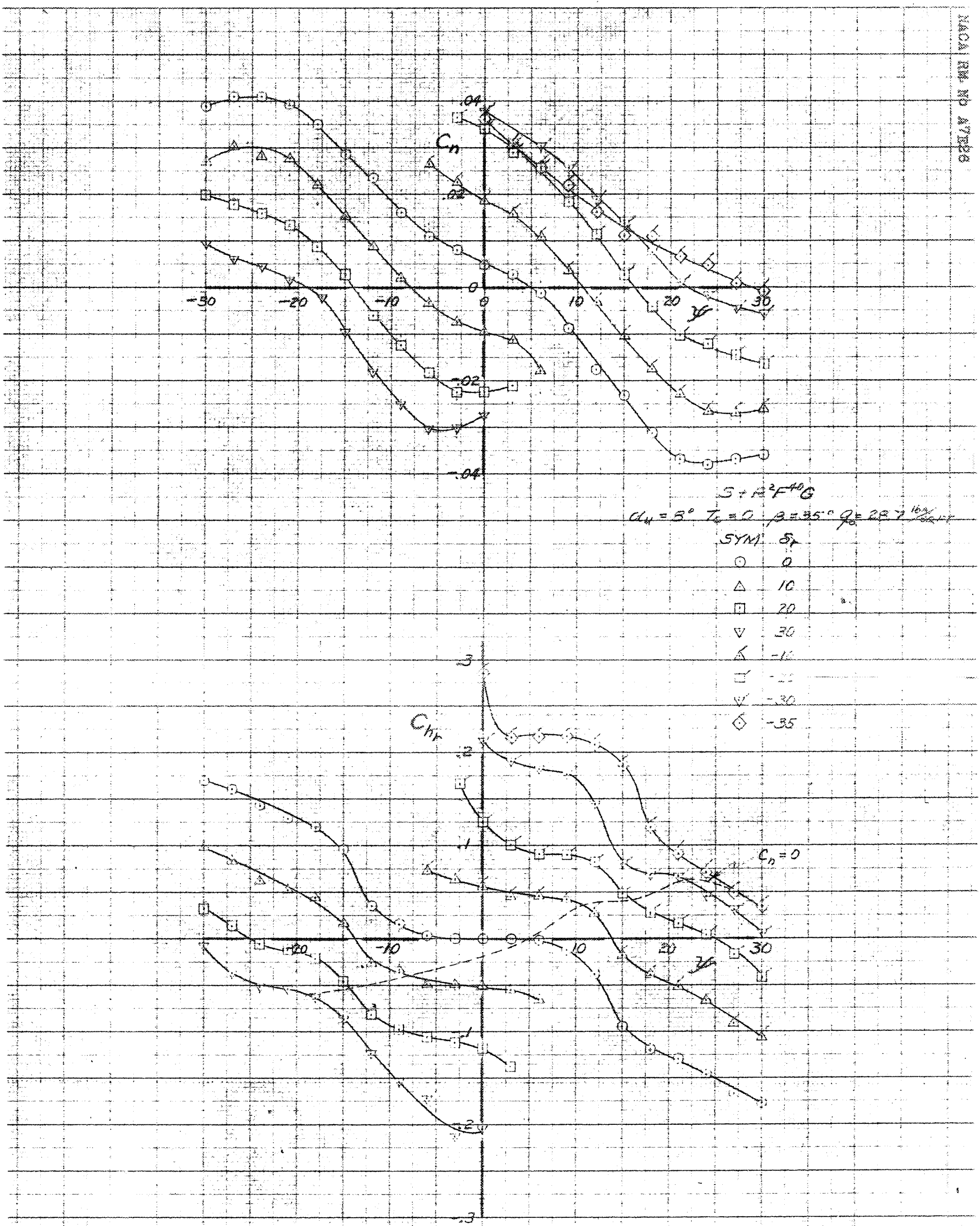

(a) C_n, C_{h_f} vs β

FIGURE 46 - AERODYNAMIC CHARACTERISTICS OF THE 1/5-SCALE MODEL OF THE RYAN X-22 AIRPLANE IN YAW. POWER-OFF APPROACH CONDITION WITH FLAPS DEFLECTED 40° AND GEAR EXTENDED.

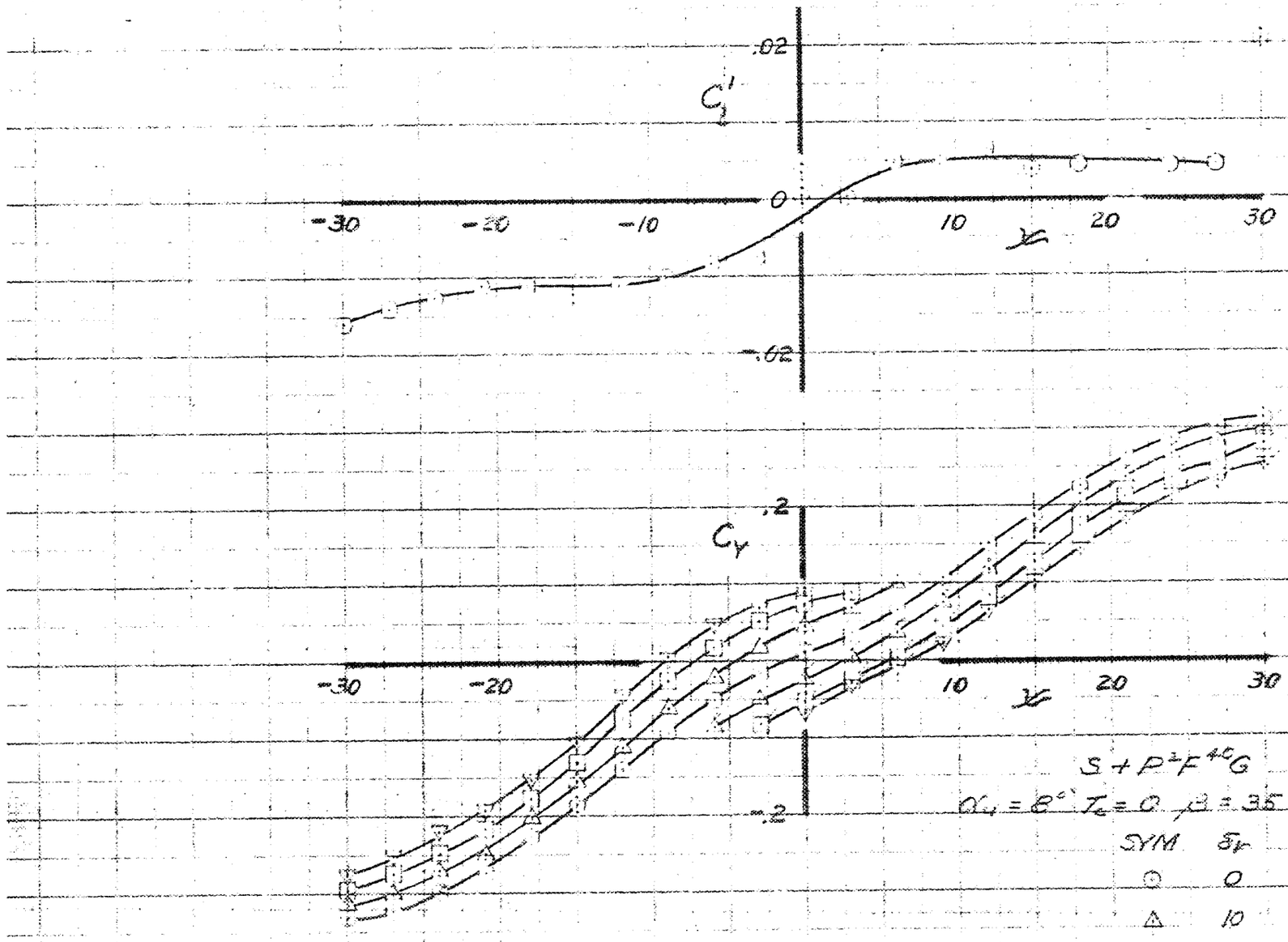

(b) C_l', C_Y vs γ_c

FIGURE 46. - CONCLUDED. 1/5-SCALE MODEL OF THE RYAN XF2R AIRPLANE.

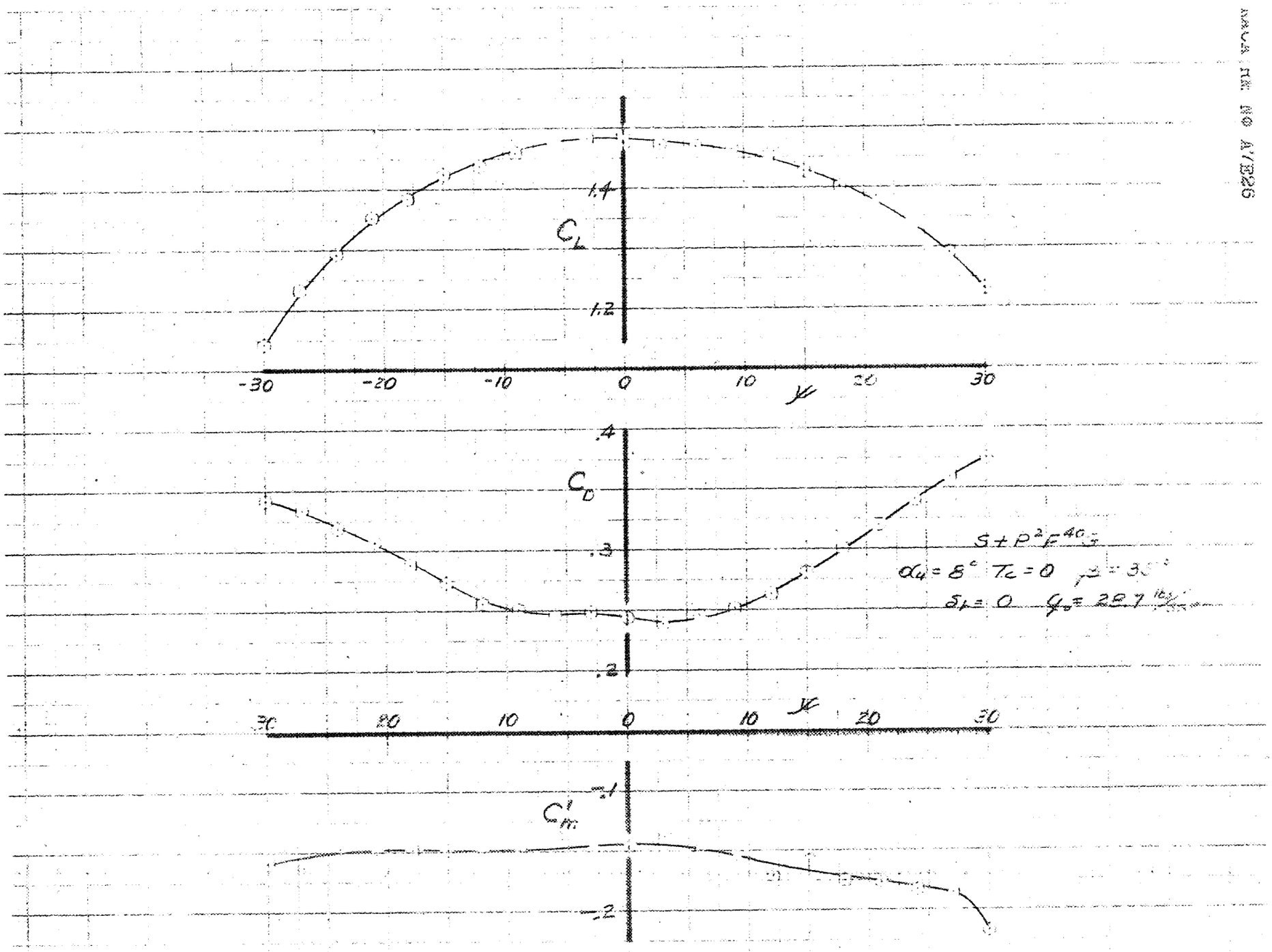

(c) C_L, C_D, C'_m vs α

FIGURE 46 - CONCLUDED. 1/6-SCALE MODEL OF THE RYAN XF2R AIRPLANE.

NACA RM No A7I26

C_n

.04
.02
-.02
-.04
-.06

-30 -20 -10 0 10 20 30

$C_Y = 0$

$S + P^2 F^{40} G$

$\alpha_w = 8°$ $T_c = 0.4$ $\beta = 25°$ $q = 25$ lb/sq ft

○	0
△	10
□	20
▽	30
△	-10
□	-20
▽	-30
◇	-35

C_{l_n}

.5
.4
.3
.2
.1

$C_n = 0$

-30 -20 -10 0 10 20 30

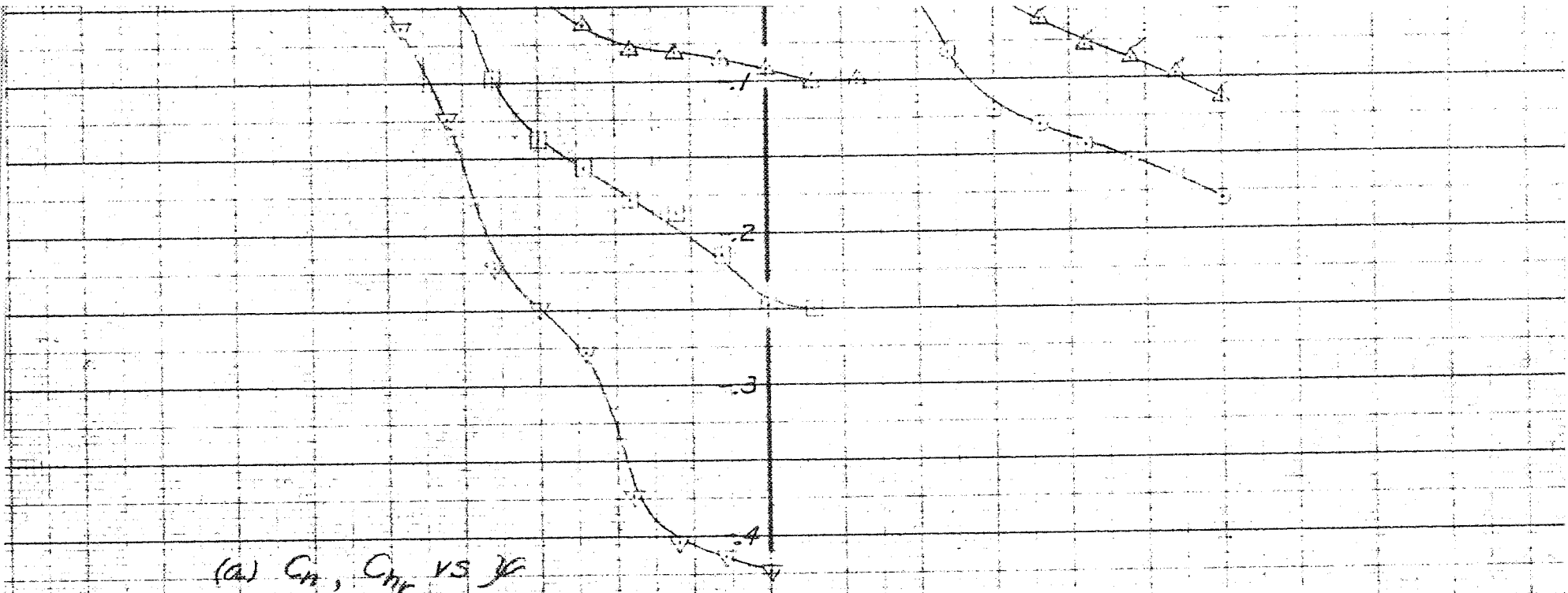

(a) C_n, C_{n_r} vs β

FIGURE 47.- AERODYNAMIC CHARACTERISTICS OF THE 1/5-SCALE MODEL OF THE RYAN XFZR AIRPLANE IN YAW. POWER-ON APPROACH CONDITION WITH FLAPS DEFLECTED 40° AND GEAR EXTENDED

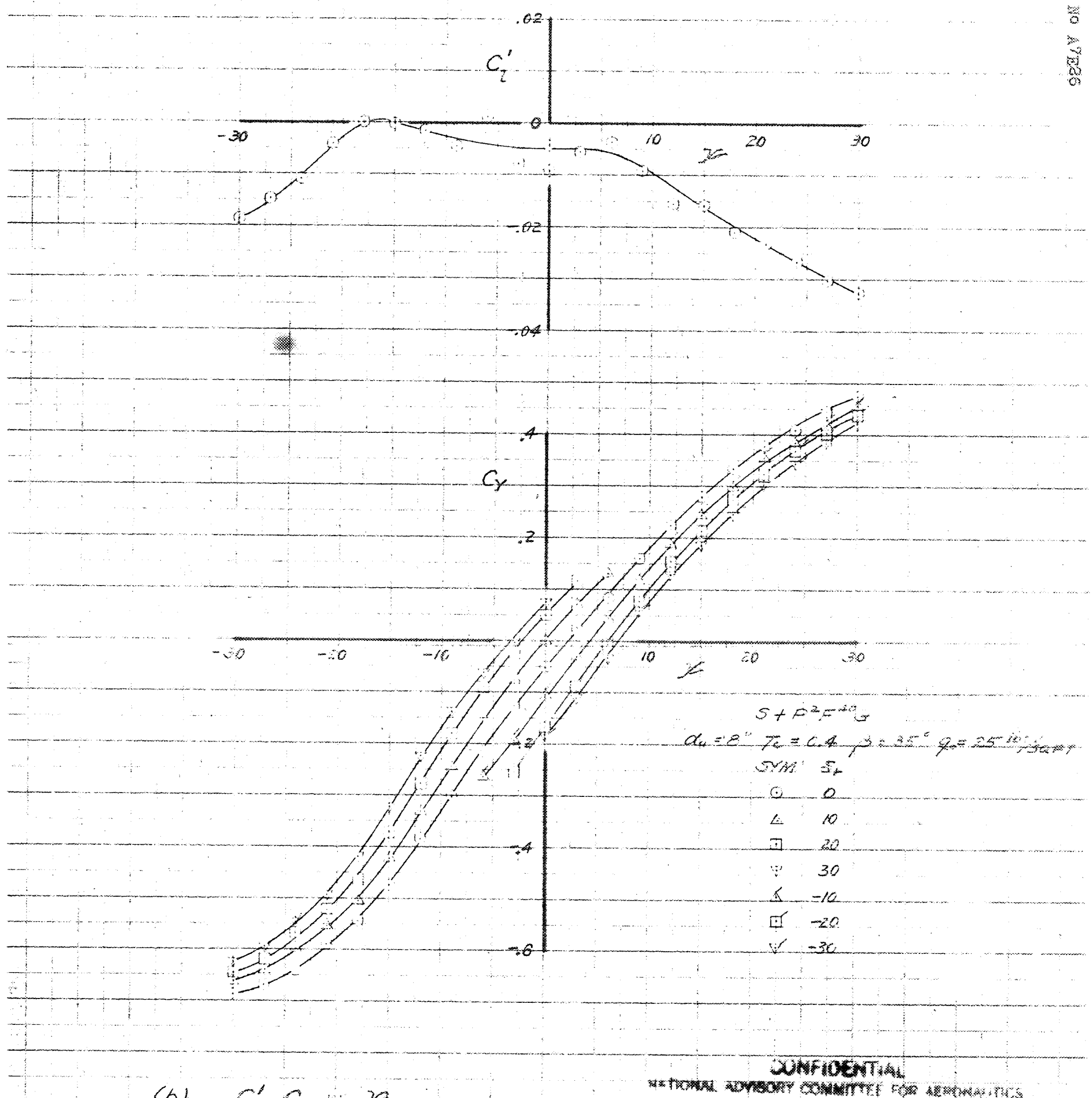

(b) C_l', C_y vs ψ

CONFIDENTIAL
NATIONAL ADVISORY COMMITTEE FOR AERONAUTICS

FIGURE 47.- CONTINUED. 1/5-SCALE MODEL OF THE RYAN XF2R AIRPLANE.

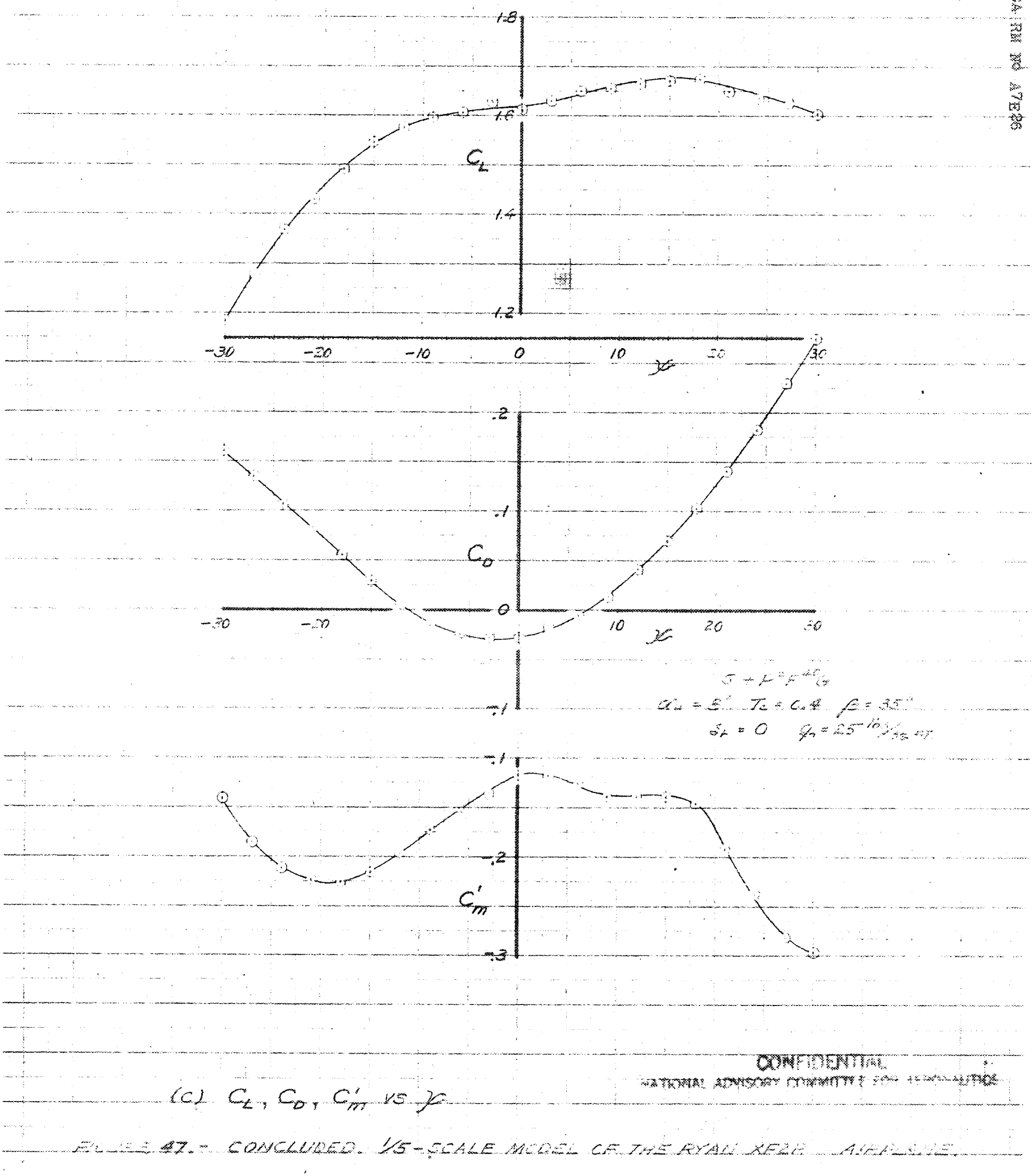

(c) C_L, C_D, C'_m vs α

FIGURE 47.- CONCLUDED. 1/5-SCALE MODEL OF THE RYAN XF2R AIRPLANE.

C_n

.04
.02
0
-.02
-.04
-.06
-.08
-.10
-.12

-30 -20 -10 0 20 30

C_{l_r}

.5
.4
.3
.2

$C_l = 0$

$C_n = 0$

$S + P^2 F^{1/2} G$

$\alpha_1 = 8$ $T_c = 0.69$ $\beta = 35°$ $\phi_0 = 16$ knots

SYM	S_1
○	0
△	10
□	20
▽	30
◁	-10
◻	-20
▽	-30
◇	-35

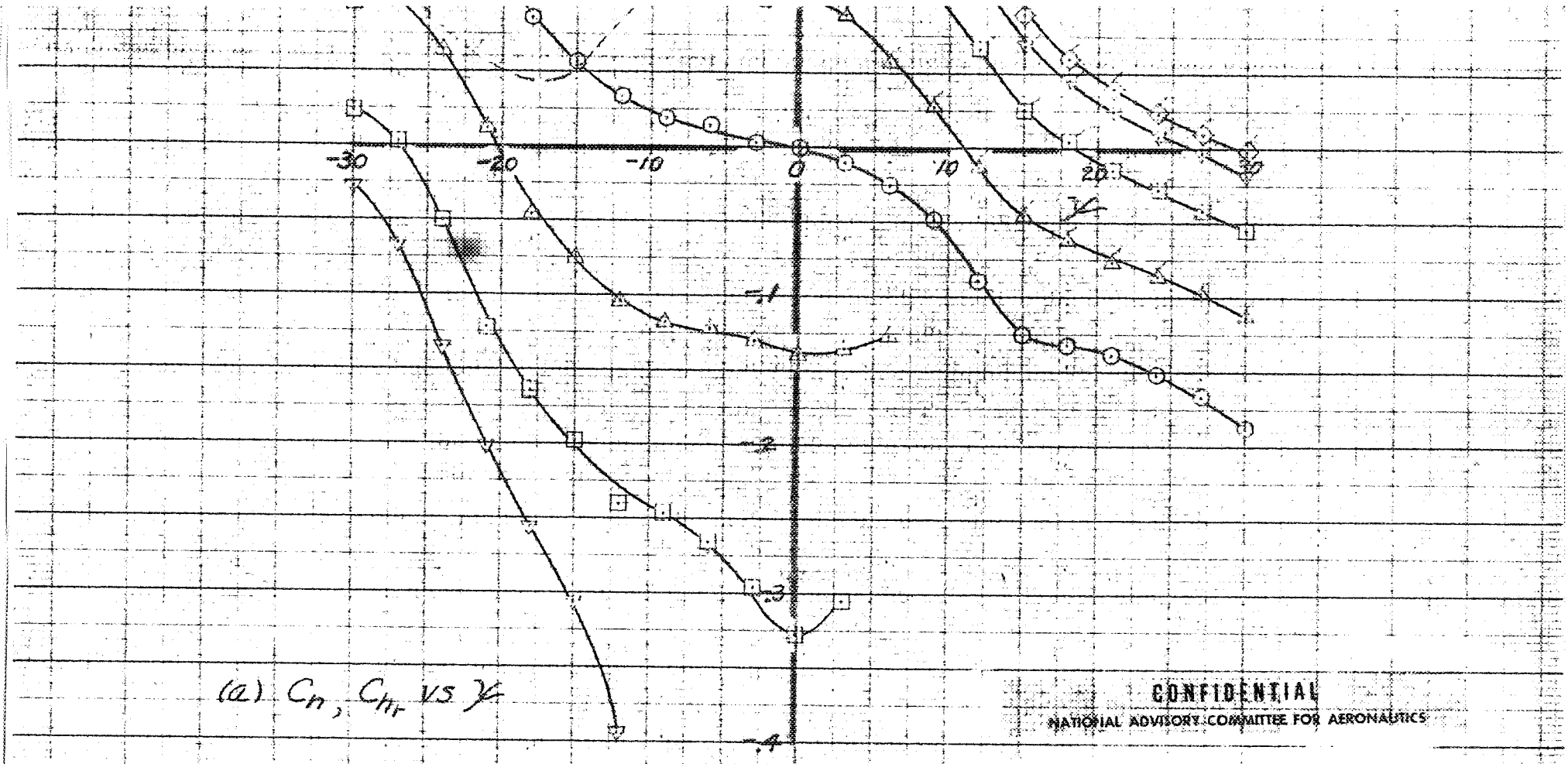

FIGURE 48 - AERODYNAMIC CHARACTERISTICS OF THE 1/5-SCALE MODEL OF THE RYAN XF2R AIRPLANE. WAVE-OFF CONDITION WITH FLAPS DEFLECTED 40° AND GEAR EXTENDED.

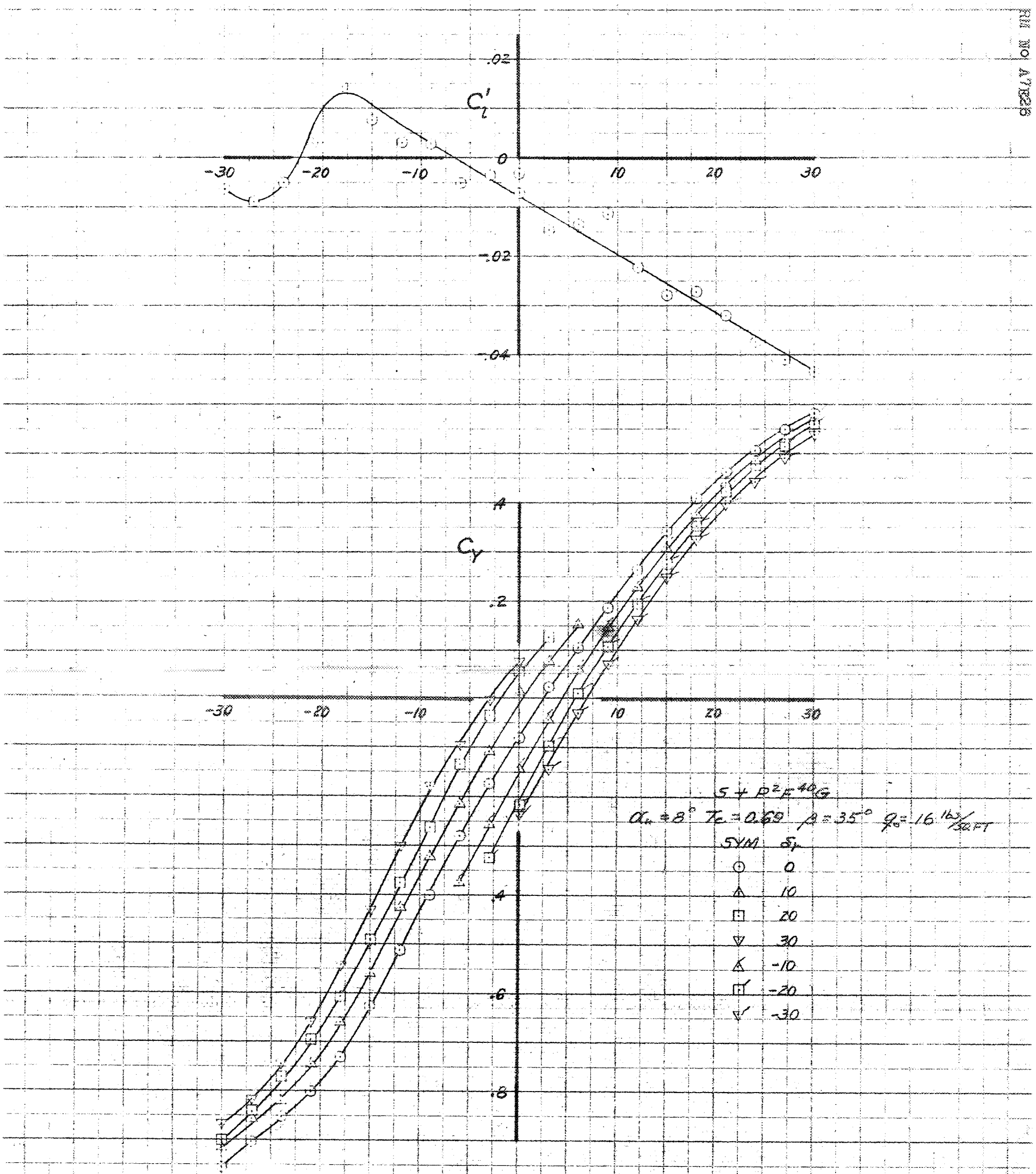

(b) C_l', C_Y vs β_F

FIGURE 18.- CONTINUED. 1/5-SCALE MODEL OF THE RYAN XFR-1 AIRPLANE

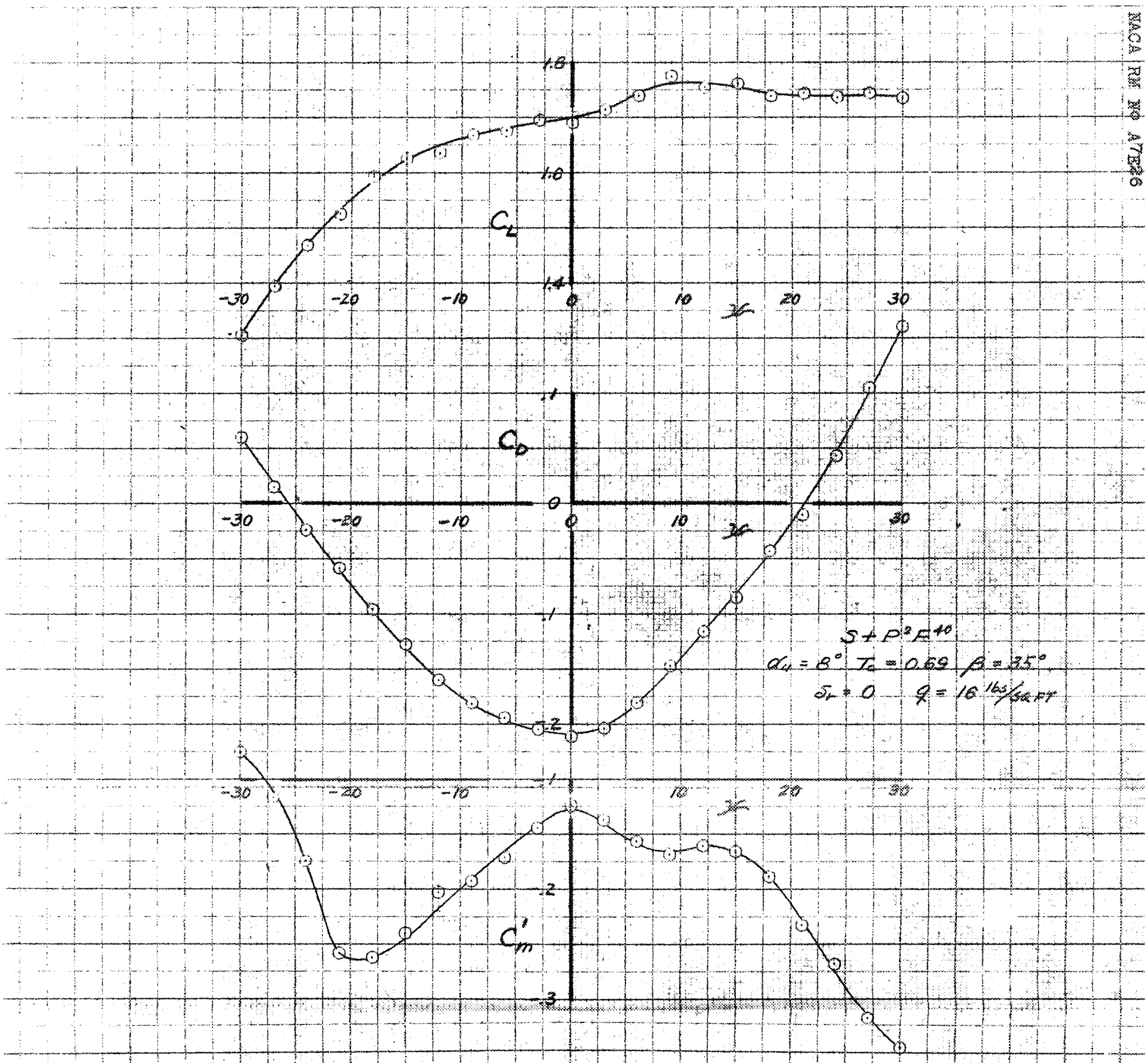

(c) C_L, C_D, C_m' vs α_c

FIGURE 48 - CONCLUDED. 1/5-SCALE MODEL OF THE RYAN XF2R AIRPLANE.